

THE RHEOLOGY OF A BITUMINOUS COAL

Thesis by

John Cary Stevenson

In Partial Fulfillment of the Requirements  
for the Degree of  
Doctor of Philosophy

California Institute of Technology  
Pasadena, California

1982

(Submitted May 24, 1982)

### ACKNOWLEDGMENT

I would like to express my gratitude and thanks to my thesis advisor, Professor W. H. Corcoran, for his invaluable assistance, guidance and advice throughout the course of the present work. Thanks also go to Dr. Chris England who expressed a continuing interest in this research work and for his many helpful suggestions and comments. I would also like to thank Professors A. J. Acosta and C. E. Brennen for their support and the support of the Mechanical Engineering Department.

I would like to thank my colleague Sam Feinstein and the Jet Propulsion Laboratory for their assistance with the experimental equipment. Additionally, I would like to thank Ray Kushida and Max Clayton for discovering the funds that allowed the completion of this experiment. I am also grateful to the Chemical Engineering Department for financial support.

Finally, I would like to thank all the members of my family for their support and patience.

### **Abstract**

The fluidity of a rapidly heated, bituminous coal was studied with a capillary rheometer. Quantitative measurements of overall fluidity, of transition from no flow to flow, and of the effects of presence of the gaseous phase were the principal objectives.

Separate measurements of the density of the coal indicated that the major changes in density with time were due to the production of gas by decomposition. The volume fraction of gas was calculated from the density measurements.

The relationships between volumetric flow rate and pressure drop were expressed in terms of an overall, or "effective," viscosity. The overall viscosity displayed values as low as thirty poise, and its rheological classification was Newtonian within the accuracy of the experimental equipment. The transition from no flow to flow was quite sudden, and it was independent of the volume of gas present in the reservoir.

The multi-component, multi-phase flow of coal was considered to be a two-component, two-phase, liquid-gas system. Various correlations found in the literature were applied to the overall viscosity data, and estimates of the viscosity of the liquid phase were made. A constitutive relationship for the density as a function of temperature, time, and pressure was developed. Closed-form solutions of the simplified momentum equation were generated based on definitions of a mean viscosity as a function of the viscosities of the liquid and the gas, and the volume fractions of the liquid and the gas. Because of the magnitude of the volume fraction of gas, the viscosity of the liquid phase was greater than the overall viscosity of the mixture.

"In the beginning, we saw the mountains as mountains  
and the sea as sea.  
During our studies, we saw the mountains as sea  
and the sea as mountains.  
Now that we have completed our studies we again see the  
Mountains as mountains and the sea as sea."

Lao Tze Tung

List of Symbols

$a$	constant fitted to the data
$A$	area
$A_c$	cross-sectional area of the capillary tube
$A_p$	area of the piston head
$b$	constant fitted to the data
$B$	intermediate result (Equation 4.65)
$c$	constant fitted to the data
$C$	circumference of the capillary tube
$C_{E-CGS}$	conversion factor, psi to dynes/cm <sup>2</sup>
$C_f$	wetted circumference
$C_g$	circumference in contact with gas
$C_l$	circumference in contact with liquid
$C_1$	constant of integration
$d\vec{A}$	elemental surface-area vector
$E$	net volumetric force due to evaporation
$F$	force
$F_p$	force exerted on the piston
$g$	gravitational acceleration constant
$\vec{g}$	gravitational acceleration vector
$G$	forces related to the gravitational field
$G_T$	total-mass velocity
$h_p$	position of the piston head
$I_g$	inertia force of the gas
$I_l$	inertia force of the liquid
$k$	constant fitted to the experimental data
$k_1$	constant defined by Equation 7.26

$k_2$	constant defined by Equation 7.27
$k_3$	constant defined in Equation 6.18
$L$	length of the capillary tube
$\dot{m}$	mass-flow rate
$m_l$	mass of the liquid and solid phases
$m_t$	total mass of the coal sample
$\dot{m}_i$	mass-flow rate into the capillary tube
$\dot{m}_o$	mass-flow rate out of the capillary tube
$P$	pressure
$P_g$	pressure in the hydraulic cylinder
$P_i$	pressure at the entrance to the capillary tube
$P_o$	pressure at the exit of the capillary tube
$P_r$	pressure in the reservoir
$P^*$	constant defined by Equation 7.2
$Q$	volumetric flow rate
$Q_i$	volumetric flow rate into the capillary
$Q_l$	volumetric flow rate of the liquid
$Q_o$	volumetric flow rate at the exit to the capillary tube
$r$	radial variable
$\tau_g$	mass fraction of gas not in solution
$\tau_o$	radius of the capillary tube
$\tau_i$	total-mass fraction of gas
$R$	function of radius only (Equation 3.2)
$R_o$	radius of the reservoir
$R^*$	specific gas constant
$t$	temporal variable
$t_o$	time at the start of constant-flow rate

$t_e$	time at the end of constant-flow rate
$t_o$	initial time
$T$	temperature
$T_c$	temperature at the centerline of the capillary tube
$T_o$	initial or boundary temperature
$T_w$	temperature at the wall
$u$	velocity in the axial direction
$\vec{u}$	velocity vector
$u_m$	intermediate result (Equation 4.62)
$u_p$	velocity of the piston head
$U$	relative velocity of a bubble in a liquid
$V$	instantaneous volume of the reservoir
$V_c$	volume of the capillary tube
$V_L$	reservoir volume occupied by the liquid and solid phases
$V_{rc}$	instantaneous volume of the reservoir and the capillary tube
$w$	intermediate result (Equation 4.63)
$X_s$	intermediate result (Equation 4.68)
$z$	axial variable
$\alpha$	a constant (Equation 4.61)
$\alpha_g$	volume fraction of gas
$\bar{\alpha}_g$	length-averaged volume fraction of gas
$\alpha_g _{in}$	volume fraction of gas at the entrance to the capillary tube
$\alpha_g _o$	volume fraction of gas at the exit of the capillary tube
$\alpha_l$	volume fraction of liquid
$\beta$	bubble radius
$\gamma$	separation constant (Equation 3.3)
$\kappa$	thermal diffusivity

$\varphi$	correlation function
$\rho$	overall density
$\bar{\rho}$	length-averaged overall density
$\rho_b$	density of a bubble
$\rho_i$	density at the entrance to the capillary tube
$\rho_l$	density of the liquid phase
$\rho_o$	density at the exit of the capillary tube
$\rho_r$	overall density in the reservoir
$\Theta$	function of time only (Equation 3.2)
$\tau$	shear stress
$\ddagger$	shear stress tensor
$\tau_{rz}$	shear stress in the axial direction acting on the r-normal plane
$\tau_w$	shear stress at the wall of the capillary tube
$\bar{\tau}_w$	length-averaged shear stress at the wall
$\tau_{wg}$	shear stress at the wall exerted by the gas
$\tau_{wl}$	shear stress at the wall exerted by the liquid
$\tau_{zz}$	shear stress acting in the axial direction and on the axial plane
$\mu$	apparent viscosity
$\bar{\mu}$	mean-apparent viscosity
$\mu_c$	constant defined by Equation 6.26
$\mu_g$	viscosity of the gas
$\mu_l$	viscosity of the liquid
$\mu_o$	initial viscosity (Equation 2.3)
$\mu_T$	true viscosity
$\mu_{TP}$	overall viscosity of a two-phase mixture
$\nu$	kinematic viscosity
$\omega$	mass-flow rate

$\omega_g$	mass-flow rate of the gas
$\omega_l$	mass-flow rate of the liquid
$\chi$	correlation variable

FIGURE CAPTIONS

- Figure 2.1 Schematic diagram of the experimental equipment.
- Figure 2.2 Detailed diagram of piston-head system.
- Figure 2.3 Detailed diagram of viscometer-block system.
- Figure 2.4 The viscosity of a calibration standard versus temperature.
- Figure 3.1 The density of a Pitt 8 coal at 410°C and a nominal pressure of 75 psi.
- Figure 3.2 The density of a Pitt 8 coal at 410°C and a nominal pressure of 100 psi.
- Figure 3.3 The density of a Pitt 8 coal at 410°C and a nominal pressure of 150 psi.
- Figure 3.4 The density of a Pitt 8 coal at 410°C and a nominal pressure of 200 psi.
- Figure 3.5 The density of a Pitt 8 coal at 450°C and a nominal pressure of 50 psi.
- Figure 3.6 The density of a Pitt 8 coal at 450°C and a nominal pressure of 75 psi.
- Figure 3.7 The density of a Pitt 8 coal at 450°C and a nominal pressure of 100 psi.
- Figure 3.8 The density of a Pitt 8 coal at 450°C and a nominal pressure of 125 psi.
- Figure 3.9 The volume fraction of gas versus time at a nominal pressure of 75 psi.
- Figure 3.10 The volume fraction of gas versus time at a nominal pressure of 100 psi.
- Figure 5.1 The viscosity of a Pitt 8 coal at 410°C and a nominal pressure drop of 75 psi.
- Figure 5.2 The viscosity of a Pitt 8 coal at 410°C and a nominal pressure drop of 100 psi.

- Figure 5.3 The viscosity of a Pitt 8 coal at 410°C and a nominal pressure drop of 150 psi.
- Figure 5.4 The viscosity of a Pitt 8 coal at 410°C and a nominal pressure drop of 200 psi.
- Figure 5.5 The viscosity of a Pitt 8 coal versus time at 450°C and a nominal pressure drop of 50 psi.
- Figure 5.6 The viscosity of a Pitt 8 coal at 450°C and a nominal pressure drop of 75 psi.
- Figure 5.7 The viscosity of a Pitt 8 coal at 450°C and a nominal pressure drop of 100 psi.
- Figure 5.8 The viscosity of a Pitt 8 coal versus time at 450°C and a nominal pressure drop of 125 psi.
- Figure 5.9 The overall viscosity of a Pitt 8 coal versus nominal pressure drop.
- Figure 8.1 The total-mass fraction of gas versus time and the standard deviation of the prediction of the overall density based on total-mass fraction of gas in the reservoir at 410°C.
- Figure 8.2 The total-mass fraction of gas in the reservoir versus time and the standard deviation of the prediction of the overall density based on the total-mass fraction of gas at 450°C.

LIST OF TABLE HEADINGS

- Table 2.1 Characterization of the Pitt 8 Coal
- Table 3.1 An Empirical Fit to the Measurement of the Density
- Table 4.1 The Maximum Values of Various Measured Quantities
- Table 4.2 The Magnitude of Various Terms in the Momentum Equation
- Table 4.3 The Modeling of Potential, Experimental Errors
- Table 5.1 An Empirical Fit to the Measurements of Overall Viscosity
- Table 5.2 The Mean, Overall Viscosity
- Table 5.3 An Estimate of the Time Rate of Change of Viscosity
- Table 6.1 An Estimate of the Viscosity of the Liquid Based on the Correlation by Lockhart and Martinelli
- Table 6.2 An Estimate of the Viscosity of the Liquid Based on the Correlation by Happel
- Table 6.3 An Estimate of the Viscosity of the Liquid Based on the Correlation by Husain
- Table 6.4 A Summary of the Estimates of the Viscosity of the Liquid
- Table 7.1 Estimate of the Mass Fraction of Gas in the Reservoir at 410°C.
- Table 7.2 Estimate of the Mass Fraction of Gas in the Reservoir at 450°C.
- Table 7.3 The Mass Fraction of Gas Not in Solution
- Table 7.4 An Estimate of the Viscosity of the Liquid
- Table 8.1 Summary of the Viscosity Measurements

TABLE OF CONTENTS

	Page
ACKNOWLEDGMENTS	ii
ABSTRACT	iii
LIST OF SYMBOLS	v
LIST OF FIGURE CAPTIONS	x
LIST OF TABLE HEADINGS	xii
TABLE OF CONTENTS	xiii
CHAPTER 1:	1
1.1 Introduction	1
1.2 Overview	1
1.3 History of the Measurement of the Fluidity of Coal	2
1.4 History of the Experimental Apparatus	4
1.5 Goals	5
1.6 Assumptions	6
CHAPTER 2:	8
2.1 Introduction	8
2.2 Overview	8
2.3 Coal Characterization	9
2.4 Starting Procedure	13
2.5 Pressure System	13
2.6 Piston-Head System	14
2.7 Viscometer-Block System	15
2.8 Thermal System	15
2.9 Density Calibration	15

2.10	Viscosity Calibration	16
CHAPTER 3:		19
3.1	Introduction	19
3.2	The Need for Density Measurements	19
3.3	Heat Transfer	19
3.4	Density Measurements	22
3.5	Volume Fraction of Gas	32
3.6	Conclusion	34
CHAPTER 4:		37
4.1	Introduction	37
4.2	Macroscopic Continuity Equation	37
4.3	Macroscopic Momentum Equation	41
4.4	Rate of Strain	47
4.5	Error Estimation	51
4.6	Conclusion	57
CHAPTER 5:		58
5.1	Introduction	58
5.2	Rheological Equations	58
5.3	Data	59
5.4	Behavior of the Overall, Apparent Viscosity	71
5.5	The Rate of the Reduction of Viscosity	71
5.6	Conclusion	74
CHAPTER 6:		76
6.1	Introduction	76
6.2	The Two-Component, Two-Phase Model	76

6.3	Flow Regime Determination	77
6.4	Equations of Motion	78
6.5	Liquid-Gas Correlations	80
6.6	Conclusion	91
CHAPTER 7:		93
7.1	Introduction	93
7.2	The Two-Component, Two-Phase Model	93
7.3	Density Model	94
7.4	Viscosity Model	98
7.5	Conclusion	107
CHAPTER 8:		
8.1	Summary and Results	108
8.2	Conclusions	114
LIST OF REFERENCES		120
APPENDIX A: DENSITY DATA		125
APPENDIX B: VISCOSITY DATA		138
APPENDIX C: GIESELER PLASTOMETER DATA		146

## Chapter 1

### 1.1 Introduction

This chapter begins by providing a brief overview of the experimental procedure. A history of the measurement of the fluidity of coal is provided from two points of view: the general literature and the apparatus. The goals of the present research are stated, and the assumptions used are presented in chronological order.

### 1.2 Overview

Industrial interest in coal research varies inversely with the perceived supply of other hydrocarbon sources, principally oil. In countries with very large, proved reserves, coal is the first source to be considered in times of scarcity and the last to actually be used. The problems associated with large scale use of coal are plentiful. The field of coal research, therefore, is wide open. Gorbaty et. al.<sup>1</sup> discussed at length the many and varied opportunities in coal research. In addition, they stated that:

*"More fundamental knowledge of coal (knowledge of its structure and its behavior during coal conversion processes) is essential before we can generate new technologies necessary for the efficient use of coal in the future."*

In order to understand better the behavior of bituminous coals upon rapid heating, a new experimental technique has been developed and applied. With this technique, a

small sample of coal is rapidly heated from room temperature to 410 °C to 450 °C. Once isothermal conditions have been approximated, the experiment continues in a manner similar to measurements with a capillary viscometer or rheometer. A pressure gradient is applied by piston, and the velocity of the piston is determined by a measurement of the position of the piston versus time. The directly measured variables are, therefore, temperature, pressure, radius of the capillary, position of the piston, and time. Of course, rapidly heated coal is a very heterogeneous, multi-phase substance which undergoes many chemical changes. Although the equipment resembles many conventional capillary rheometers, the analytical procedure is much more complex.

### **1.3 History of the Measurement of the Fluidity of Coal.**

The fluidity of rapidly heated, bituminous coals has been studied for the last fifty years with one principal instrument, the Gieseler plastometer. This instrument was developed by Gieseler<sup>2</sup> in 1934, and with some minor modifications it is now an ASTM standard procedure<sup>3</sup>. Lloyd<sup>4</sup> described the instrument's use with coal as follows:

*"This method measures the resistance of a mass of well-packed, pulverized coal to the rotation of a rabble-arm stirrer which is driven through a constant-torque clutch."*

The principle is that the speed of rotation should be some function of the viscosity of the sample. Two criticisms are immediately apparent. One is that the measurement is only qualitative. Any attempt to make a quantitative measurement of viscosity based on this extremely complicated flow would be hazardous at best. Second, there is a free surface between the coal and the environment through which products of devolatilization will pass. No attempt was made to contain these gaseous products.

The temperature history of the coal sample is crucial to understanding and modeling the behavior of the coal during rapid heating. Of particular interest are the

'isothermal' measurements made by Fitzgerald<sup>5</sup>, van Krevelen<sup>6</sup>, and Lloyd<sup>7,8</sup>. Based on these isothermal measurements and the resultant fluidity curves, a large body of literature has attempted to explain and model the fluidity data. Though these models match the fluidity data well, the models can not be considered any better than the data upon which they were built.

Lloyd's<sup>7,8</sup> measurements on the Gieseler plastometer are of particular interest since he measured a Pitt 8 coal from the same batch that was used in these experiments. Lloyd found that the time of maximum fluidity occurred approximately twenty minutes into the run, and the estimated two to three minutes to achieve the isothermal conditions were not significant when compared to the fluidity time-scale of twenty minutes. The data of van Krevelan, Huntjens and Dormans<sup>9</sup> showed a very similar time scale of fluidity with the maximum fluidity again occurring at ten to twenty minutes. In all of these measurements, the maximum fluidity was followed by a decrease in fluidity due to coking. Because the coking of bituminous coals is of vital importance to the metallurgical industries, the time scale for coking may be independently confirmed by various instruments. Davis<sup>10</sup> provided a good review of the coking process and its dependency on temperature and heating rate. It would appear reasonable, therefore, to attribute the reduction in fluidity at the ten to thirty-minute time-scale to be due to coking. The time-scale to maximum fluidity of ten to twenty minutes, however, could not be verified with the present experiment and may be an artifact of the Gieseler plastometer.

Of course, the data acquired from the Gieseler plastometer have been used for physical and chemical modeling since its inception. Almost immediately, two different interpretations of the increase in fluidity were enunciated. Audibert<sup>11</sup> was the first to suggest, even before the use of a plastometer, that the coal was melting. Waters<sup>12</sup> showed that the increase in fluidity measured by a Gieseler plastometer was reversible, thereby suggesting some sort of melting process. Fitzgerald<sup>5</sup> thought the increase in

fluidity was due to a intermediary product called a "metaplast". Van Krevelen and Chermin<sup>13</sup> and Lloyd<sup>7</sup> built upon this chemical-change model. Lloyd<sup>8</sup> even combined the two processes of melting and "metaplast" to explain the plastometry data.

Even if the isothermal data from the Giesler plastometer were accepted as valid, use of the fluidity values in modeling has at least one serious flaw. All of the models assumed that the concentration of either the "metaplast" or the melted fraction was proportional to the fluidity values. The actual flow, however, contained significant volume fractions of gas and perhaps solids. The relationship, therefore, between a metaplast or meltable fraction and fluidity is complex and unknown.

#### **1.4 History of the Experimental Apparatus**

The first application of capillary-rheometer techniques to coal in its plastic state was described by England and Ryason<sup>14</sup> as part of the coal-pump project at JPL. Their experimental work was intended to support the application and development of extrusion technology for the introduction of coal into high-pressure reaction vessels. The rheometer used by England and Ryason had a capillary diameter of 0.15 centimeter and an approximate heat-up time of seven minutes. A constant-force compression cage was used to apply a pressure gradient across the capillary. The instrument was used principally to determine the temperature at which extrusion would begin.

Further work in support of the coal-pump project was conducted by Feinstein<sup>15</sup> with a rheometer which had a capillary diameter of 0.053 centimeter and an approximate heat-up time of ninety seconds. The piston for this experiment was driven at a constant velocity which was found to complicate greatly the rheological equations. A modified form of this equipment was developed by Feinstein<sup>16</sup>. It applied a constant force to the piston head by means of a hydraulic cylinder. The capillary tube and the heat-up rates remained the same. This capillary rheometer, designed by Feinstein, was essentially the same instrument used in this investigation. It is discussed in more

detail in Chapter 2.

In addition to the rheometer, JPL also supplied the coal used in this investigation. Analysis of this coal was subcontracted to W. Lloyd at the University of Kentucky, and the results of his analysis are given in Chapter 2.

### 1.5 Goals

The principal goal of this research was to provide a technique of experimentation and analysis that would allow a more quantitative examination of the rheology of bituminous coals in their plastic state. Included within this objective was determination of the principal phases present and their effect upon the measurements. Ideally, the analysis of the experimental data would allow an estimate of the viscosity of the liquid phase of the coal. The information so gathered is important for process design, especially in the scaling of equipment.

In order to establish the viscosity of the liquified coal, the flow regime of this multi-component, multi-phase fluid had to be estimated. Then the effect of the non-continuous phase or phases had to be estimated so that the viscosity of the continuous phase could be determined. In the particular case of the Pitt 8 coal, the viscosity of the continuous phase was estimated from the overall, apparent viscosity and the volume fraction of gas. A model that estimated the mass fraction of gas based on the temperature and time was developed in order to estimate better the viscosity of the continuous phase.

A nother goal was a closer look than previously available at the transition of coal into its plastic state. This information would apply directly to the understanding of chemical change and melting models and might even allow an estimate of the molecular weight of the continuous phase.

## 1.6 Assumptions

Because of the complexity in characterizing coal that is being rapidly heated, many assumptions were necessary. Great efforts were made to minimize the number and extent of these assumptions. These assumptions were developed in the analysis and are discussed below in the order in which they were applied.

In Chapter 2, the principal assumption made and used for the remainder of this work was that all the coal samples were similar. This assignment was difficult because the variability of coal even within the same seam is often significant. In addition, it was assumed that the calibration runs for density and viscosity made at temperatures less than 60 °C demonstrated significant accuracy for the high temperatures encountered during measurements of the coal.

In Chapter 3, the assumption of thermal equilibrium after ninety seconds was based on a conservative analysis of heat transfer. Also, the volume fraction of gas was estimated using one further assumption. The maximum density displayed by the coal was assumed to be a good estimate of the density of the solid and liquid phases. It should be noted, however, that the assumption used to estimate the volume fraction of gas did not enter into the measurement of the overall, apparent viscosity.

In Chapter 4, the continuity and momentum equations were developed in macroscopic form with a minimum of assumptions. The principal assumption was that the density in the capillary tube was not a function of angular or radial coordinates. The neglect of the angular coordinate is common in this geometry, but the assumption that the density was not a function of the radius was obviously wrong and implied an overall measurement. This assumption is discussed in more detail at the beginning of Chapter 4. Because of the presence of significant volumes of gas and a large pressure drop, the density was treated as a function of axial position.

In Chapter 6, a two-component, two-phase fluid was assumed in order to apply the correlations developed in the literature. In addition, the flow regime was assumed to be frothy, based on various flow-regime analyses found in the literature.

In Chapter 7, the density was modeled on the assumption of an incompressible liquid and an ideal gas. Detailed assumptions on solubility and equilibrium were also made in this chapter, and the effects of surface tension between the phases was neglected. In addition, the development of a mean viscosity of the liquid assumed that the viscosity of the gaseous products could be assumed to be the viscosity of methane.

## Chapter 2

### 2.1 Introduction

This chapter begins with an overview of the experimental equipment, including a discussion for the design objectives and a grouping of the equipment by function. The variables that are actually measured are discussed in light of the overall system. The calibration of measurement modes for both density and viscosity is described. Finally, the performance of the system is discussed relative to design objectives and further improvements.

### 2.2 Overview

The measurement of the viscosity of a multicomponent, heterogenous, chemically-reacting material is a difficult engineering challenge. When this material is coal, the additional problems of coal variability, even within the same seam, aging, and preparation are encountered. Surprisingly, the final form of the equipment is a straightforward application of the technology of capillary rheometry. The equipment was originally designed by Sam Feinstein of JPL. His major design objectives were stated as

15

1. retention of all decomposition products

2. rapid and reproducible heating
3. uniform and isothermal conditions after heating
4. measurement of bulk density under viscosity conditions for viscosity
5. constant monitoring of temperature within the viscometer block.

The final configuration of the equipment is shown schematically in Figure 2.1. The equipment is divided into five functional systems: control of pressure, temperature, movement of piston head, operation of viscometer block, and introduction of coal sample. Mechanically, the system is similar to a capillary rheometer with a constant pressure-drop. Thermally, the system has the ability to maintain a constant high temperature, and the viscometer block provides a large thermal inertia for rapid heat-up and accurate control of temperature. Additionally, all components in contact with the coal have high conductivity to ensure rapid heat transfer. The system is discussed by functional groups in greater detail below.

Measurements of bulk density were made with the same equipment by replacing the hollow capillary tube with a solid rod of the same outer diameter. In this way, bulk density measurements were made under essentially the same conditions encountered during a viscosity measurement.

### **2.3 Coal Characterization**

Most of the measured variables were independent of time. The variables were temperature, pressure drop (or pressure for density measurements), sample mass, and type and preparation of coal. In this work, the coal used was a large sample of Pittsburgh Number 8 seam coal, referred to as Pitt 8, from West Virginia. The coal was dried and tumbled in an environment of nitrogen and then ground to -80 mesh. (Tyler sieve size.) Proximate and ultimate analyses of a portion of this sample were performed by Dr. Lloyd and are given in Table 2.1.<sup>17</sup>

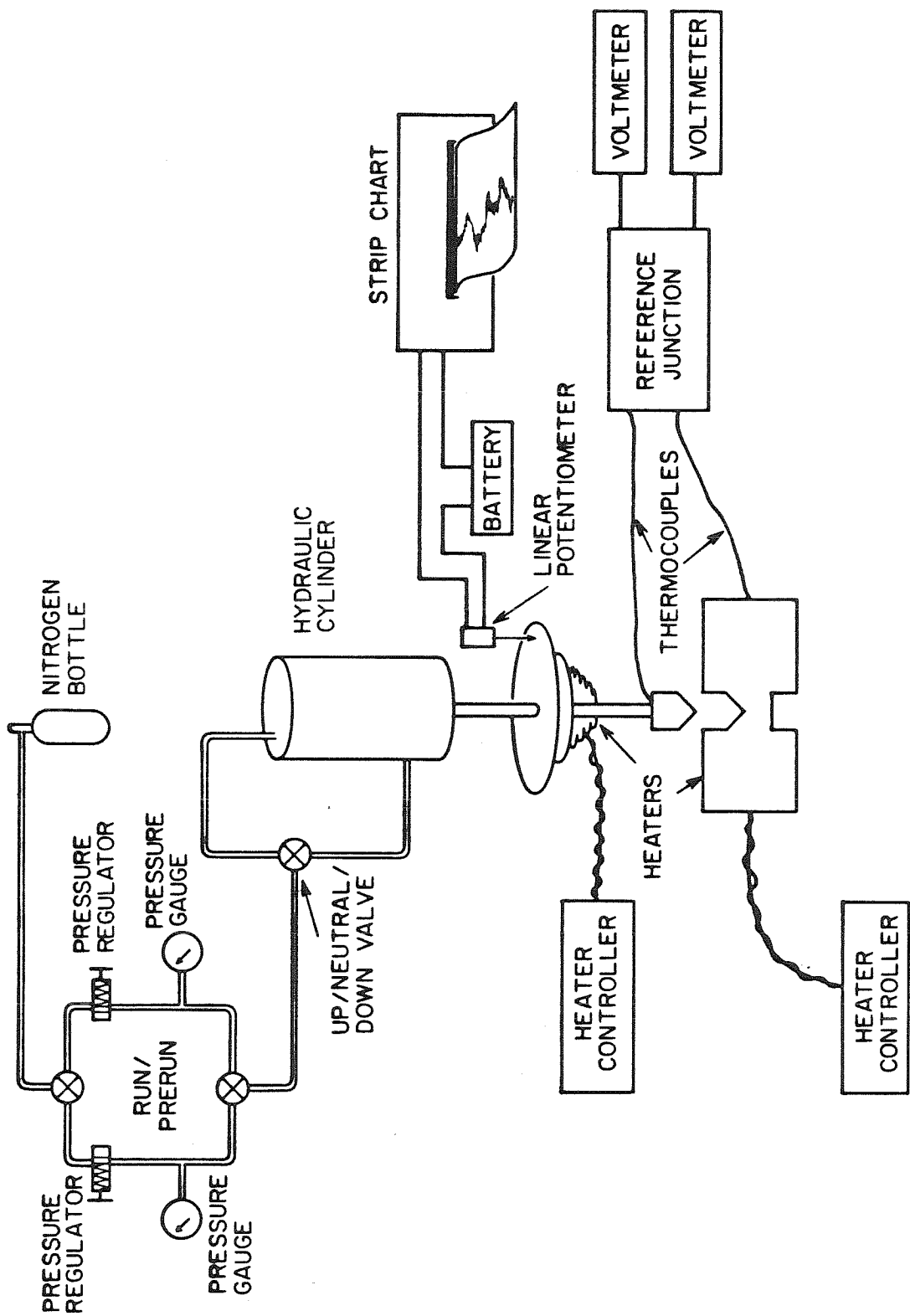


Figure 2.1. Schematic Diagram of the Experimental Equipment

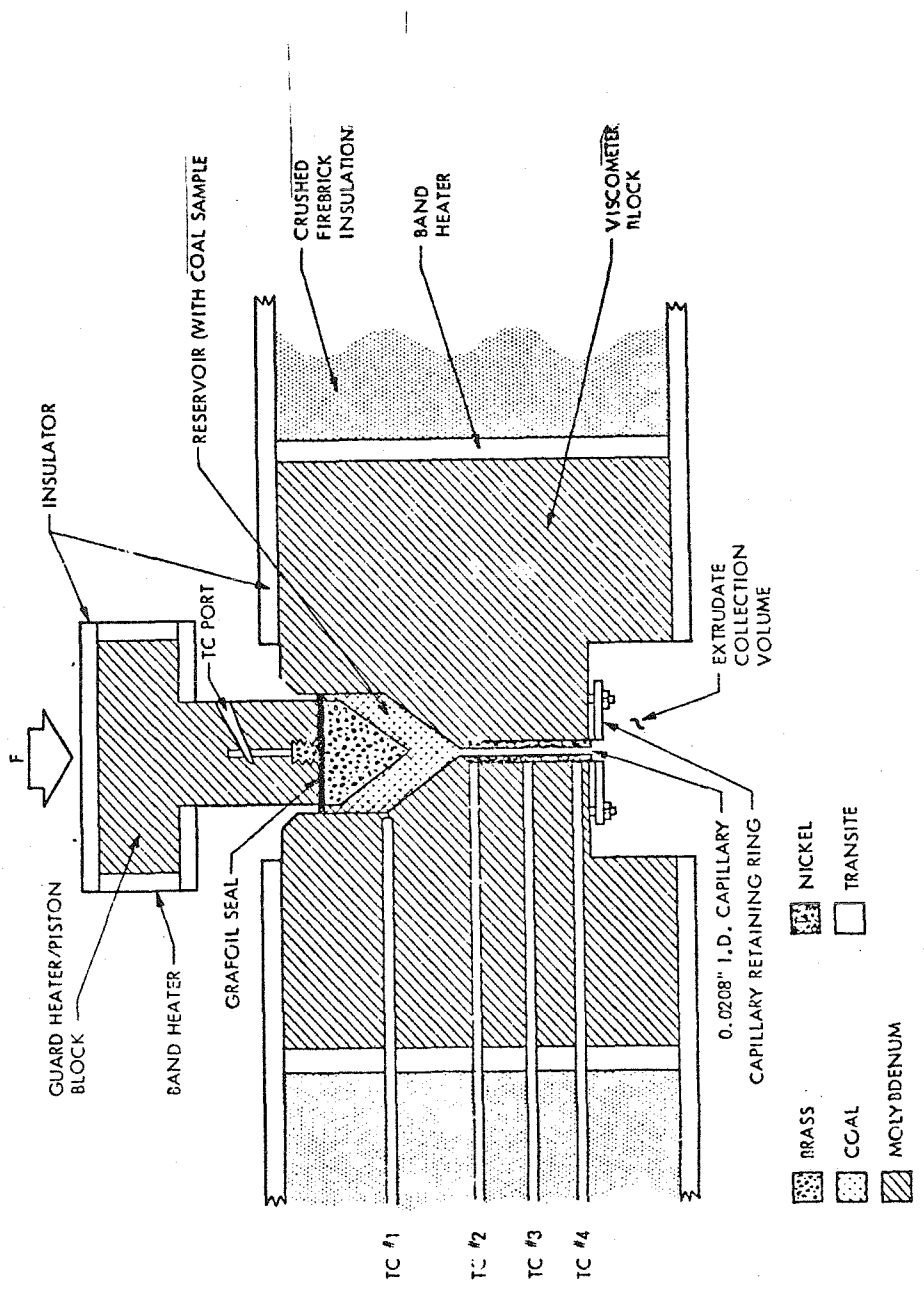


Figure 2.2. A detailed diagram of the piston head and viscometer block.  
( from Feinstein 15 )

Table 2.1 Characterization of the Pitt 8 Coal <sup>17</sup>	
Proximate	
Property	Percentage by M ass
Moisture	0.25
Ash	8.08
Volatile M atter	39.61
Fixed Carbon	52.06

Ultimate	
Property	Percentage by M ass
Carbon	77.17
Hydrogen	5.16
Nitrogen	0.97
Sulfur	2.36
Oxygen ( by difference )	6.26

## 2.4 Starting Procedure

The time-dependent variable was the position of the piston head which established the volume occupied by the coal and its decomposition products. The overall viscosity of the heated coal was computed from the data taken during a viscosity run. Density data that were taken under the same conditions were also used to compute the overall viscosity. The computation is discussed in detail in Chapter 4. Further analysis was needed to include the effects of the multiphase nature of the heated coal. This analysis is described in detail in Chapter 6.

Because of the strong dependence on time of the density and viscosity of heated coal in the apparatus, it is important to understand how time was measured. Upon insertion of the room-temperature coal into the high-temperature viscometer block, the time was recorded with an initial value of zero. The piston head was then inserted into the viscometer block. For the runs at 450 °C, a nominal pressure of 50 psi was applied during the warm-up period. For the runs at 410 °C, the run pressure was applied immediately. It appeared necessary to reduce the pressure during heat-up for the higher temperature runs to insure an adequate supply of coal in the reservoir for the viscosity measurement. After 80 seconds, thermal equilibrium was assumed, and the run pressure was applied for the 450 °C runs. The data reported elsewhere in this report were based upon this procedure.

## 2.5 Pressure System

The pressure for the rheometer was supplied by high-density nitrogen from a pressurized tank connected to a hydraulic cylinder whose piston was mechanically connected to the piston-head system. A pressure gauge provided a measurement of the pressure in the hydraulic cylinder. The reading of the pressure gauge was referred to as the nominal pressure for all subsequent measurements. This measurement was converted to the force provided by the piston in order to determine the absolute pres-

sure in the reservoir of the viscometer-block system. The radius of the hydraulic cylinder was 3.2 centimeters, and the force transmitted to the piston head was given by:

$$F_p = \pi 3.2^2 \times (P_g + 14.7) \times C_{E-CGS} \text{ dynes} \quad (2.1)$$

where  $F_p$  is the force,  $P_g$  is the pressure gauge reading, and  $C_{E-CGS}$  converted the pressure reading to the cgs system. Two pressure regulators were arranged in parallel and were selected by a switch. This arrangement allowed two different pressures to be available for the schedule of heating described in the start-up section of this chapter.

## 2.6 Piston-Head System

The piston-head system accepted the force generated by the hydraulic cylinder and transmitted this force through a molybdenum rod to the reservoir in the viscometer-block system. There was an electric heater which elevated the piston head to the run temperature. Also connected to the electric heater were a controller and two thermocouples. Figure 2.2 shows the details of the piston head and seal. The seal was cloth of woven carbon fiber and had a thickness of 0.030 in. The material was manufactured by Durametallic Corporation of Kalamazoo, Michigan and is called Grafoil. This Grafoil seal was able to withstand the high temperatures and still retain the products of decomposition. Its sliding friction against the reservoir wall was negligible. The piston head itself was made of brass to improve heat transfer. The conical shape of the piston head also improved heat transfer by increasing the surface area. A linear potentiometer was connected to the piston-head system to provide a voltage that was directly proportional to the vertical position of the piston head. This voltage was recorded on a strip-chart and provided the volume occupied by the coal in the reservoir. The force provided by the hydraulic cylinder produced a pressure in the reservoir based on the area of the piston head normal to the applied force:

$$P_r = \frac{F_p}{\pi R_o^2} \frac{\text{dynes}}{\text{cm}^2} \quad (2.2)$$

where  $P_r$  is the pressure in the reservoir, and  $R_o$  is the radius of the reservoir.

### 2.7 Viscometer-Block System

The viscometer system consisted of the reservoir, capillary tube, and thermocouples surrounded by an electric heater and insulation. The viscometer block was made of molybdenum to facilitate heat transfer. Figure 2.3 shows the system in greater detail, and includes the placement of the two thermocouples. The disposable capillary tube was made of a nickel alloy and had an interior diameter of 0.026 centimeter, a length of 2.7 centimeters, and a length-to-diameter ratio of 51. An estimate of the expansion of both the radius and the length of the capillary tube due to temperature change was based on the thermal expansion coefficient<sup>18</sup> and was found to be not significant for either measurement. The reservoir was tapered to match the shape of the piston head. This shape also reduced the effect of any entrance losses due to constricting flow.

### 2.8 Thermal System

The temperature of the viscometer was controlled by an electric heater with variable power. Thermocouple number 2 in Figure 2.3 provided the feedback for temperature control. The temperature of the piston head and rod was controlled by an on/off, electric heater. Thermocouple number 1 in Figure 2.2 gave feedback for control. Thermocouple number 2 in Figure 2.2 and number 1 in Figure 2.3 provided independent measures, respectively, of the temperature of the head and viscometer block.

### 2.9 Density Calibration

The density of ordinary tap water at 23 °C was measured by a modification of the capillary rheometer. A solid rod replaced the capillary, and the piston-head-position

measurement provided the volume occupied by a sample of water. The mass of the water was also measured, and the density was calculated. Ten independent samples were measured, and the resulting mean density was  $0.993 \text{ gm/cm}^3$  with a standard deviation of  $0.0267 \text{ gm/cm}^3$ . The published value<sup>19</sup> of the density of water at  $23^\circ \text{C}$  is  $0.997538 \text{ gm/cm}^3$ . The results indicated that operation of the equipment and analysis for density were sufficiently accurate.

## 2.10 Viscosity Calibration

Figure 2.4 presents the results of the calibrations of the capillary viscometer. In addition, the four points measured by the manufacturer of a calibration standard provided by Canon Instruments<sup>44</sup> are plotted.

The experimental results and the manufacturer's data were compared by independently fitting the function of the form

$$\mu = \mu_0 e^{k(T-T_0)} \quad (2.3)$$

where  $\mu$  and  $\mu_0$  are viscosities,  $k$  is a constant, and  $T$  and  $T_0$  are temperatures, to each group of data. A representative point,  $\mu_0$  and  $T_0$ , was chosen, and the constant  $k$  was chosen to produce the minimum least-squares error. The Arrhenius equation<sup>20</sup> might have been more appropriate, but the manufacturer provided information on the change of viscosity with temperature, and this information appeared to be worth using. The constant,  $k$ , represents a fractional rate of change of viscosity. This result may easily be seen by differentiating Equation 2.3 to produce

$$\frac{\frac{d\mu}{\mu}}{\frac{dT}{T_0}} = k \quad (2.4)$$

The manufacturer reported that  $k$  ranged from  $-0.096$  at  $20^\circ \text{C}$  to  $-0.074$  at  $40^\circ \text{C}$ . The constant that produced the minimum least-squares error for the manufacturer's data was found to be equal to  $-0.084$ . The standard deviation for the manufacturer's

fit for viscosity in Equation 2.2 was 0.499 poise. The approximation is plotted in Figure 2.4 and labeled as Equation 2.5.

When Equation 2.3 was applied to the experimental results,  $k$  was found to be -0.1085. The standard deviation of the viscosity for this approximation was 0.385 poise. This function is also plotted in Figure 2.4 and labeled as Equation 2.6.

To summarize, the manufacturer's data were fitted to the function

$$\mu = \mu_0 e^{-0.084(T - T_0)} \quad (2.5)$$

with  $\mu_0 = 17.48$  poise and  $T_0 = 35.0^\circ C$ . The experimental data were fitted to the function

$$\mu = \mu_0 e^{-0.1085(T - T_0)} \quad (2.6)$$

with  $\mu_0 = 17.20$  poise and  $T_0 = 35.0^\circ C$ .

Figure 2.4 indicates that the measurements of the viscosity and temperature by means of the capillary-rheometer system were reasonably accurate. The apparent differences in the values for  $k$  are probably related to two factors. First, the least-squares fit was based on an arbitrary point,  $\mu_0$ ,  $T_0$ , which was not varied to reduce the error. Also, the fit for the experimental data was weighted toward the lower temperatures because there were more measurements per temperature at the lower end. Second, Equation 2.3 is not the best empirical function for the correlation of viscosity and temperature. Although it might be possible to refine further the analysis of the data in order to provide a closer fit, the results of the calibration trials show a sufficient accuracy relative to the expected performance of the equipment and to the total error in the experiment.

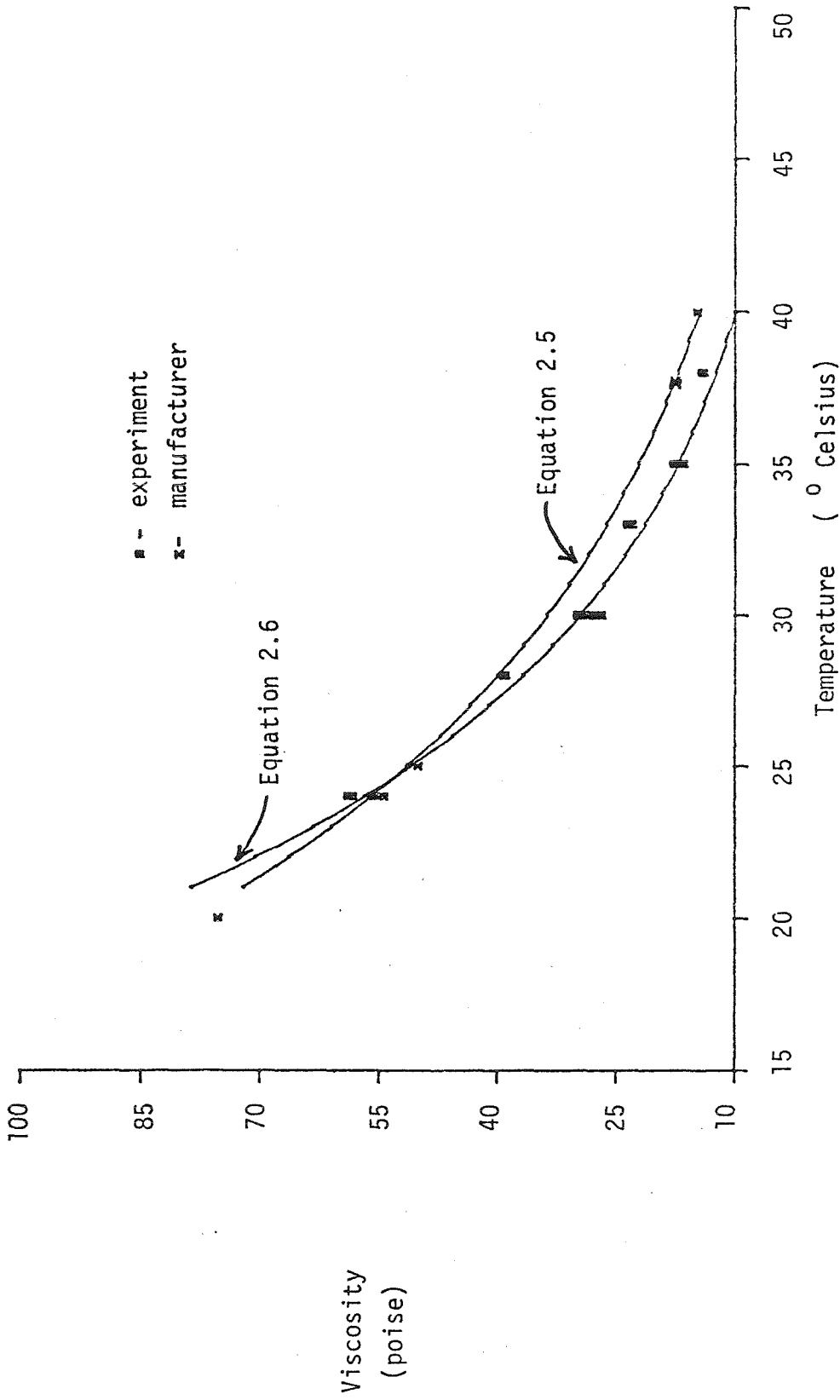


Figure 2.4. The viscosity of a calibration standard<sup>44</sup> versus temperature.

## **Chapter 3**

### **3.1 Introduction**

This chapter discusses the measurement of the density of coal in the modified rheometer. The usefulness of independent measurements of density is outlined. The temperature history of the coal sample is estimated, and actual density measurements are presented and correlated. Behavior of the coal upon rapid heating is discussed, and volume fractions of gas are deduced. Results of the density measurements are summarized.

### **3.2 The Need for Density Measurements**

The density of the coal upon rapid heating is a strong function of the type of coal, temperature, reservoir pressure, and time. Measurement of the density under run-conditions allowed a direct application of the momentum equation to determine the viscosity. In addition, measurement of the density allowed observation of the behavior of the coal under much simpler conditions than those that prevailed during measurement of the viscosities. Thus questions concerning degasification rates and modeling were more easily addressed.

### **3.3 Heat Transfer**

One of the advantages of the experimental equipment was the ability to heat the sample rapidly. Its thermal history in the reservoir was estimated using a simplified, two-dimensional analysis. Assumptions necessary for this analysis are reviewed.

The geometry of the sample of coal within the reservoir was a cylinder with conic end sections, convex at the top, and concave at the bottom. Neglect of the conic end sections reduced the surface area available for heat transfer without changing the total volume. This procedure gave a conservative estimate of the rate of temperature rise, i.e., a longer time to reach thermal equilibrium. Further, by considering the cylinder to be of infinite length, a two-dimensional analysis was used so that the governing energy equation was again conservatively estimated.

Another simplification assumed no dependence of temperature on the angular coordinate. This assumption is common for the symmetrical geometry under consideration. Initially, the density, heat capacity, and thermal conductivity were treated as constant even though they would most certainly be functions of both position and time. A heat-transfer analysis based on a two-dimensional slab was also developed. This analysis estimated more accurately both the areas available for heat transfer and the maximum distance from a boundary.

The two-dimensional energy equation in cylindrical coordinates with no heat sources, no angular dependencies, and constant coefficients is given as

$$\frac{1}{r} \frac{\partial}{\partial r} \left( r \frac{\partial T}{\partial r} \right) = \frac{1}{\kappa} \frac{\partial T}{\partial t} \quad (3.1)$$

where  $r$  is the radial coordinate,  $t$  is the time,  $\kappa$  is the thermal diffusivity of coal, and  $T$  is the temperature. Assume a product solution of the form:

$$T(r,t) = R(r)\Theta(t) \quad (3.2)$$

where  $R$  is a function of radius only, and  $\Theta$  is a function of time only. Equation 3.1 separates to

$$\frac{1}{R(r)r} \frac{\partial}{\partial r} \left( r \frac{\partial R(r)}{\partial r} \right) = \gamma = \frac{1}{\kappa \Theta(t)} \frac{\partial \Theta(t)}{\partial t} \quad (3.3)$$

where  $\gamma$  is the separation constant. The solution of the temporal equation is exponential, and the solution of the radial equation yields Bessel functions. Based on Carslaw and Jaeger<sup>21</sup>, the solution to Equation 3.1 is available with the following boundary conditions:

$$T = 25^\circ C \quad \text{for } t < 0, R_0 \geq r \geq 0 \quad (3.4)$$

$$T = T_0 \quad \text{for } t \geq 0, r = R_0 \quad (3.5)$$

where  $R_0$  is the radius of the coal sample, and  $T_0$  is the temperature applied at the boundary. The thermal diffusivity of coal was estimated from Van Krevelen and Schuyer<sup>22</sup> as  $2.5 \times 10^{-3} \frac{cm^2}{sec \ ^\circ C}$ . Based on this value, Equation 3.1, and the boundary conditions, the temperature at the centerline after ninety seconds was estimated as sixty percent of the applied temperature.

An estimate of the temperature history of the coal sample that would more closely reflect both the areas available for heat transfer and the maximum distance to a boundary would be based on the two-dimensional, semi-infinite slab. The area available for heat transfer would be conservatively estimated by assuming the depth of the sample to be the thickness of the slab. Since the depth of the sample was a time-dependent variable, a conservative value based on a corresponding density of the sample of  $0.75 \text{ gm/cm}^3$  was used. With the same estimate of the thermal diffusivity as before, the temperature at the center of the sample after forty seconds was within ten percent of the temperature applied at the boundary.

A number of important physical parameters have been simplified to make the estimate of the temperature history tractable. The diffusivity of the coal was assumed constant when, in fact, it would be a function of temperature. Increasing temperature would increase the heat capacity and thereby reduce the diffusivity of the coal. Based

on the available data<sup>22</sup>, the change in diffusivity would not significantly alter the estimates of the temperature history. Any endothermic or exothermic reactions, while likely, were neglected because the small quantity of coal could not store or release enough energy to significantly affect the estimates of the temperature history. The change in overall diffusivity due to the presence of gaseous products was also neglected because isothermal conditions were achieved before a significant volume of gas had been produced. It would appear likely, based on these estimates of the temperature history, that the assumption of isothermal conditions after ninety seconds is justified.

### 3.4 Density Measurements

Figures 3.1 through 3.8 display the density versus time of a Pitt 8 coal at 410 °C and nominal pressures of 75, 100, 150, and 200 psig respectively. The solid lines in these figures represent the best least-squares approximation based on the general equation

$$\rho_r(t) = a + be^{-k(t-t_0)} \quad (3.6)$$

where  $\rho_r$  is the density in the reservoir,  $t$  is time, and  $a$ ,  $b$ ,  $k$ , and  $t_0$  are the constants to be established. Table 3.1 shows the values of these constants for each pressure and temperature and the standard deviation arising from each fit. This exponential fit was chosen for convenience and did not imply any physical interpretation. These measurements gave density as a function of time, temperature, and pressure with a maximum standard deviation of 3 percent of the minimum value of the density. Greater accuracy was prevented by a systematic error in the experimental procedure and efforts to eliminate this error were unsuccessful.

Coal in the reservoir could be inspected by opening the piston and aborting a density run after 90 seconds. The appearance of the coal in the reservoir was as might be expected. Reduction of the pressure in the reservoir to atmospheric caused gas

pockets of various sizes to form throughout the coal. The coal was sticky and fluid, giving the appearance of a froth. This visual evidence reinforced the assumption that the coal behaved as a viscous fluid, not as a solid. The apparent fluidity of a rapidly heated coal is more of a liquid-gas than a gas-solid flow.

Table 3.1 An Empirical Fit to the Measurements of the Density						
Temperature	Pressure	a *	b *	k *	t <sub>0</sub> *	Standard Deviation
(°Celsius)	(psig nominal)	(gm/cm <sup>3</sup> )	(gm/cm <sup>3</sup> )	(1/second)	(second)	(gm/cm <sup>3</sup> )
410	200	0.86	0.47	0.0038	90	0.0045
410	150	0.60	0.56	0.0017	90	0.0058
410	100	0.48	0.51	0.0017	90	0.0060
410	75	0.51	0.39	0.0042	90	0.0054
450	125	0.33	0.64	0.0053	90	0.0055
450	100	0.30	0.41	0.0054	90	0.0059
450	75	0.36	0.26	0.0081	90	0.0057
450	50	0.31	0.23	0.0204	90	0.0090

\* constants fit to Equation 3.6,  $\rho_r(t) = a + be^{-k(t-t_0)}$ .

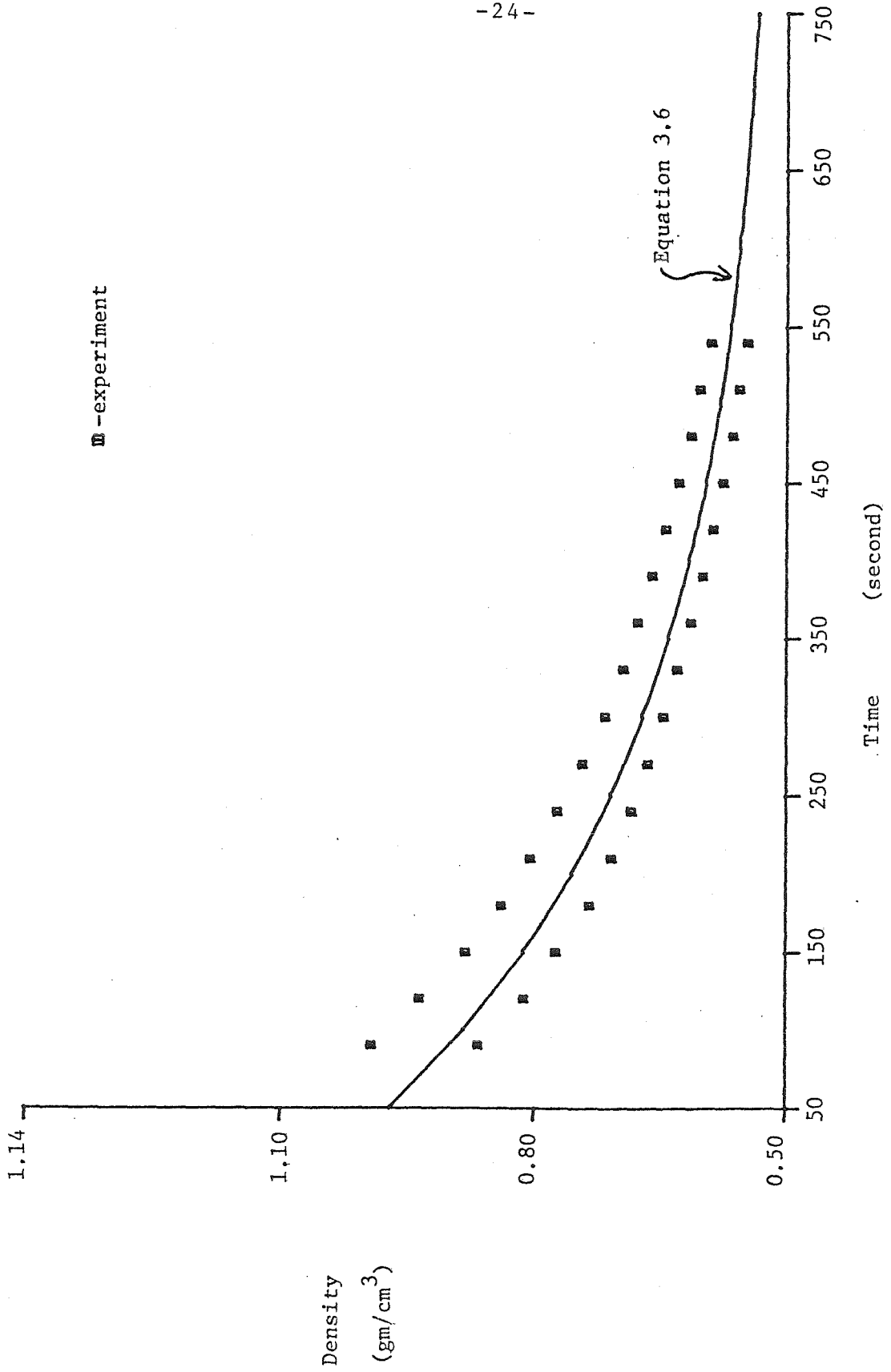


Figure 3.1. The density of a Pitt 8 coal at 410 °C and a nominal pressure of 75 psi.

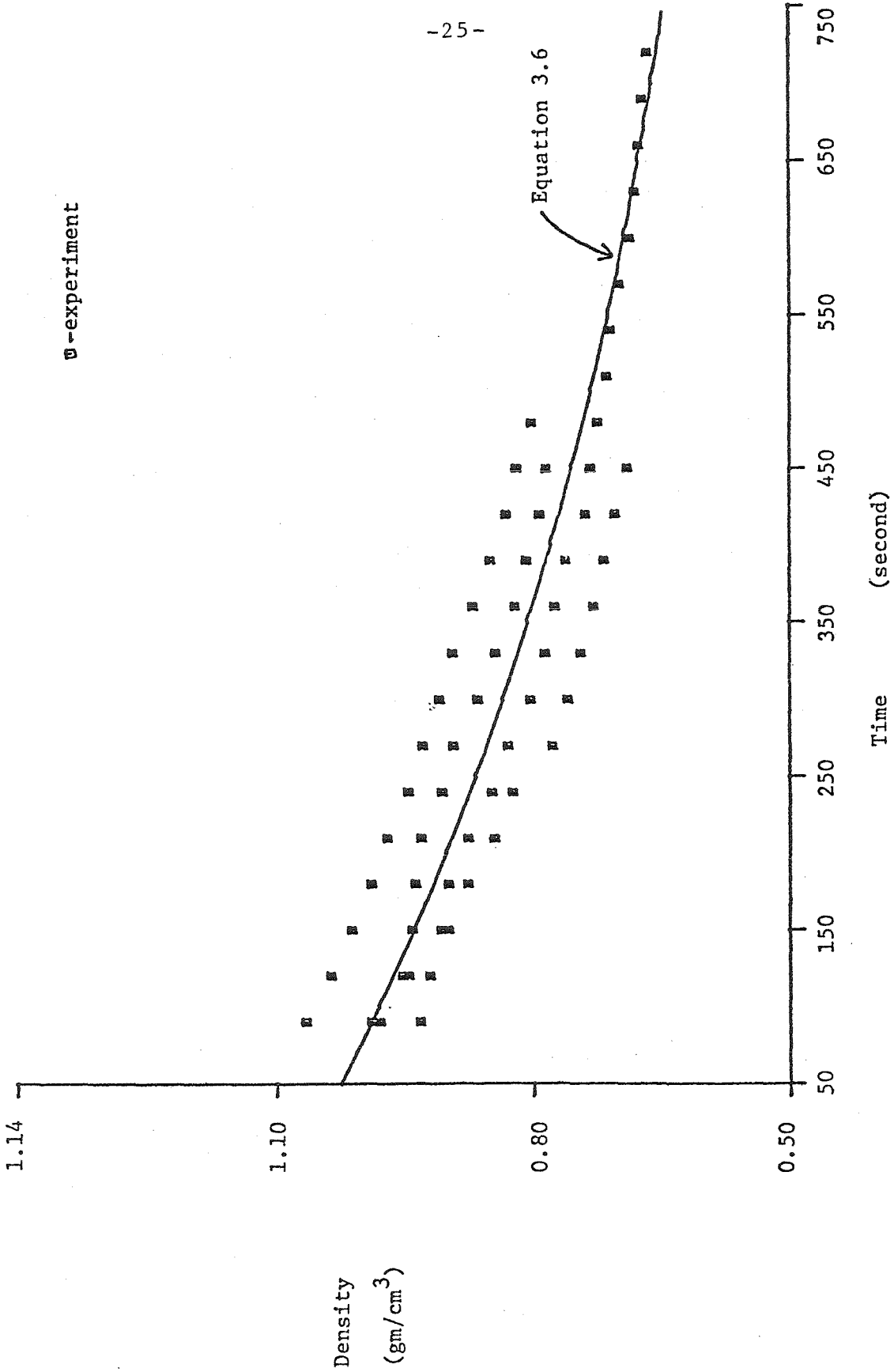


Figure 3.2. The density of a Pitt 8 coal at 410 °C and a nominal pressure of 100 psi.

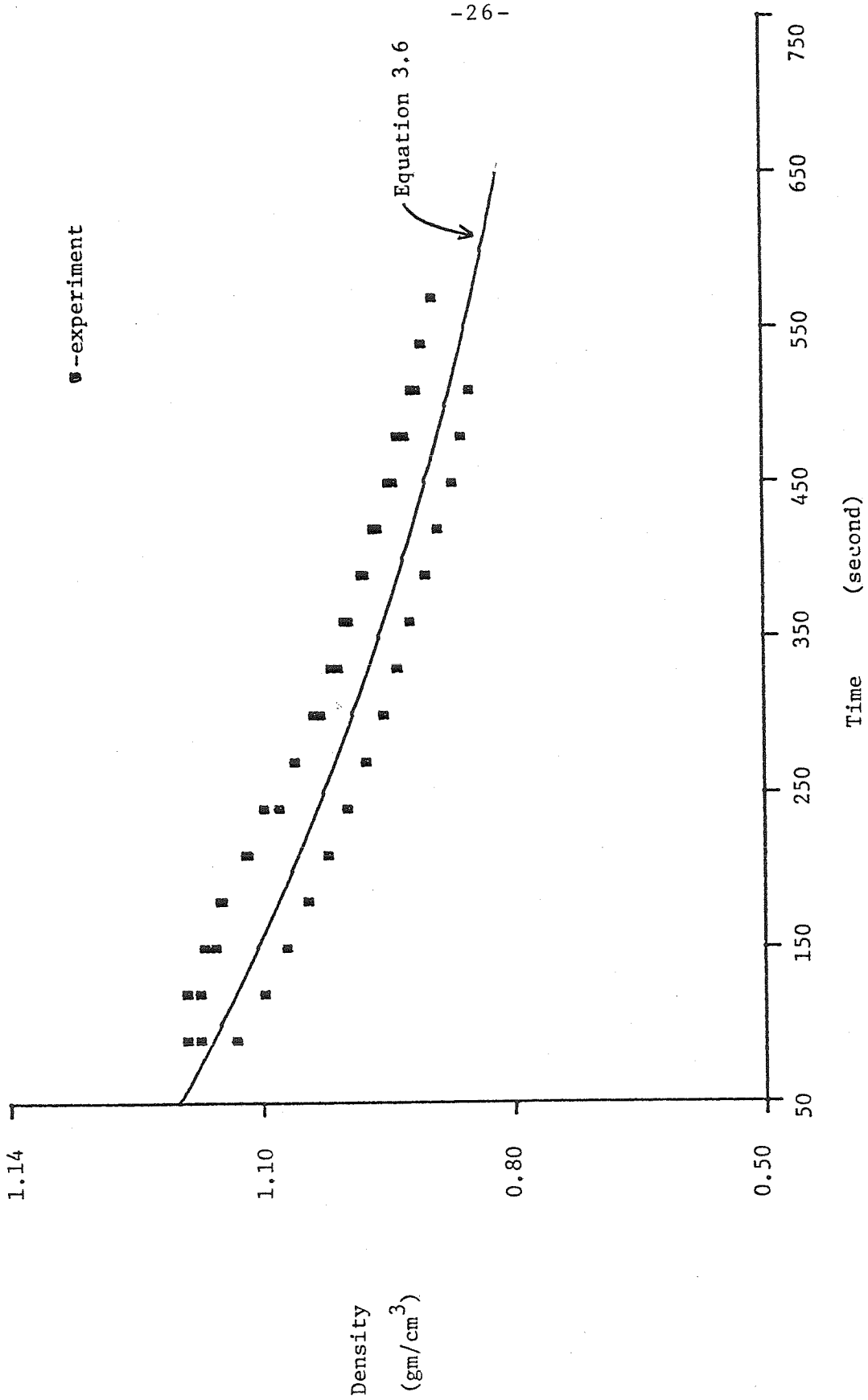


Figure 3.3. The density of a Pitt 8 coal at 410 °C and a nominal pressure of 150 psi.

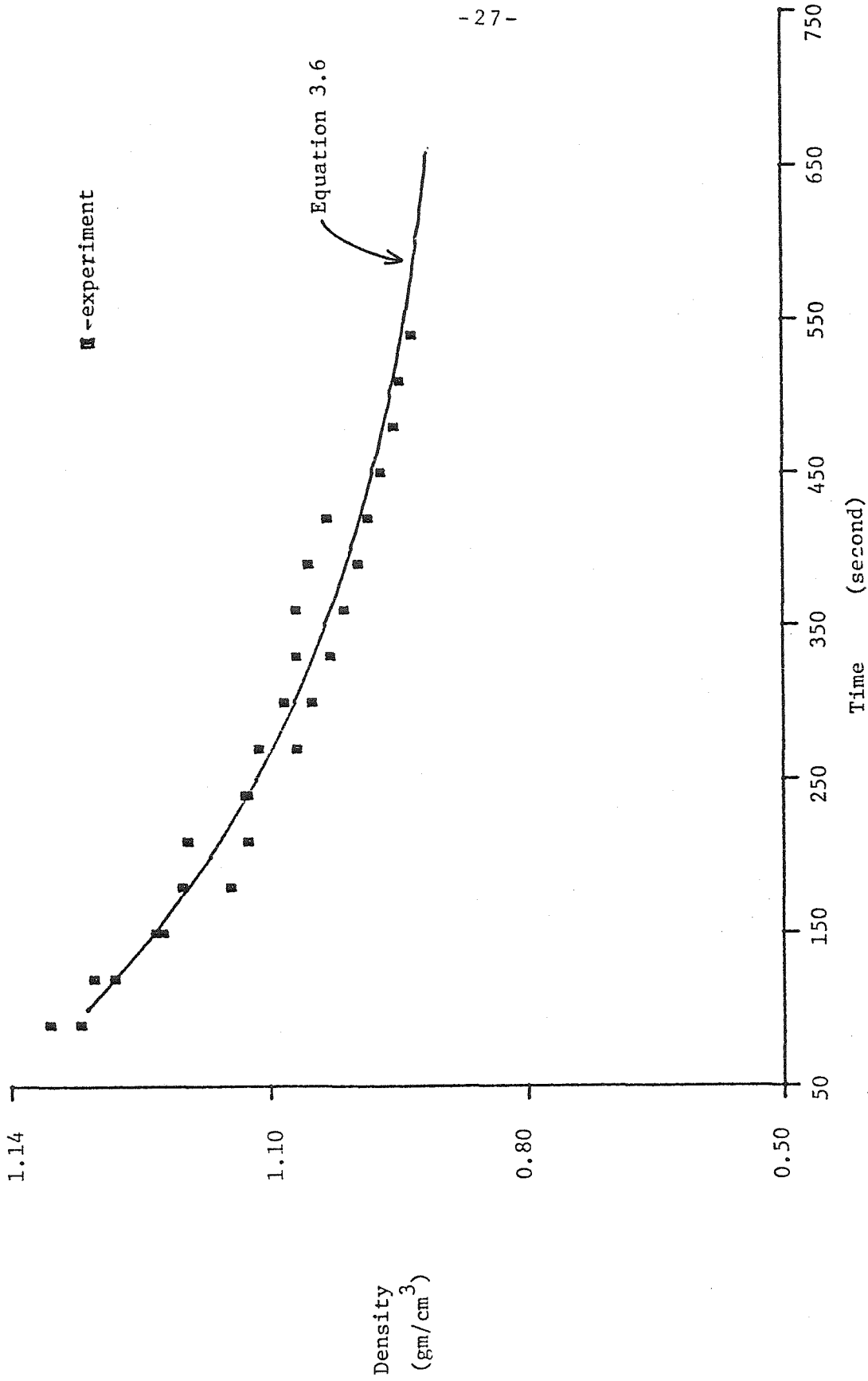


Figure 3.4. The density of a Pitt 8 coal at 410 °C and a nominal pressure 200 psi.

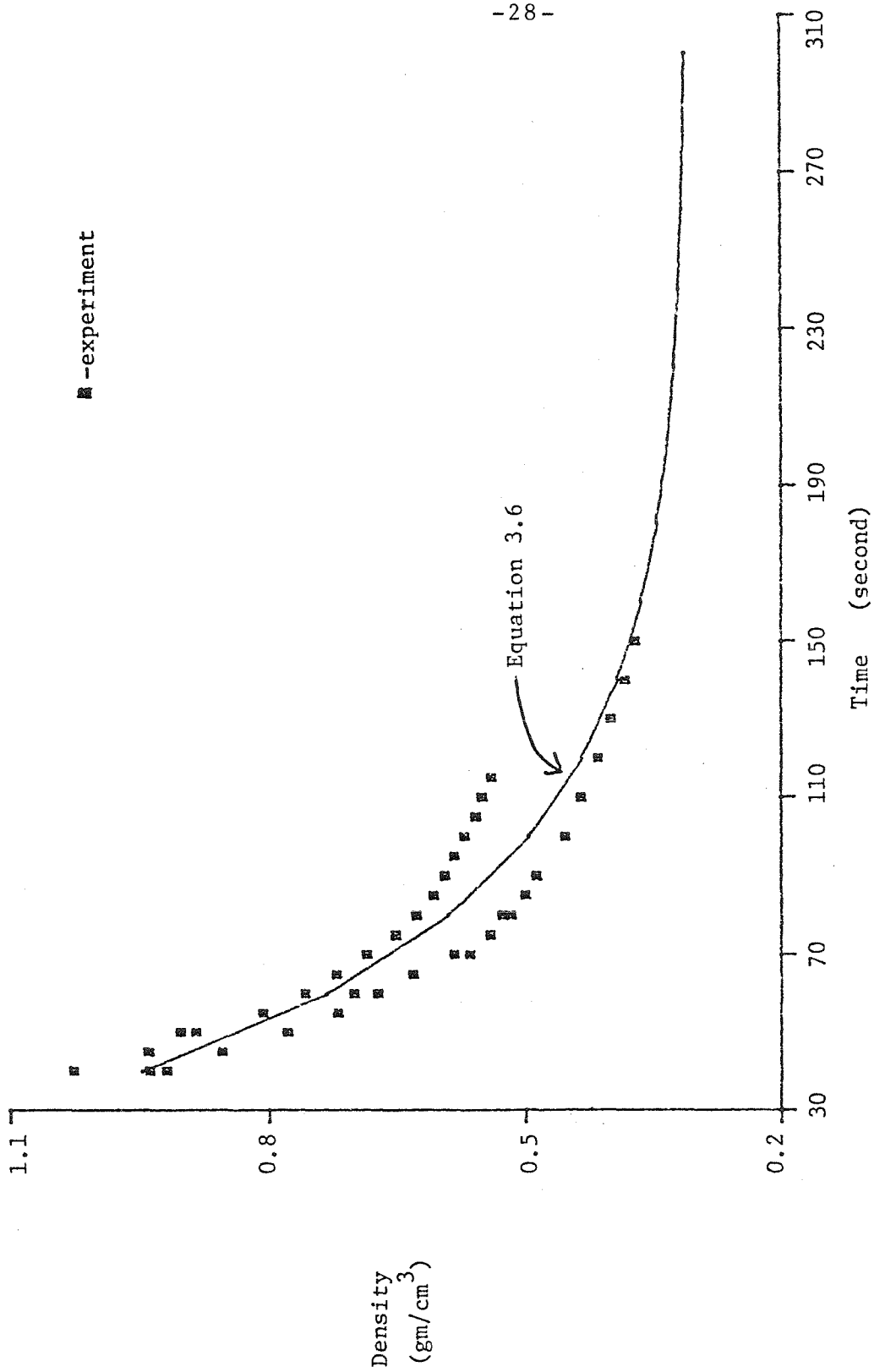


Figure 3.5. The density of a Pitt 8 coal at 450 °C and a nominal pressure of 50 psi.

□ -experiment

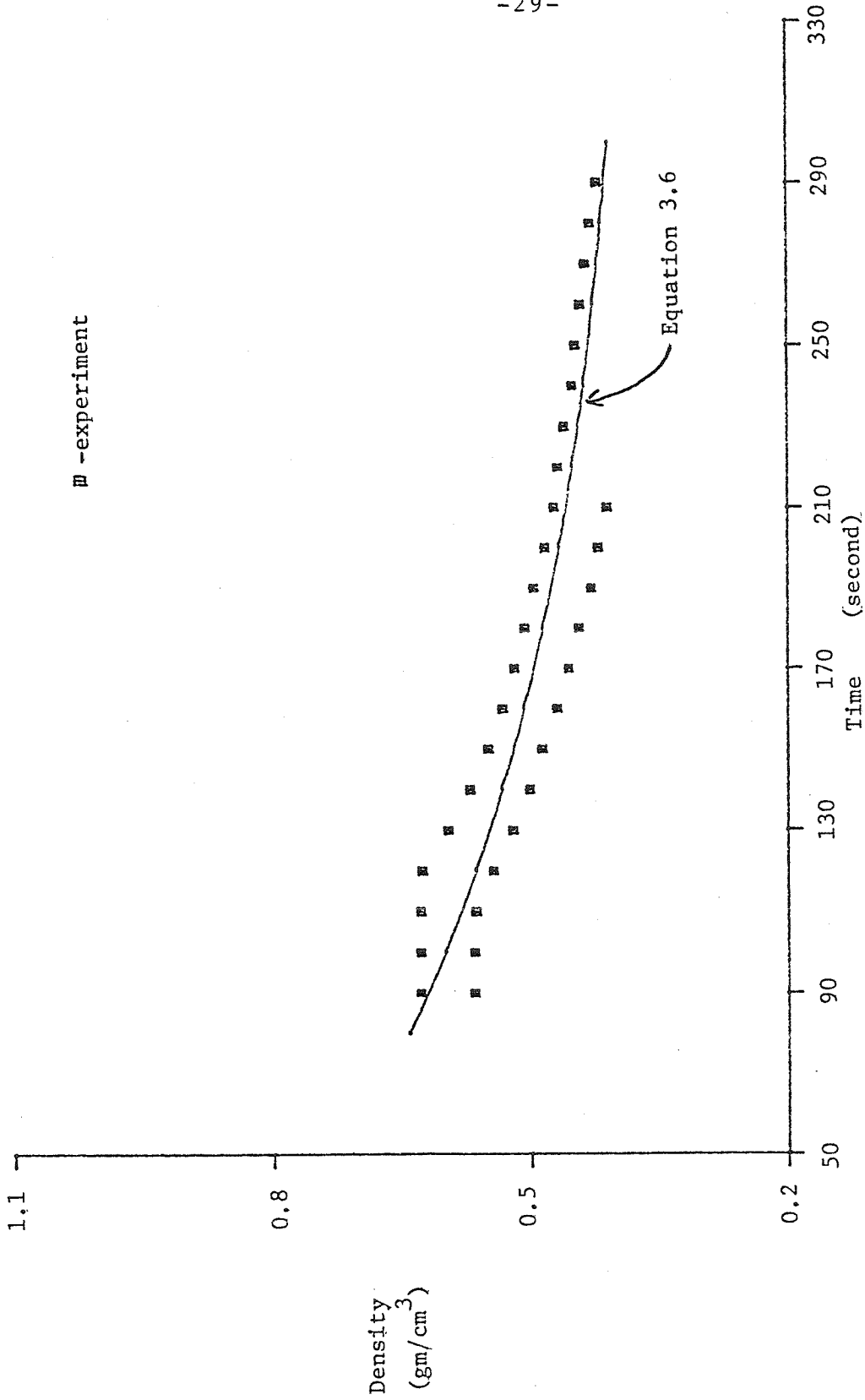


Figure 3.6. The density of a Pitt 8 coal at 450 °C and a nominal pressure of 75 psi.

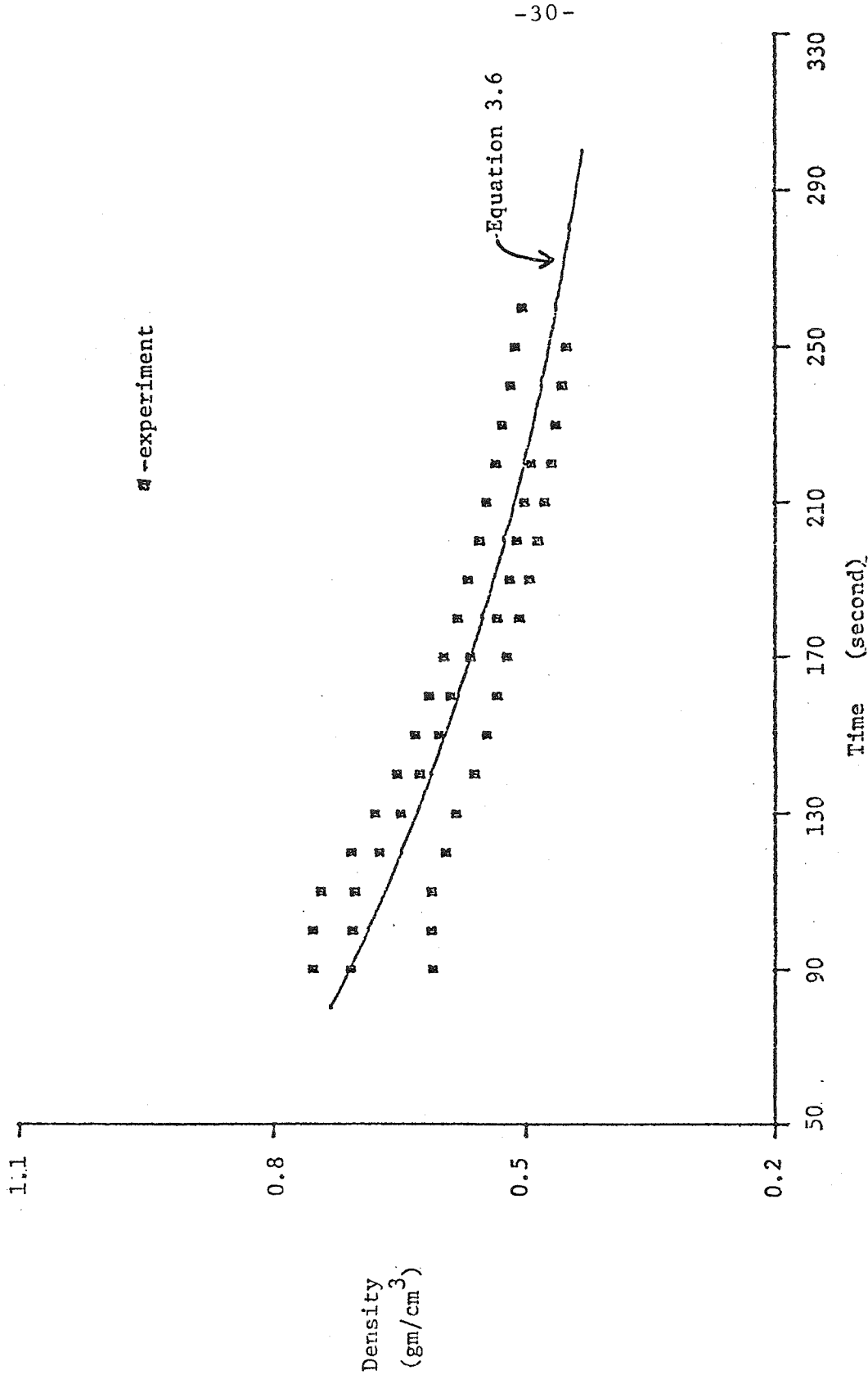


Figure 3.7. The density of a Pitt 8 coal at 450 °C and a nominal pressure of 100 psi.

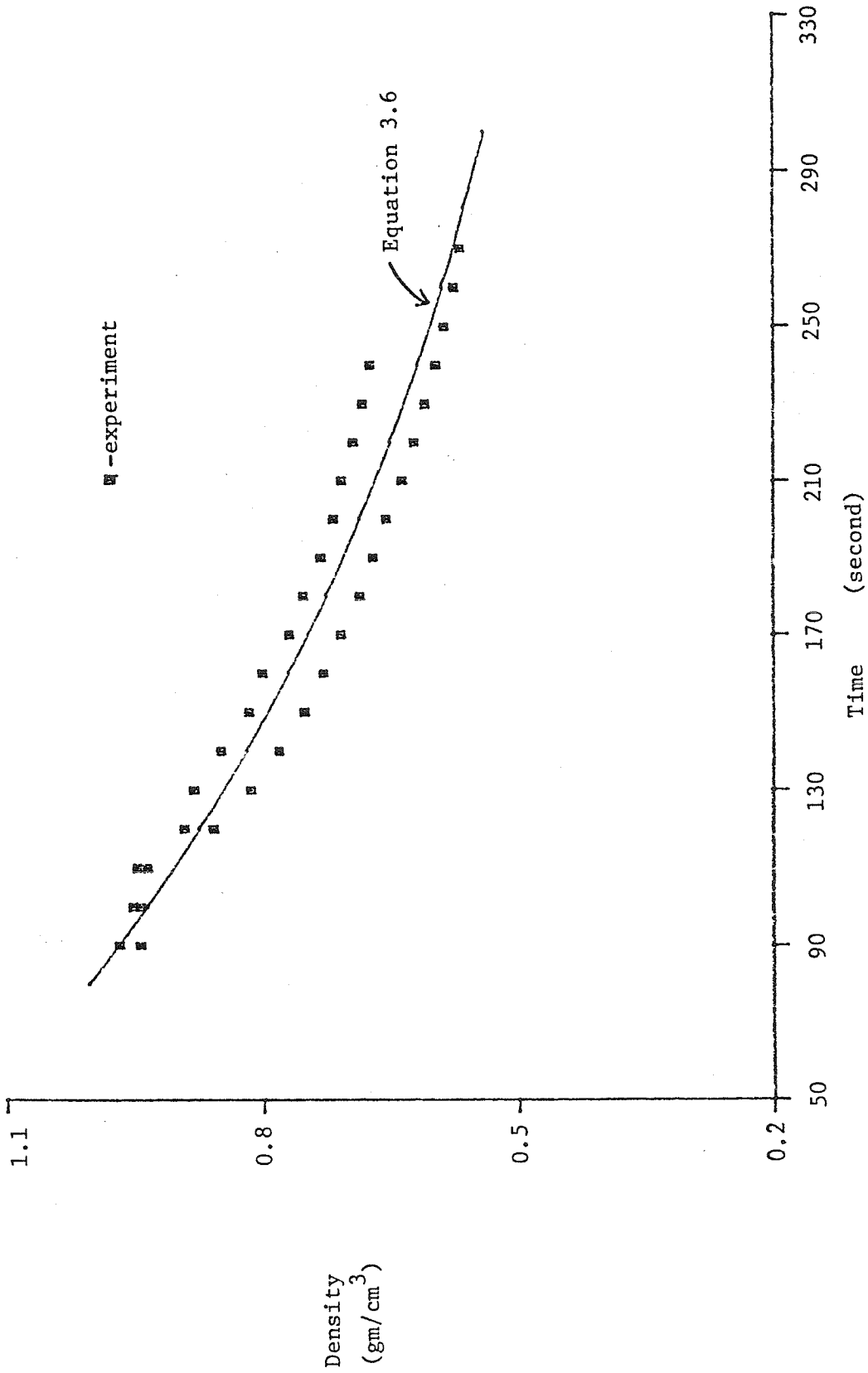


Figure 3.8. The density of a Pitt 8 coal at 450 °C and a nominal pressure of 125 psi.

### 3.5 Volume Fraction of Gas

One of the most important factors in measuring the viscosity of a multicomponent system is the volume occupied by the gaseous phase. Therefore the amount and volume of the gas present in the rapidly heated coal must be estimated.

Density decreased rapidly with time, and that result probably was caused by gas being produced during devolatilization. The bulk density of bituminous coals at standard temperature and pressure is approximately  $1.2 \text{ gm/cm}^3$ .<sup>22</sup> Upon insertion and pressurization of the coal in the reservoir, the density increased to a maximum value after 10-20 seconds. The maximum density appeared to be a function of the temperature only. The maximum density for the runs at  $410^\circ \text{C}$  was measured as  $1.32 \text{ gm/cm}^3$  with a standard deviation of  $0.057 \text{ gm/cm}^3$ . The maximum density for the runs at  $450^\circ \text{C}$  was measured as  $1.14 \text{ gm/cm}^3$  with a standard deviation of  $0.032 \text{ gm/cm}^3$ . Thus, by neglecting any further density change of this solid and liquid phase with time, the reduction of density represented the production of a gas. Admittedly, the solid and liquid phase probably changed density with increasing temperature. Large ( 50% ) density reductions will be considered, however, to be due to gas production only. Any further thermal expansion of the solid and liquid phase will be neglected.

With the above assumptions, the volume fraction of gas may be deduced from the density data as follows. The volume fraction of liquid,  $\alpha_l$ , is given by

$$\alpha_l = \frac{V_L}{V} \quad (3.7)$$

where  $V_L$  is the volume occupied by the liquid and solid phase, and  $V$  is the total volume. Though this ratio may be computed directly from the density measurements, it is easier to use the overall density values reported earlier. Thus Equation 3.7 becomes

$$\alpha_l = \frac{\rho_r m_l}{\rho_l m_t} \quad (3.8)$$

where  $\rho_r$  is the density in the reservoir,  $\rho_l$  is the density of the liquid and solid phase,  $m_l$  is the mass of the solid and liquid phase, and  $m_t$  is the total mass of the sample measured at the beginning of the run. By assuming the ratio of masses to be unity, Equation 3.8 becomes

$$\alpha_l = \frac{\rho_r}{\rho_l} \quad (3.9)$$

the error in assuming the mass ratio to be unity is proportional to the mass fraction of gas and is not believed to be significant. This assumption is equivalent to stating the volume occupied by the solid and liquid phase does not significantly change during devolatilization.

Because the volume fraction of gas,  $\alpha_g$ , is given by

$$\alpha_g = 1 - \alpha_l \quad (3.10)$$

Substituting Equation 3.9 into 3.10 gives

$$\alpha_g = 1 - \frac{\rho_r}{\rho_l} \quad (3.11)$$

By using the empirical relationship for the overall density, Equation 3.8, and the measurement of the solid and liquid density, Equation 3.11 becomes

$$\alpha_g = 1 - \frac{1}{\rho_l(T)} (a + b e^{-k(t-t_0)}) \quad (3.12)$$

where  $a$ ,  $b$ ,  $k$ , and  $t_0$  are functions of temperature, pressure, and coal type, and  $\rho_l$  is a function of temperature. Figures 3.9 and 3.10 give the volume fractions of gas versus time for a Pitt 8 coal at 410 °C and 450°C and a nominal pressures of 75 and 100 psig respectively. All of the density measurements given in Table 3.1 were used with Equation 3.12 to produce the volume fractions of gas.

### 3.6 Conclusion

The overall density of a Pitt 8 coal was measured as a function of time, temperature, and pressure. The change of the overall density with time was shown to be significant for the calculation of the volumetric flow rate into the capillary tube. The history of the temperature of the coal in the reservoir was estimated and the coal was considered to be at thermal equilibrium with the rheometer within ninety seconds. The major changes in density with time were recognized to be principally caused by the production of gas. The density of the liquid phase was measured as a function of temperature and the volume fraction of gas as a function of time, temperature and pressure was calculated.

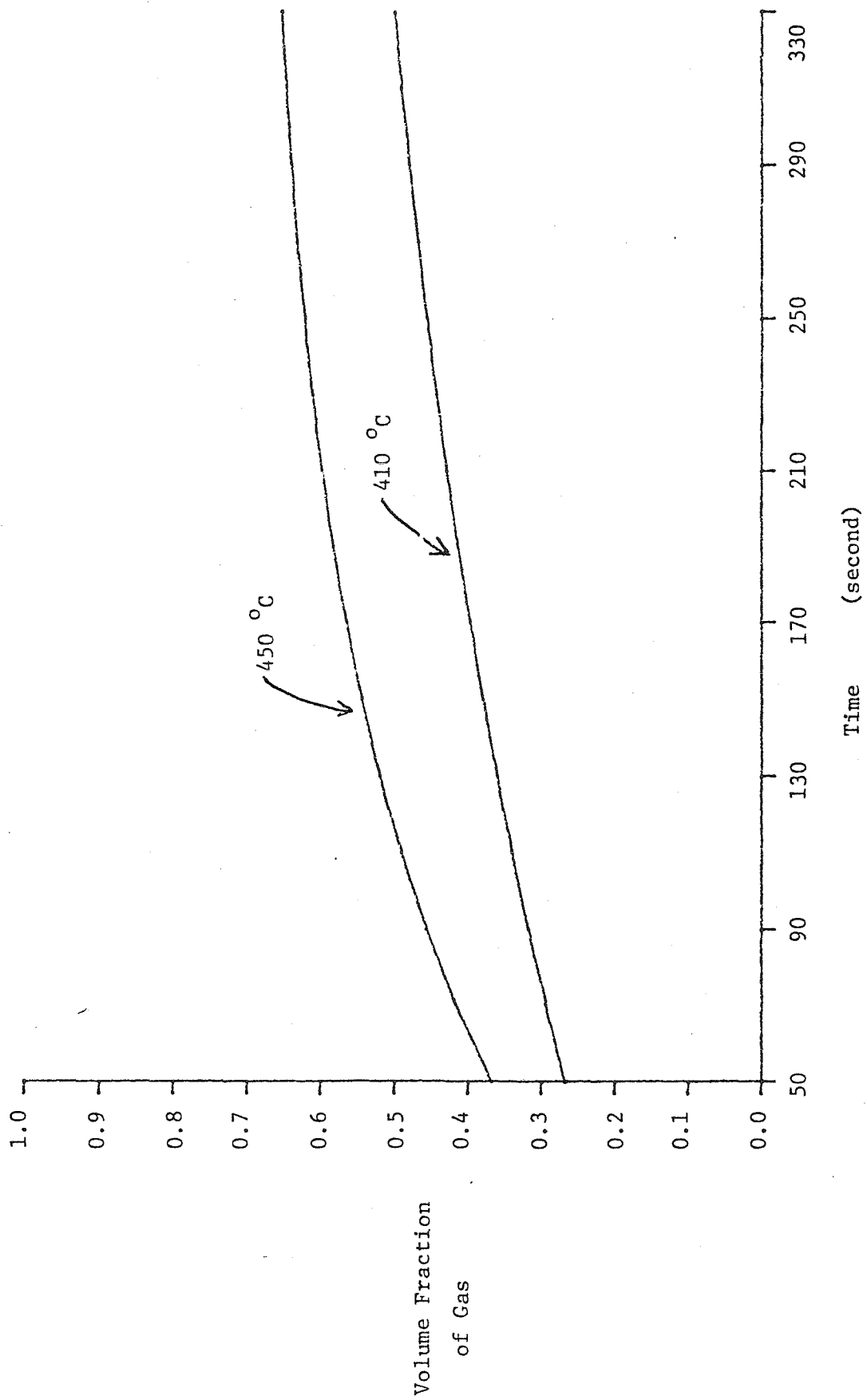


Figure 3.9. The volume fraction of gas versus time at a nominal pressure of 75 psi.

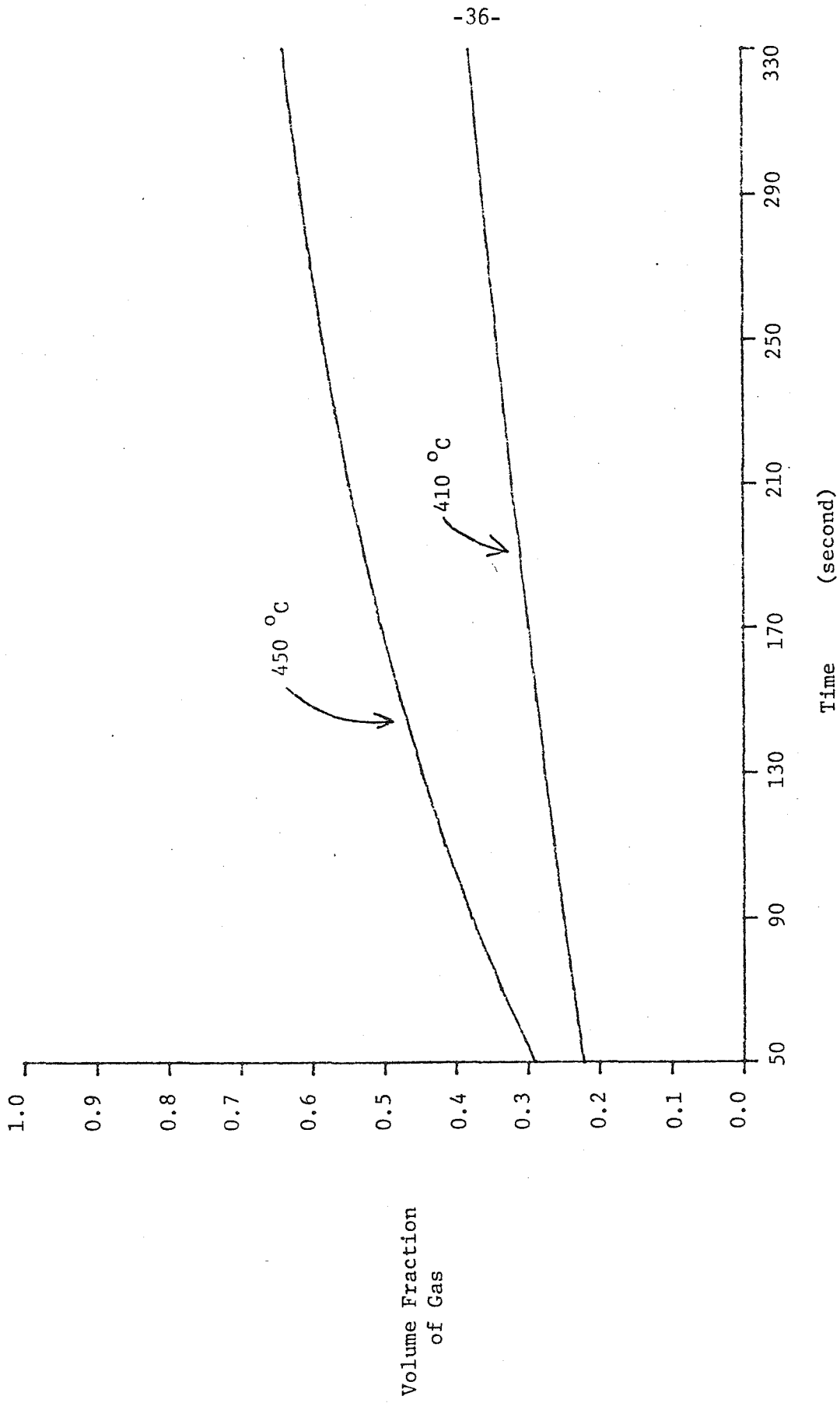


Figure 3.10. The volume fraction of gas versus time at a nominal pressure of 100 psi.

## Chapter 4

### 4.1 Introduction

This chapter applies the equations of motion to the rheometer under flow conditions. The continuity equation was used to develop the volumetric flow rate from the position of the piston head. The momentum equation was used to establish the wall-shear stress and to determine the magnitude of the various forces. For a given run, the density was considered to be a function of time and pressure, and the volumetric flow rate was shown to be a function of pressure and position of the piston. Rate of strain was developed as a function of the volumetric rate of flow. Difficulties in interpreting the meaning of an apparent, overall viscosity for the multiphase system are discussed. Finally, various potential errors arising from the use of a capillary-rheometer are estimated.

### 4.2 Macroscopic Continuity Equation

The control volume was first taken to be the reservoir, with coal streaming out into the capillary tube and the volume shrinking with time due to the movement of the piston head. The macroscopic continuity equation states

$$\frac{\partial}{\partial t} \int \rho dV + \int \rho \vec{u} \cdot d\vec{A} = 0 \quad (4.1)$$

where  $\rho$  is the density,  $V$  is the instantaneous control volume,  $\vec{u}$  is the velocity vector of the coal,  $t$  is the time, and  $A$  is the surface area of the control volume.

The only flux across the control volume was at the entrance of the capillary tube. Furthermore, since the reservoir was at uniform pressure, the density was not considered to be a function of spatial position. Hence, Equation 4.1 becomes

$$\frac{\partial}{\partial t} (\rho_r V) + \rho_r Q_i = 0 \quad (4.2)$$

where  $Q_i$  is taken to be the volumetric flow rate into the capillary tube and  $\rho_r$  is the density in the reservoir.

Throughout this development, the density was taken to be a function of time, temperature, and pressure only, thereby eliminating the need for detailed knowledge of the distribution of gas. This assumption was consistent with the macroscopic development of the equations of motion and was not considered to significantly effect the results of the continuity equation or the force balance. Measurement of the viscosity, however, depends strongly on knowledge of the distribution of gas. Problems that arise from a lack of this knowledge are discussed in Section 4.4

Differentiation and rearrangement of Equation 4.2 yields

$$Q_i = - \frac{V}{\rho_r} \frac{\partial \rho_r}{\partial t} - \frac{\partial V}{\partial t} \quad (4.3)$$

Since

$$V = A_p h_p \quad (4.4)$$

where  $A_p$  is the cross-sectional area of the piston head and  $h_p$  is the height of the piston from the bottom. The time derivative of the control volume becomes

$$\frac{\partial V}{\partial t} = A_p \frac{\partial h_p}{\partial t} = A_p u_p \quad (4.5)$$

where  $u_p$  is the velocity of the piston-head. Therefore, Equation 4.3 yields

$$Q_i = -\frac{V}{\rho_r} \frac{\partial \rho_r}{\partial t} - A_p u_p \quad (4.6)$$

The instantaneous volume and the velocity of the piston-head were derived from the measurement of the position of the piston-head. The density as a function of time was available from the measurements of the density.

The control-volume was extended to include the capillary tube in order to determine the volumetric flow rate out of the capillary tube,  $Q_o$ . With  $V_\pi$  taken to be the instantaneous volume of the reservoir and capillary tube, and assuming that the density is not a function of radial position, Equation 4.1 becomes

$$\frac{\partial}{\partial t} \int \rho dV_\pi + \rho_o Q_o = 0 \quad (4.7)$$

where  $\rho_o$  is the density at the exit of the capillary tube. The volume integral may be split into two integrals, for the reservoir and for the capillary tube. Thus,  $Q_o$  becomes

$$Q_o = -\frac{1}{\rho_o} \left[ \frac{\partial}{\partial t} \left( \int \rho dV + \int \rho dV_c \right) \right] \quad (4.8)$$

where  $V_c$  is the volume of the capillary tube. Since the density was constant in the reservoir volume, Equation 4.8 becomes

$$Q_o = -\frac{1}{\rho_o} \left[ \frac{\partial}{\partial t} (\rho_r V) + \frac{\partial}{\partial t} \int \rho dV_c \right] \quad (4.9)$$

And, as before

$$Q_o = -\frac{1}{\rho_o} \left[ V \frac{\partial \rho_r}{\partial t} + \rho_r A_p u_p + \frac{\partial}{\partial t} \int \rho dV_c \right] \quad (4.10)$$

or

$$Q_o = -\frac{\rho_r}{\rho_o} \left[ \frac{V}{\rho_r} \frac{\partial \rho_r}{\partial t} + A_p u_p \right] - \frac{1}{\rho_o} \frac{\partial}{\partial t} \int \rho dV_c \quad (4.11)$$

Because the capillary tube had a constant cross-section, and assuming the density was not a function of angular position, Equation 4.11 may be written as

$$Q_o = -\frac{\rho_r}{\rho_o} \left[ \frac{V}{\rho_r} \frac{\partial \rho_r}{\partial t} + A_p u_p \right] - \frac{1}{\rho_o} A_c \frac{\partial}{\partial t} \int \rho dz \quad (4.12)$$

where  $A_c$  is the cross-sectional area of the capillary tube. Defining

$$\bar{\rho} \equiv \frac{1}{L} \int_0^L \rho dz \quad (4.13)$$

where  $\bar{\rho}$  is the length-averaged density, and  $L$  is the length of the capillary tube, Equation 4.12 becomes

$$Q_o = -\frac{\rho_r}{\rho_o} \left[ \frac{V}{\rho_r} \frac{\partial \rho_r}{\partial t} + A_p u_p \right] - A_c \frac{L}{\rho_o} \frac{\partial \bar{\rho}}{\partial t} \quad (4.14)$$

By taking the worst-case values and assuming the time rate of change of the length-averaged density was of the same order of magnitude as for the measured densities, as noted in Chapter 3, the final term in Equation 4.14 may be neglected in comparison with the other terms. Thus the volumetric flow rate out of the capillary tube is

$$Q_o = -\frac{\rho_r}{\rho_o} \left[ \frac{V}{\rho_r} \frac{\partial \rho_r}{\partial t} + A_p u_p \right] \quad (4.15)$$

The added complexity of this result when compared with Equation 4.6 shows the difficulties associated with the density being a function of pressure as well as time.

Finally, a relationship between the density and the volumetric flow rate at the entrance and the exit is developed with the continuity equation as follows

$$\dot{m}_i = \dot{m}_o = \rho_r Q_i \quad (4.16)$$

and

$$\rho_r Q_i = \rho_o Q_o = \rho Q \quad (4.17)$$

where  $\dot{m}_i$  is the mass flow rate at the entrance of the capillary tube,  $\dot{m}_o$  is the mass flow rate at the exit, and  $Q$  is the volumetric flow rate as a function of axial position.

### 4.3 Macroscopic Momentum Equation

The control volume for the macroscopic momentum equation was taken to be the capillary volume, yielding

$$\frac{\partial}{\partial t} \int \rho \vec{u} dV + \int (\rho \vec{u}) \vec{u} \cdot d\vec{A} = \int \rho \vec{g} dV - \int P d\vec{A} - \int \vec{\tau} \cdot d\vec{A} \quad (4.18)$$

where  $\vec{g}$  is the gravitational acceleration,  $P$  is the pressure, and  $\vec{\tau}$  is the shear stress tensor. The velocity was assumed to be in the axial direction only. The axial components of Equation 4.18 were developed individually, starting from the left and moving across. Expansion of the first term gives

$$\frac{\partial}{\partial t} \int \rho u dV = \frac{\partial}{\partial t} 2\pi \int \int \rho u r dr dz \quad (4.19)$$

where  $u$  is the velocity in the axial direction, and no dependence on the angular coordinate is assumed. Furthermore, by assuming the density was not a function of radial position, Equation 4.19 yields

$$\frac{\partial}{\partial t} 2\pi \int \int \rho u r dr dz = 2\pi \frac{\partial}{\partial t} \int dz \rho \int u r dr = \frac{\partial}{\partial t} \int \rho Q dz \quad (4.20)$$

Substitution of Equations 4.16 and 4.17 yields

$$\frac{\partial}{\partial t} \int \rho u dV = L \frac{\partial}{\partial t} \dot{m}_i \quad (4.21)$$

The second term of Equation 4.18 in the axial direction gives

$$\int (\rho u) u dA = \int_o (\rho u) u dA - \int_i (\rho u) u dA \quad (4.22)$$

Then, again neglect any angular dependencies to obtain

$$\int (\rho u) u dA = 2\pi \left[ \int_0 (\rho u) u r dr - \int_i (\rho u) u r dr \right] \quad (4.23)$$

Equation 4.23 is recognized to represent the change in the kinetic energy of the flow from the input to the output. Because of the pressure dependence of the density, the exit stream had a higher velocity than the entrance stream. The error incurred by neglecting Equation 4.23 was estimated in a conventional manner in Section 4.5. Additionally, the magnitude of this term was estimated by use of the following:

$$2\pi \left[ \int_0 (\rho u) u r dr - \int_i (\rho u) u r dr \right] \approx (\rho \bar{u}^2 A)_o - (\rho \bar{u}^2 A)_i \quad (4.24)$$

where  $\bar{u}$  is the mean velocity at the indicated positions. Rearrangement and substitution gives

$$\int (\rho u) u dA \approx \frac{\dot{m}}{A_c} (Q_o - Q_i) \quad (4.25)$$

The third term in Equation 4.18 was expanded to yield

$$\int \rho \vec{g} dV = g \int \int 2\pi r \rho r dr dz \quad (4.26)$$

where  $g$  is the axial component of the acceleration of gravity, and  $\vec{g} = (0, 0, g)$ . Again, no density dependence on angular position is assumed. Furthermore, by assuming no radial variations of the density, Equation 4.26 becomes

$$gA \int \rho dz = gV_c \bar{\rho} \quad (4.27)$$

where  $\bar{\rho}$  is the length-averaged density, and  $V_c$  is the volume of the capillary tube. The fourth term of Equation 4.18 represents the pressure exerted on the control volume at the entrance and exit of the capillary tube, that is

$$\int P d\hat{A} = (P_o - P_i) A_c \quad (4.28)$$

where  $P_i$  and  $P_o$  are respectively the pressures at the entrance and exit of the capillary tube.

The fifth term of Equation 4.18 represents the shear force acting on the surface of the control volume. In the axial direction, this term was written as <sup>23</sup>

$$\int_V^* d\hat{A} = -\int \tau_w C dz - \left[ \int_0^r \tau_{zz} 2\pi r dr - \int_i \tau_{zz} 2\pi r dr \right] \quad (4.29)$$

where  $\tau_w$  is the shear stress in the axial direction acting on the r-normal plane and evaluated at the wall,  $\tau_{zz}$  is the shear stress in the axial direction acting on the z-normal plane, and  $C$  is the circumference of the capillary tube. Examination of the first term of Equation 4.29 gives

$$-\int \tau_w C dz = -C \int \tau_w dz \quad (4.30)$$

Thus, the macroscopic momentum equation in the axial direction becomes, through Equations 4.22, 4.25, 4.27, 4.28, 4.29, and 4.30 :

$$L \frac{\partial \rho_i Q_i}{\partial t} + \frac{\dot{m}}{A_c} (Q_o - Q_i) = g V_c \bar{\rho} - (P_o - P_i) A_c - C \int \tau_w dz - 2\pi \left[ \int_0^r \tau_{zz} r dr - \int_i \tau_{zz} r dr \right] \quad (4.31)$$

where  $\rho_i$  is the density in the reservoir, also referred to as  $\rho_r$ .

Equation 4.31 represents the full macroscopic momentum equation with the axial velocity as a function of  $r$  and  $z$ , and the density as a function of time and pressure. With the above restrictions, Equation 4.31 represents a precise description of the forces acting on a complex, multicomponent, multiphase flow through a capillary tube. From laboratory data, the magnitude of the various forces was estimated, and resulting simplifications were made with confidence. The final term in Equation 4.31, which contains the  $\tau_{zz}$  term, may not be determined, however, without further modeling. The area on which this force acts was small, and the total force was not expected to be significant. After the introduction of an apparent viscosity, the  $\tau_{zz}$  term was examined in detail.

Expansion of Equation 4.31 to input the laboratory data and neglect of the  $\tau_{zz}$  term for the moment, gives

$$L \left[ \frac{\partial \rho_i}{\partial t} Q_i + \frac{\partial Q_i}{\partial t} \rho_i \right] + \frac{\dot{m}}{A_c} [Q_o - Q_i] = g V_c \bar{\rho} - (P_o - P_i) A_c - C \int \tau_w dz \quad (4.32)$$

Development of the difference in the volumetric flow rates into and out of the capillary tube by use of Equations 4.6 and 4.15 produces

$$Q_o - Q_i = - \left[ \frac{V}{\rho_r} \frac{\partial \rho_r}{\partial t} + A_p u_p \right] \left( \frac{\rho_r}{\rho_o} - 1 \right) \quad (4.33)$$

Substitution of Equation 4.33 into 4.32 leads to the final form of the macroscopic momentum equation:

$$L \left[ \frac{\partial \rho_r}{\partial t} Q_i + \frac{\partial Q_i}{\partial t} \rho_r \right] + \frac{\dot{m}}{A_c} \left[ - \left( \frac{V}{\rho_r} \frac{\partial \rho_r}{\partial t} + A_p u_p \right) \left( \frac{\rho_r}{\rho_o} - 1 \right) \right] = \bar{\rho} V_c g - (P_o - P_i) A_c - C \int_0^L \tau_w dz \quad (4.34)$$

All the terms on the left-hand side of Equation 4.34 were evaluated with the laboratory data and compared with the right-hand side. Table 4.1 shows the maximum values for these various terms. Table 4.2 compares the magnitude of the resultant forces with the magnitude of the smallest pressure force used. From these comparisons, Equation 4.34 was simplified to

$$-(P_o - P_i) A_c = C \int_0^L \tau_w dz \quad (4.35)$$

Though this result is similar to simple capillary flow, it is based on laboratory measurements of a complex fluid. Finally, by defining the length-averaged shear stress,

$$\bar{\tau}_w \equiv \frac{1}{L} \int_0^L \tau_w dz \quad (4.36)$$

Equation 4.35 becomes

$$\frac{-(P_o - P_i) A_c}{CL} = \bar{\tau}_w \quad (4.37)$$

which completes the force balance.

Table 4.1 The M aximum Values of Various M easured Quantities		
Term	M aximum Value	Run Number
$\frac{\partial \rho_r}{\partial t}$	0.005	38
$Q_i$	0.20	87
$\frac{\partial Q_i}{\partial t}$	0.055	85
$\frac{\dot{m}}{A_c}$	31.63	95
$\frac{V}{\rho_r}$	2.813	94
$A_p u_p$	0.115	95
$\frac{\rho_r}{\rho_o} - 1$	2.1	35

Table 4.2 The Magnitude of Various Terms in the Momentum Equation		
Force	Magnitude	Ratio to Minimum Pressure Force
(dyne)	(dyne)	
$(P_o - P_i)A_c$	7704	1.0
$L \frac{\partial \rho_r}{\partial t} Q_i$	0.0027	$3.5 \times 10^{-7}$
$L \rho_r \frac{\partial Q_i}{\partial t}$	0.193	$2.5 \times 10^{-5}$
$\frac{\dot{m}}{A_c} \left( \frac{V}{\rho_r} \frac{\partial \rho_r}{\partial t} \right) \left( \frac{\rho_r}{\rho_o} - 1 \right)$	0.442	$5.7 \times 10^{-5}$
$\frac{\dot{m}}{A_c} (A_p u_p) \left( \frac{\rho_r}{\rho_o} - 1 \right)$	3.63	$4.7 \times 10^{-4}$
$\bar{p} V_c g$	5.91	$7.7 \times 10^{-4}$

#### 4.4 Rate of Strain

The volumetric flow rate was defined as

$$Q \equiv 2\pi \int_0^{\tau_0} u(r) dr \quad (4.38)$$

where the velocity was assumed to be independent of angular position, and  $\tau_0$  was the radius of the capillary tube. Integration by parts yields

$$Q = -2\pi \int_0^{\tau_0} \frac{\partial u}{\partial r} \frac{r^2}{2} dr \quad (4.39)$$

By using the estimates of the magnitudes of force from the previous section, the momentum Equation for a differential volume within the capillary tube gives

$$\frac{\partial P}{\partial z} = -\frac{1}{r} \frac{\partial}{\partial r} (r\tau_{rz}) \quad (4.40)$$

where  $\tau_{rz}$  is the shear stress in the axial direction acting on the r-normal plane. Integration over the entire radius yields

$$\int_0^{\tau_0} \frac{\partial P}{\partial z} r dr = d(r\tau_{rz}) \quad (4.41)$$

$$\frac{dP}{dz} \frac{\tau_0^2}{2} = \tau_0 \tau_w \quad (4.42)$$

Integration to any position  $r$  yields

$$\frac{dP}{dz} \frac{r^2}{2} = r\tau_{rz} \quad (4.43)$$

Dividing Equation 4.43 by 4.42 and rearranging yields

$$\frac{r}{\tau_0} = \frac{\tau_{rz}}{\tau_w} \quad (4.44)$$

Finally, defining the true viscosity,  $\mu_T$ , in a conventional manner, and neglecting any yield or viscoelastic effects,

$$\mu_T \left( \frac{\partial u}{\partial r} \right) = - \frac{\tau}{\frac{\partial u}{\partial r}} \quad (4.45)$$

and substituting into 4.39 for the rate of strain yields

$$Q = 2\pi \int_0^{\tau_0} \frac{\tau}{\mu_T} \frac{r^2}{2} dr \quad (4.46)$$

Equation 4.45 shows that the viscosity is a function of rate of strain or shear stress due to the potential of a non-Newtonian fluid. Following Van Wazer,<sup>24</sup> the apparent viscosity ( $\mu$ ) was used as a constant, and any variation of its magnitude with flow conditions will indicate a non-Newtonian constitutive equation. If necessary, the true viscosity may then be determined from the behavior of the apparent viscosity versus, say, volumetric flow rate. Substitution for the shear stress with Equation 4.44 produces

$$Q = 2\pi \int_0^{\tau_0} \left( \frac{\tau_w}{\mu} \frac{r}{\tau_0} \right) \frac{r^2}{2} dr = \frac{\pi \tau_w}{\mu \tau_0} \int_0^{\tau_0} r^3 dr \quad (4.47)$$

Thus

$$Q = \frac{\pi \tau_w \tau_0^3}{4\mu} \quad (4.48)$$

The viscosity may be obtained by rearrangement:

$$\mu = \frac{\pi \tau_w \tau_0^3}{4Q} \quad (4.49)$$

where both  $\tau_w$  and  $Q$  are functions of axial position.

At this point in the development, the difficulties of a multicomponent fluid become evident. The macroscopic momentum equation showed that the changing density with pressure does not produce a significant change in the kinetic energy of the flow. In addition, evaluation of the continuity equation showed that though the time rate of change of the density within the capillary did not significantly alter the volumetric flow

rate, the changing gradient of the density did affect the actual volumetric flow and, therefore, the rate of strain. Thus, Equation 4.38 was stated in terms of the length-averaged shear stress, and Equation 4.49 was dependent on the axial position. In order to obtain a value for the overall viscosity, it was necessary to carefully define what is meant by the overall viscosity. By substitution for  $\tau_w$ , from Equation 4.49, in Equation 4.36 yields

$$\int_0^L \frac{4Q\mu}{\pi r_o^3} dz = \frac{-(P_o - P_i)A_c}{C} \quad (4.50)$$

where  $Q$  is a function of axial position. Additionally, since the apparent viscosity is defined for a given  $\tau_w$ , and  $\tau_w$  is a function of axial position, Equation 4.50 can not be used to experimentally determine the apparent viscosity.

The usual method to overcome this difficulty was to define an overall viscosity based on the value of the volumetric flow rate at the entrance to the capillary tube. Substitution of Equation 4.38 into 4.49 yields

$$\mu = \frac{\pi r_o^3}{4Q_i} \times \frac{-(P_o - P_i)A_c}{CL} \quad (4.51)$$

where the mean shear stress was used for  $\tau_w$  and the volumetric flow rate was taken to be the value it had at the entrance of the capillary tube. Such a procedure was necessary to define the overall viscosity of a multi-component, multi-phase fluid.

Note that Equation 4.51 uses an arbitrary definition of an overall viscosity. While this definition is common in the literature, it must be recognized that the measurement of an overall viscosity was, at least, a function of the length of the capillary tube. Chapters 6 and 7 will develop a relationship for density as a function of pressure, and then solve the differential momentum equation to find the pressure distribution. The constraint of an arbitrary definition of viscosity based on the volumetric flow rate at the entrance was a serious drawback to any meaningful measurements. This treatment

should be helpful, however, in estimating the flow performance of rapidly-heated coals.

Finally, an estimate of  $\tau_{zz}$  from Equation 4.31 was made. The force ( $F$ ) may be written as

$$F = \int_0^{r_0} 2\pi r \tau_{zz} dr \quad (4.52)$$

and its estimation will produce the magnitude of the last two terms in Equation 4.31. From Bird, et al.<sup>25</sup>,  $\tau_{zz}$  may be written as

$$\tau_{zz} = -\mu \left[ 2 \frac{\partial u}{\partial z} - \frac{2}{3} (\nabla \cdot \vec{u}) \right] \quad (4.53)$$

From the general continuity equation:

$$\nabla \cdot \vec{u} = -\frac{u}{\rho} \frac{\partial \rho}{\partial z} \quad (4.54)$$

for axial flow only. Thus

$$F = -\int_0^{r_0} 4\pi r \mu \frac{\partial u}{\partial z} dr - \int_0^{r_0} 2\pi r \mu \frac{2}{3} \frac{u}{\rho} \frac{\partial \rho}{\partial z} dr \quad (4.55)$$

$$F = -\frac{\partial}{\partial z} \int_0^{r_0} 4\pi r \mu u dr - \int_0^{r_0} 2\pi r \mu \frac{2}{3} \frac{u}{\rho^2} \rho \frac{\partial \rho}{\partial z} dr \quad (4.56)$$

Equation 4.14 yields

$$\dot{m} = \int_0^{r_0} 2\pi r u \rho dr = \text{constant} \quad (4.57)$$

Substitution of Equation 4.57 into 4.56 produces

$$F = -2\mu \frac{\partial}{\partial z} \left( \frac{\dot{m}}{\rho} \right) - \frac{2}{3} \frac{\mu}{\rho^2} \frac{\partial \rho}{\partial z} \dot{m}$$

$$F = -2\mu \dot{m} \frac{\partial}{\partial z} \left( \frac{1}{\rho} \right) + \frac{2}{3} \mu \dot{m} \frac{\partial}{\partial z} \left( \frac{1}{\rho} \right)$$

$$F = -\frac{4}{3} \mu m \frac{\partial}{\partial z} \left( \frac{1}{\rho} \right) \quad (4.58)$$

The gradient of the inverse density may be estimated as

$$\frac{\partial}{\partial z} \left( \frac{1}{\rho} \right) \approx \frac{\frac{1}{\rho_o} - \frac{1}{\rho_r}}{L} \quad (4.59)$$

and use of Table 4.1 gives

$$F = 0.013 \times \mu \quad (4.60)$$

Comparison of this force with the forces in Table 4.2 showed that it could be neglected in the momentum equation.

Thus, the macroscopic momentum equation was safely simplified to the form used in Equation 4.38. After carefully noting what was meant by overall, apparent viscosity, Equation 4.51 was used with the measurements of piston-head position and applied pressure drop to deduce the viscosity.

#### 4.5 Error Estimation

Several major sources of error resulting from capillary rheometer readings must be addressed. The non-Newtonian nature of the flow somewhat complicates the estimation of these errors.

The kinetic energy of the issuing stream represents some of the energy from the total applied pressure that is not balanced by the viscous forces. Following the development by Van Wazer<sup>26</sup>, the difference is given as:

$$\Delta P_{observed} - \Delta P_{actual} = \frac{\rho Q^2}{\alpha \pi^2 r_o^4} \quad (4.61)$$

For Newtonian fluids,  $\alpha$  is unity. For non-Newtonian pseudoplastic fluids,  $\alpha$  may range from one to two. Thus, by choosing  $\alpha$  as one as the worst case, we may determine the order of magnitude of the kinetic energy effect. By using the following

representative values:

$$u_p \approx 0.05 \frac{cm}{sec} \quad A_p \approx \pi \text{ cm}^2 \quad \rho \approx 1 \frac{gm}{cm^3} \quad \tau_0 \approx 0.025 \text{ cm}$$

the volumetric flow rate is determined by the piston-head velocity and area which neglects the changing density with time. This estimate should be sufficient for an order of magnitude estimate. Forming the correction term yields:

$$32400 \frac{\text{dynes}}{\text{cm}^2} 1.45 \times 10^{-5} \frac{\text{psi}}{\frac{\text{dyne}}{\text{cm}^2}} = 0.47 \text{ psi}$$

This correction factor represents about 0.1 per cent of the applied pressure and may be neglected. If significantly different flow magnitudes are encountered, this estimate should be recalculated.

Bogue <sup>27</sup> discusses the end effect loss for non-Newtonian fluids represented by the power-law models. He presented his results by comparing the end effect losses with the kinetic energy losses. The end effect loss for pseudoplastic behavior never represented more than 17 per cent of the kinetic energy losses. From the previous estimate of kinetic energy loss we may safely neglect the end effect. In addition, Merz <sup>28</sup>, working with pseudoplastic polymer melts, states that the end effect may be neglected for L/D ratios greater than 20 to 120. Our L/D ratio of approximately 51 qualifies.

Capillary viscometer calculations are based on the assumption of laminar flow. The laminar flow regime is easily determined from the Reynold's number as

$$\frac{\rho u D}{\mu} \leq 2100$$

for Newtonian fluids. For non-Newtonian fluids, a generalized Reynold's number is generated from the power-law model. Examination of these results has shown that

pseudoplastic fluids transition at higher Reynold's numbers.<sup>29</sup> Using the same estimates of volumetric flow rate as above we find that

$$\mu \geq 0.01 \text{ poise}$$

for laminar flow. The actual Reynolds' numbers were less than  $10^{-3}$ .

A nother source of error comes from pressure losses prior to the capillary tube. This loss was due to two main sources, piston-head friction and introduction of material into the capillary. Van Wazer<sup>30</sup> states that the latter is found for highly viscous fluids with yield values. The well designed entrance for the capillary and the lack of a yield value for our coal suggest that the latter loss is not appropriate. The piston-head friction is so slight that the piston head easily drops to the bottom, even with a fresh Graphfoil seal. It would appear that these losses are not applicable.

After ninety seconds of preheat, the coal in the reservoir was considered to be isothermal. In addition, the capillary-wall temperature was assumed to be held constant at the run temperature. The temperature profile in the capillary tube during runs was estimated as shown below.

First, following Toor,<sup>31</sup> use a Newtonian relationship for rate of strain:

$$u_m = \frac{\tau_o^2}{4\mu} \left( -\frac{1}{2} \frac{dP}{dz} \right) = \frac{3.14 \times 10^2}{\mu} \frac{cm}{sec} \quad (4.62)$$

$$w = -u_m \frac{dP}{dz} = \frac{1.1 \times 10^9}{\mu} \frac{dynes}{cm^2 sec} \quad (4.63)$$

Finally, the centerline-to-wall temperature difference well past the point where there was a thermal entrance effect is given as

$$(T_c - T_w)_0 = \frac{\tau_o^2 w}{8k} = \frac{2.4}{\mu} \text{ } ^\circ C \quad (4.64)$$

Thus, even at the highest shear, the temperature difference will only be one degree Celsius. The effect of the thermal entrance length will be described after the following

calculation.

The coal melt may appear to behave as a pseudoplastic fluid. A power-law model approximates the coal melt behavior better than a Newtonian model. A thermal analysis based on the power-law model with pseudoplastic parameters should point out any discrepancies between our flow and the Newtonian thermal analysis. A gain following Toor, <sup>31</sup>

$$\tau^{n-1}B = \frac{\partial u}{\partial r} \quad (4.65)$$

where  $B$  is an intermediate result. We choose  $n=3$ , a good pseudoplastic value.

$$u_m = \frac{r_o^3}{5} B \left( -\frac{1}{2} \frac{dP}{dz} \right)^2 \quad (4.66)$$

Again approximate the pressure gradient as constant,

$$u_m = 1.17 \times 10^7 B$$

$$w = -u_m \frac{dP}{dz} = 4.04 \times 10^{13} B$$

Past the thermal entrance distance, the centerline to wall temperature difference is given as

$$(T_c - T_w)_o = \frac{1}{10} r_o^2 \frac{w}{k} = 7.01 \times 10^4 B \quad (4.67)$$

Fit of the power-law model to the worst case of flow yields,

$$n=3 \quad B = 1.1 \times 10^{-5} \frac{cm^4}{dynes^2 \ sec}$$

Substitution into our result gives

$$(T_c - T_w)_o = 0.78 \text{ } ^\circ C$$

Thus, the effect of pseudoplastic flow does not change the magnitude of viscous-

energy generation. It should be noted here that the value of thermal conductivity is taken from Van Krevelen<sup>22</sup> and is very conservative for our operating pressures.

Finally, the thermal-entrance length may be found based on a five-per-cent difference from the steady-state values. Again, following Toor,<sup>31</sup>

$$\frac{L}{r_o} = \frac{5}{6} X_s \left( \frac{2r_o u_m}{\alpha} \right) = 93.5 \text{ cm} \quad (4.68)$$

Thus, the flow never approached the steady-state value. That is, the entire flow is within the thermal entrance length. Toor<sup>31</sup> solved the entrance problem and showed that the temperature distribution, which starts uniformly, smoothly approaches the steady-state values. Therefore, our temperature difference will never reach the values calculated above.

Table 4.3 summarizes the potential errors and the model used for their estimation.

Table 4.3 The Modeling of Potential, Experimental Errors				
Error	Estimation Model			
	general	power law	Newtonian	order of magnitude
kinetic	X	X	X	X
end effect		X	X	X
turbulence		X	X	X
viscous heating		X	X	
entrance effect	X			

#### **4.6 Conclusion**

The volumetric flow rate was shown to be a function of density, time, and axial position at a temperature and pressure by application of the continuity equation to various control volumes. The macroscopic momentum equation was simplified with a minimum number of assumptions by using the experimental data and the significant terms were shown to be the pressure gradient and the shear stress at the wall. The flow was shown to be laminar and the energy generated by viscous dissipation was insignificant. Though detailed knowledge of the radial distribution of the density was not considered important for the continuity equation or the force balance, this knowledge was shown to be essential for any meaningful measurement of the viscosity. These difficulties with the application of the viscosity to multi-phase capillary flow necessitated an arbitrary definition of an overall viscosity. Benefits and drawbacks of such a definition were discussed and various potential errors arising from the use of a capillary rheometer were estimated.

## Chapter 5

### 5.1 Introduction

In this chapter the overall viscosity is determined from the experimental data and the equations developed in Chapter 4. The overall, apparent viscosity is presented in tabular and graphic forms as a function of time at a given pressure drop and temperature. A least-squares approximation is applied to the viscosity data as a function of time, and the behavior of the apparent, overall viscosity as a function of pressure drop and temperature is described. A lower bound for the time rate of change of the overall, apparent viscosity is estimated and then compared to estimates of the volume fraction of gas, the degasification rate, and the temperature.

### 5.2 Rheological Equations

Based on the position of the piston head as a function of time, and the density as a function of time, the volumetric flow rate into the capillary tube was given in Equation 4.6 as

$$Q_i = -\frac{V}{\rho} \frac{\partial \rho}{\partial t} - A_p u_p \quad (5.1)$$

By use of the length-averaged shear stress at the wall, the overall, apparent viscosity was developed in Equation 4.51 as

$$\mu = \frac{\pi r_0^3}{4Q_i} \left[ \frac{-(P_0 - P_i)A_c}{CL} \right] \quad (5.2)$$

It should be stressed that  $\mu$  is based on the convention of using the volumetric flow rate at the entrance to the capillary tube.

Equation 5.1 was substituted into Equation 5.2 to produce the overall, apparent viscosity as a function of time at constant temperature and pressure drop. After the least-squares approximation was applied to the viscosity-time data, the overall, apparent viscosity was displayed as a function of pressure drop and temperature.

### 5.3 Data

Figures 5.1 through 5.8 present a representative sample of the overall, apparent viscosity as a function of time at constant temperature and pressure drop. A least-squares approximation of the form

$$\mu = a + b(t - t_0) + c(t - t_0)^2 \quad (5.3)$$

where  $a$ ,  $b$ ,  $c$ , and  $t_0$  are constants to be established, and  $t$  is time, was applied to the viscosity data. The constants that produced the minimum error for each value of temperature and pressure drop are given in Table 5.1 with the standard deviation arising from each approximation. This parabolic fit was chosen for convenience and did not imply any physical interpretation.

As can be seen from the data, the viscosity measurements are characterized by a sudden and large reduction in viscosity, then a relatively constant value for most of the run, and finally a rise in viscosity at the end of the run. The sudden drop in viscosity at the beginning of the run was easily the most dramatic feature of the entire experiment and was looked at in more detail in Section 5.5.

The increase in viscosity at the end of the run might be attributed to the coking of the coal, to the end effects of the reservoir becoming significant, other unknown factors, or some combination of the above. Coking of the coal, which is strong function

of temperature and rate of heat transfer, would increase the measured viscosity. The effects of coking on fluidity were clearly demonstrated in the experiments with the Gieseler plastometer<sup>5,7,8,9,13</sup>. Another possible cause of the increase in viscosity at the end of the run was thought to be a result of the entrance losses becoming significant as the distance between the piston head and the reservoir wall approached the magnitude of the radius of the capillary tube. These end effects would result in a large increase in the measured viscosity, and this increase in measured viscosity would be expected to occur, and was observed to occur, at approximately the same position of the piston head. The rise in viscosity at the end of the run was, therefore, taken to be an artifact of the experimental equipment.

Table 5.2 represents a constant approximation of the viscosity data after the two large changes in the viscosity at the beginning and at the end have been removed. This approximation was applied to a time period in which the flow was considered to be both frothy and steady. This estimate of the overall, apparent viscosity,  $\mu$ , is not meant to be an accurate measure of some property of the heated coal; in fact,  $\mu$  was expected to be a function of the length of the capillary tube. Rather, the grouping of parameters of flow which  $\mu$  represents, as in Equation 5.2, was very useful in providing the estimates of the viscosity of the liquid alone. Chapters 6 and 7 take on this difficult task of estimating the viscosity of the liquid during the time spans indicated in Table 5.2.

Figure 5.7 deserves additional comment. Of the two viscosity runs plotted in this figure, one of the runs showed the expected transition to flow at 98 seconds. The other viscosity run displayed a relatively flat plot because the transition to flow had occurred before the warm-up period of ninety seconds had expired. These differences in the time-to-transition were directly related to the mass of the sample, the larger mass transitioning at a latter time.

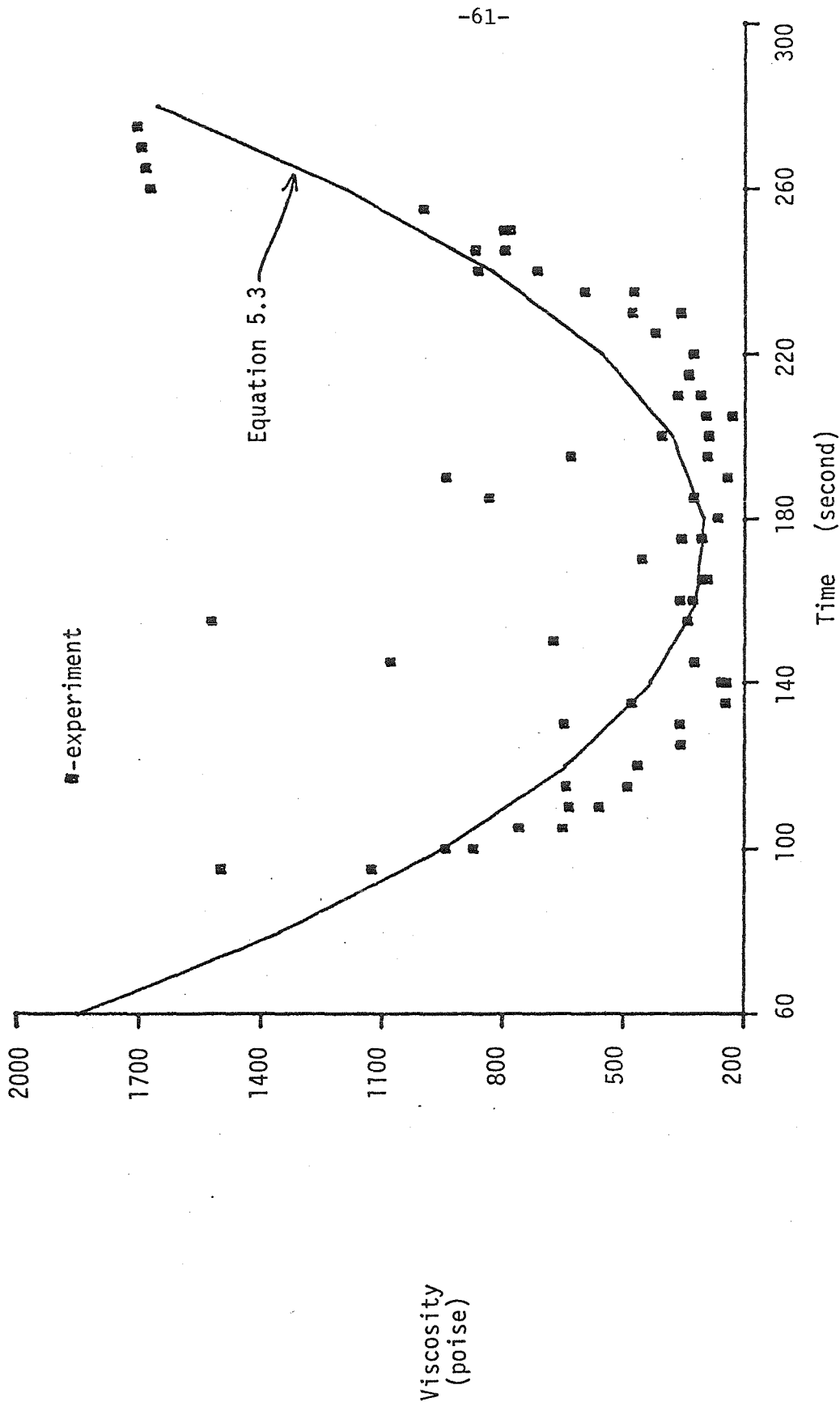


Figure 5.1. The viscosity of a Pitt 8 coal at 410 °C and a nominal pressure drop of 75 psi.

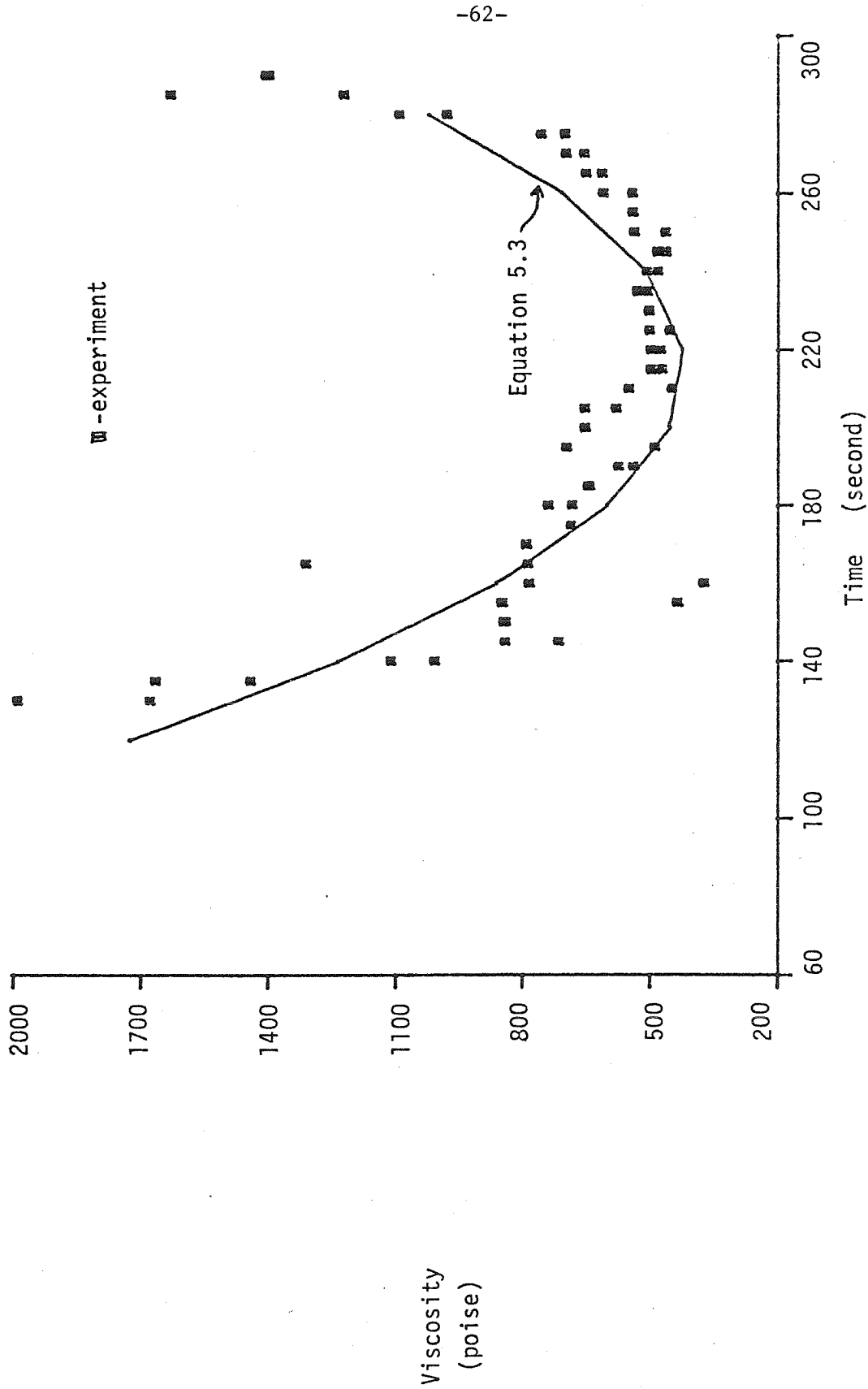


Figure 5.2. The viscosity of a Pitt 8 coal at 410 °C and a nominal pressure drop of 100 psi.

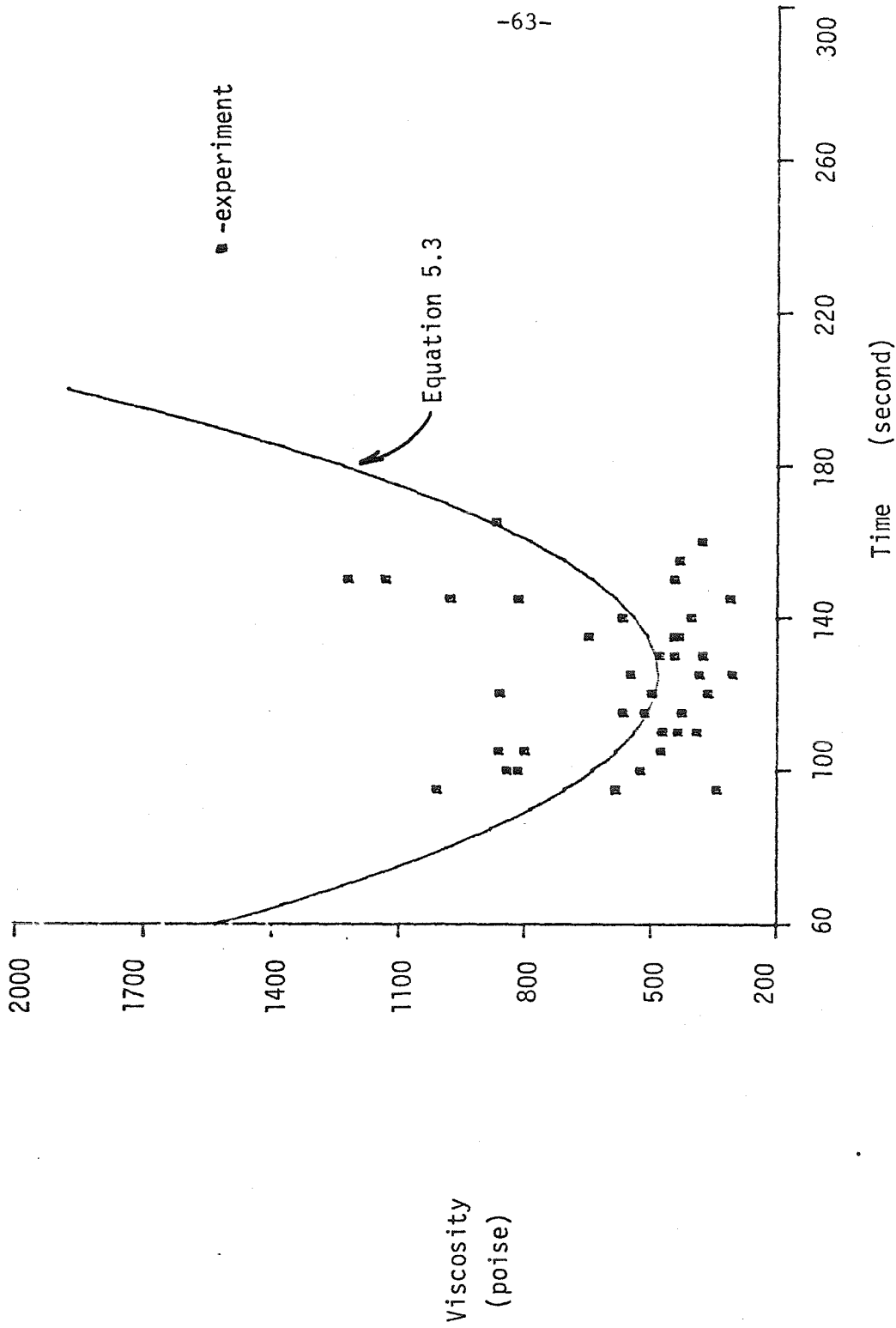


Figure 5.3. The viscosity of a Pitt 8 coal at 410 °C and a nominal pressure drop of 150 psi.

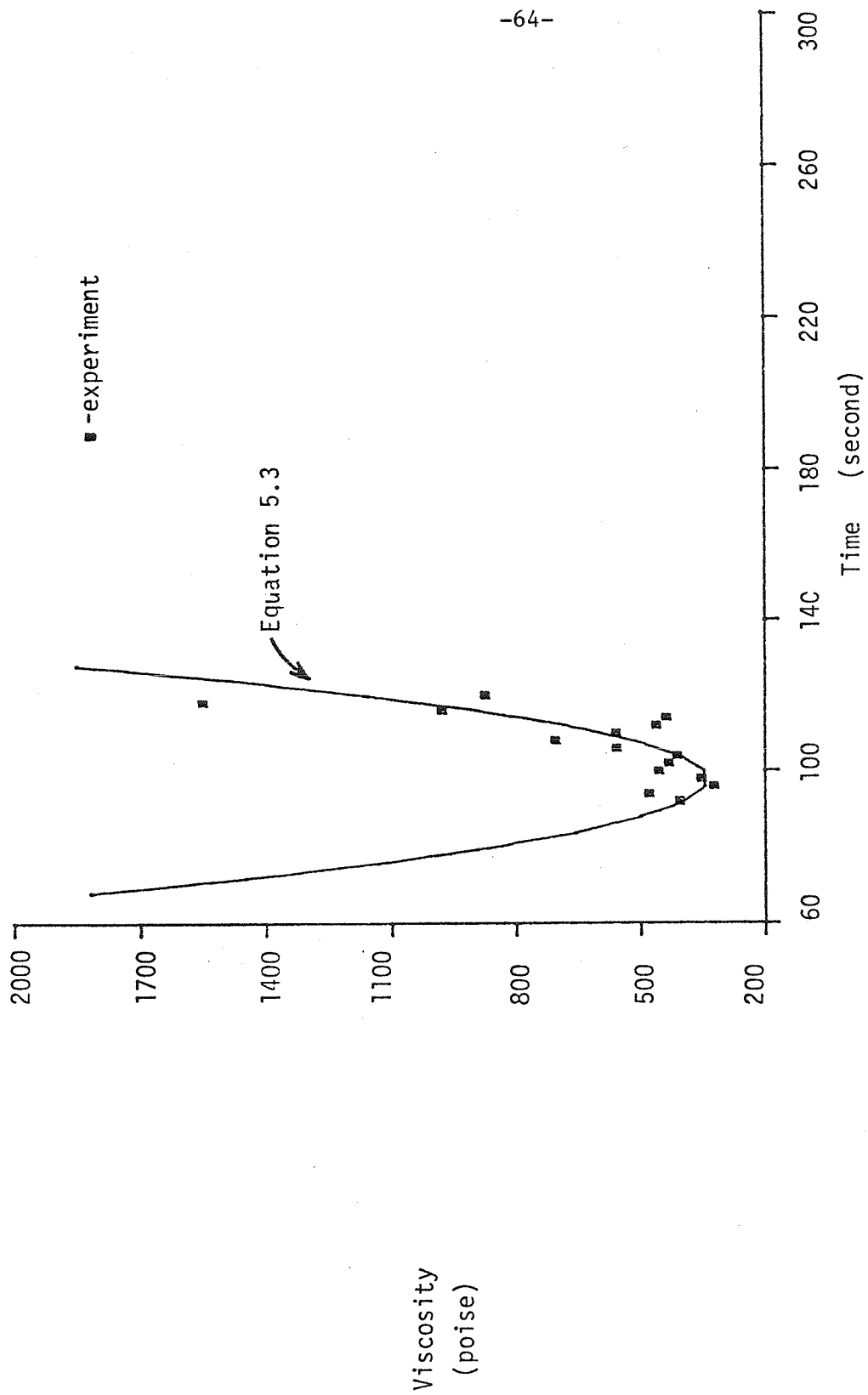


Figure 5.4. The viscosity of a Pitt 8 coal at 410 °C and a nominal pressure drop of 200 psi.

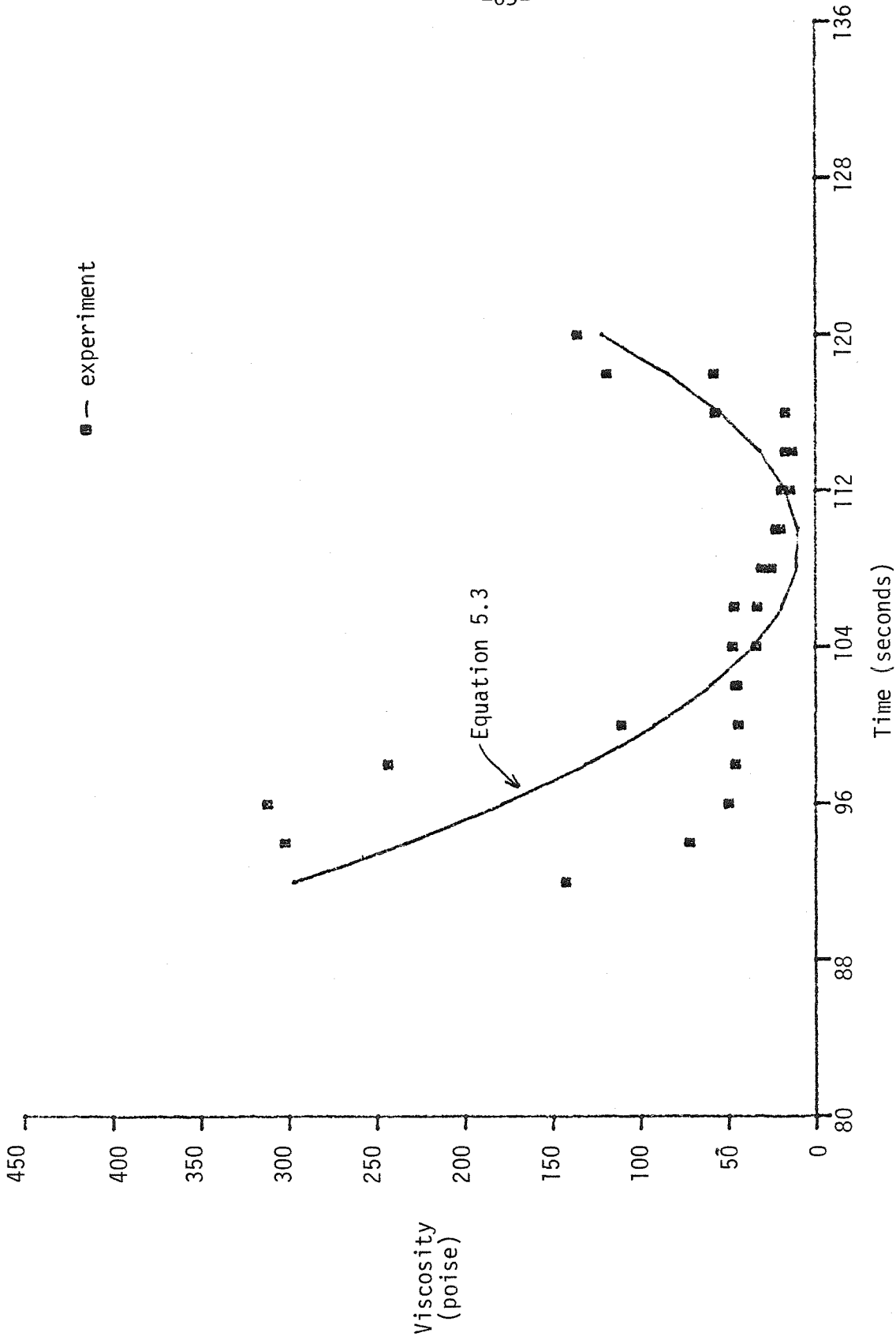


Figure 5.5 The viscosity of a Pitt 8 coal versus time at 450°C and a nominal pressure drop of 50 psi.

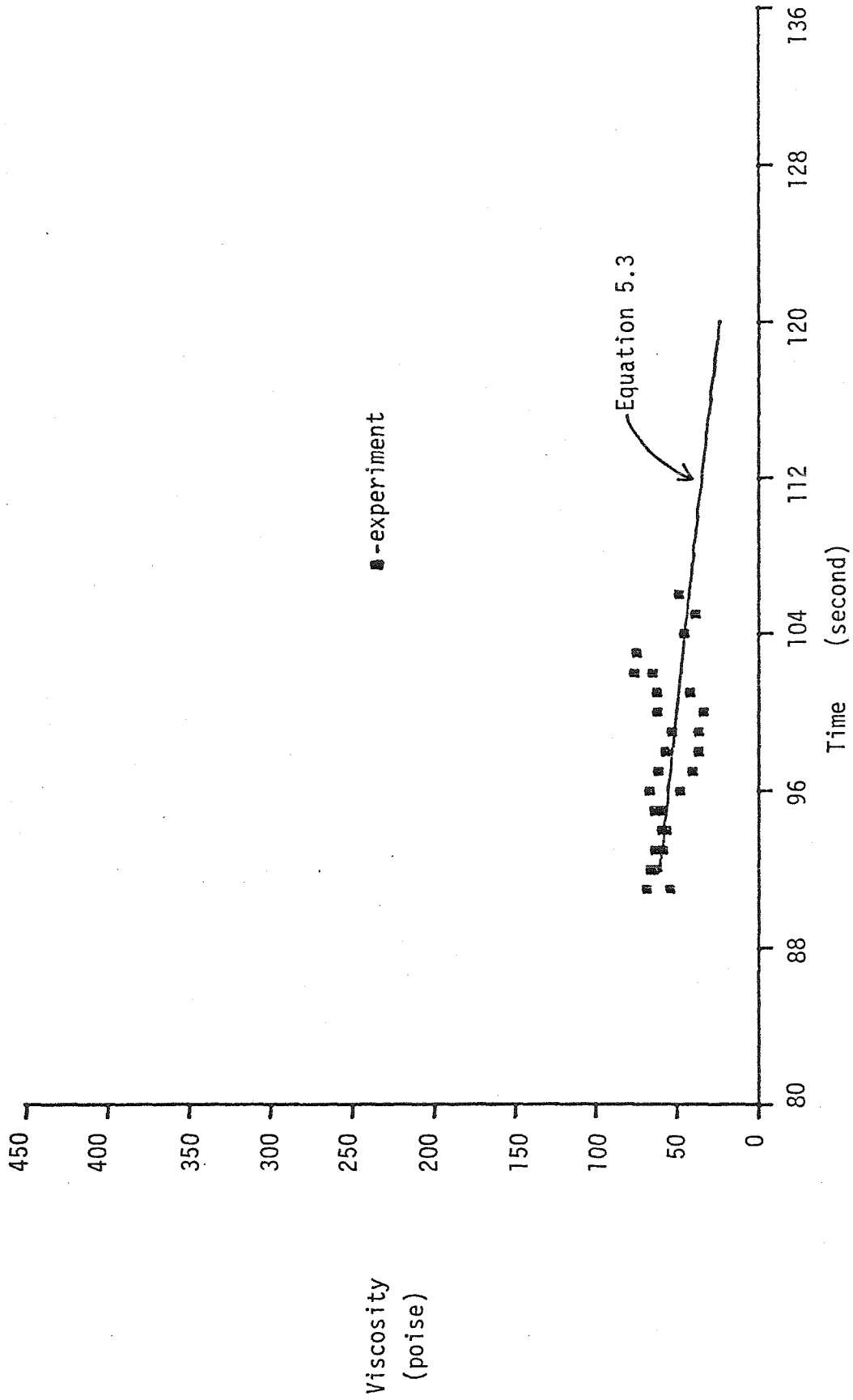


Figure 5.6. The viscosity of a Pitt 8 coal at 450 °C and a nominal pressure drop of 75 psi.

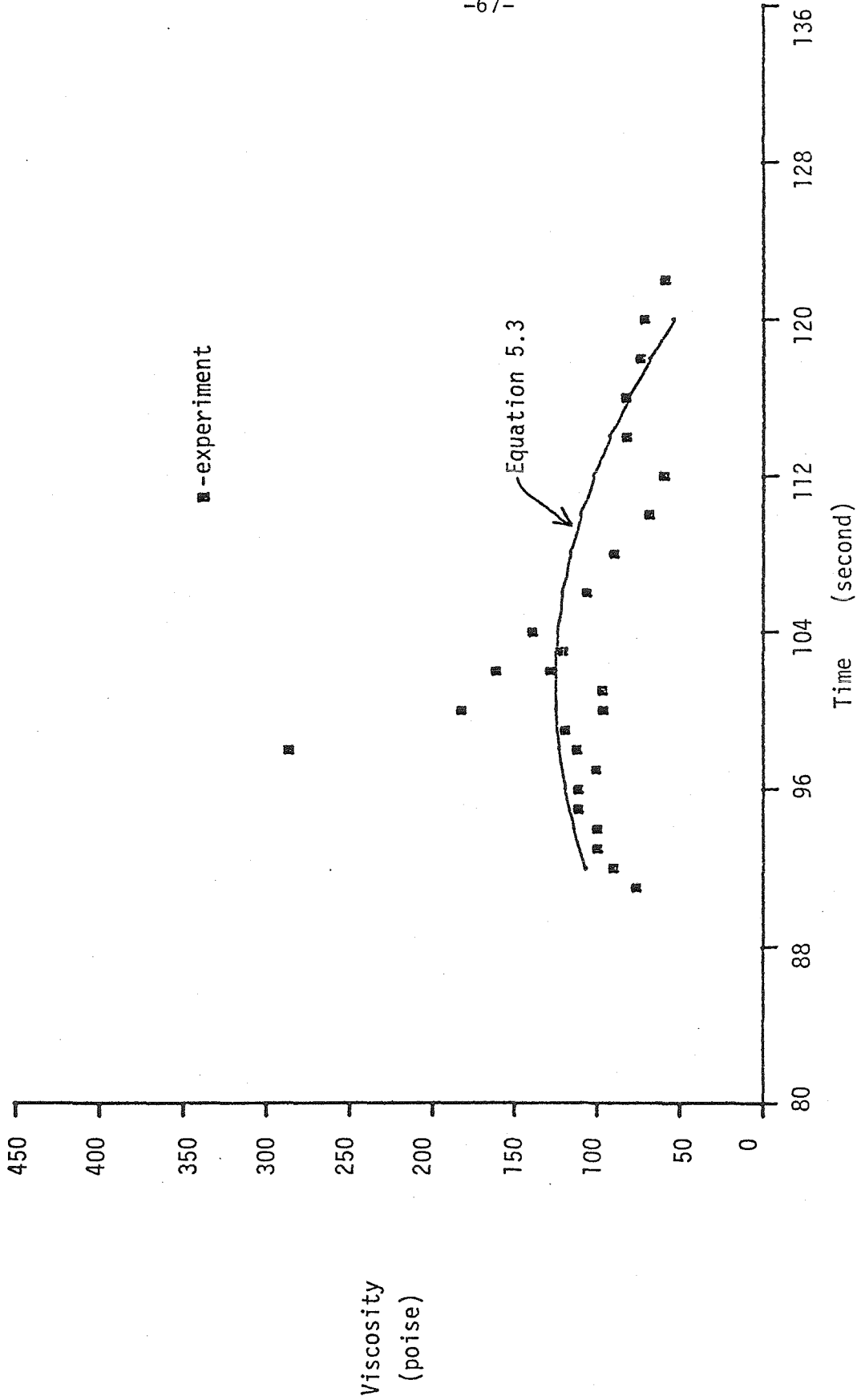


Figure 5.7. The viscosity of a Pitt 8 coal at 450 °C and a nominal pressure drop of 100 psi.

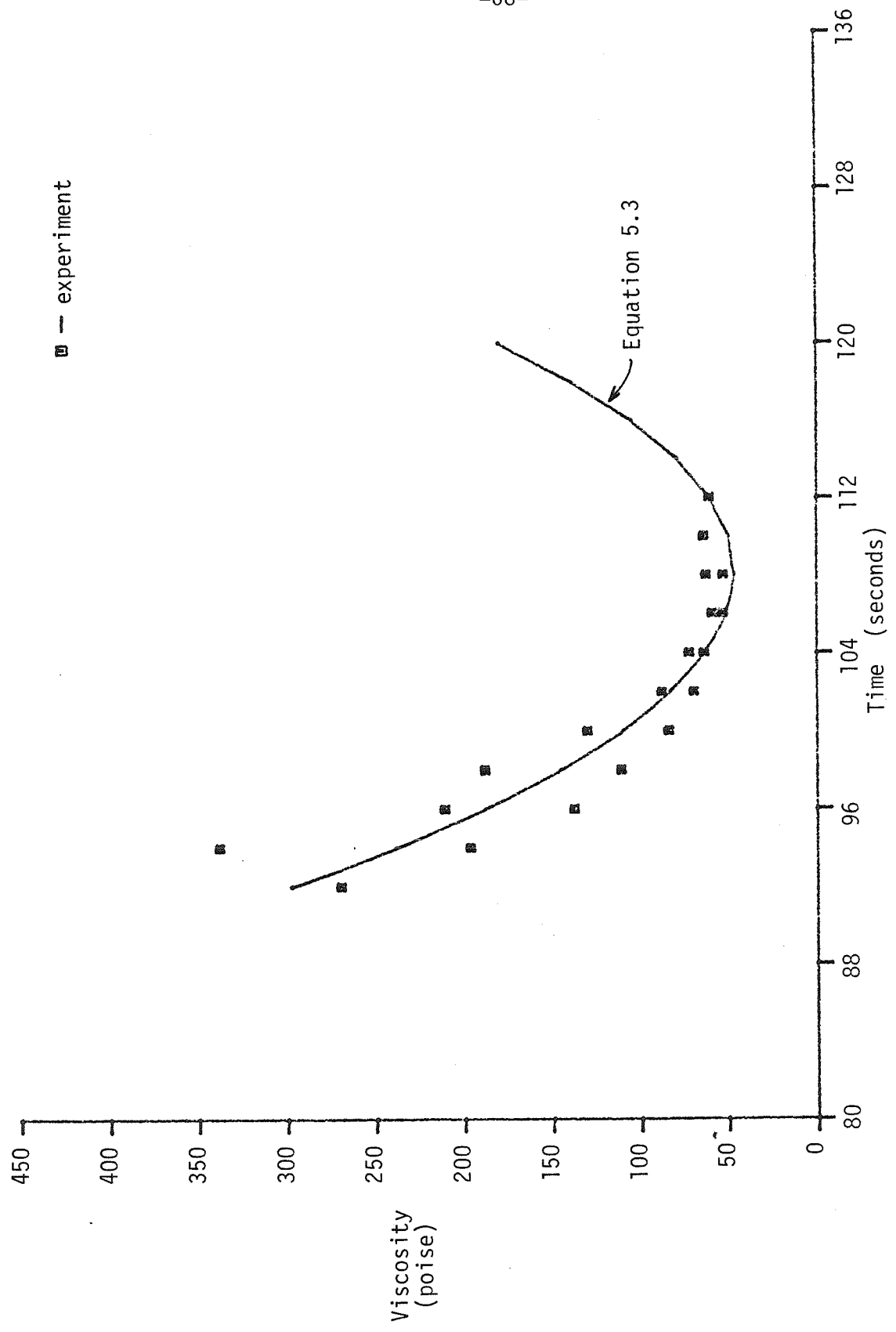


Figure 5.8 The viscosity of a Pitt 8 coal versus time at 450°C and a nominal pressure drop of 125 psi.

Table 5.1 An Empirical Fit to the Measurements of Overall Viscosity						
Temperature	Pressure	$a^*$	$b^*$	$c^*$	$t_0^*$	Standard Deviation
(°C)	(psi nominal)	(poise)	( $\frac{\text{poise}}{\text{second}}$ )	( $\frac{\text{poise}}{\text{second}^2}$ )	(second)	(poise)
410	75	296.8	-0.086	0.120	173.5	33.90
410	100	420.8	-0.422	0.143	214.0	25.24
410	150	482.6	-0.552	0.248	124.0	36.60
410	200	340.3	0.529	1.66	98.0	53.26
450	50	9.41	-0.457	0.969	109	13.74
450	75	45.0	-1.294	-0.0024	104	2.57
450	100	0.974	-10.104	-0.205	126.0	7.447
450	125	45.87	0.011	0.959	108.2	7.506

\* constants fit to Equation 5.3,  $\mu = a + b(t - t_0) + c(t - t_0)^2$

Table 5.2 The Mean, Overall Viscosity

Temperature	Pressure	Mean Viscosity	Standard Deviation	Time Range	
(°C)	(psi nominal)	(poise)	(poise)	begin	end
410	75	355.7	29.39	130	220
410	100	586.0	20.34	145	275
410	150	528.1	32.98	95	145
410	200	493.6	57.48	92	120
450	50	33.69	5.33	100	116
450	75	52.83	2.77	91	108
450	100	64.96	8.30	106	122
450	125	65.49	7.59	100	112

#### **5.4 Behavior of the Overall, Apparent Viscosity.**

Figure 5.9 displays the viscosity versus nominal pressure drop at both experimental temperatures. The behavior of the viscosity as a function of pressure drop determines the rheological classification of the fluid, Newtonian or non-Newtonian. Though the overall, apparent viscosity neglects the effects of the volume fraction of gas, which was very significant, Figure 5.9 indicates that the viscosity does not significantly vary with pressure drop. It would appear reasonable to assume that the viscosity is Newtonian within the limits of accuracy of the experimental equipment, especially for the runs at 450 °C. The large change in viscosity of approximately thirty per cent at 410 °C deserves additional comment. Reexamination of the data suggested that the lower value for the overall, apparent viscosity that was found for the run at a nominal pressure drop of 75 psi and a temperature of 410 °C was due to instabilities in the frothy regime that were excessive when compared with the instabilities found for the other runs at the same temperature. Since the overall apparent viscosity did not appear non-Newtonian within the accuracy of the experimental equipment, it would not appear reasonable to attempt to use the estimates of the viscosity of the liquid alone to classify the heated coal as Newtonian or non-Newtonian.

Figure 5.9 also displays the large change in viscosity with temperature. This viscosity reduction with temperature, which is significant within the accuracy of the equipment, may be explained as a simple physical occurrence and may be modeled by the Arrhenius equation.

#### **5.5 The Rate of the Reduction of Viscosity**

The most remarkable aspect of the flow of the heated coal was the sudden onset of flow. In contrast to the continuous viscosity reduction displayed by isothermal studies with a Geiseler plastometer by Lloyd and others <sup>5,7,8,9,12,13</sup>, the capillary-rheometer data showed a sudden and swift transition from essentially no flow to the maximum flow

rate observed. In addition, once this sudden change had occurred, the overall, apparent viscosity remained relatively constant until the end-of-the-run increase was observed. This phenomenon of sudden viscosity reduction would seem to indicate that a major structural change had occurred. Since this sudden reduction in overall viscosity occurred approximately forty to fifty seconds after isothermal conditions existed, the reduction was associated with an "induction," or waiting, period of time.

Table 5.3 displays a lower-bound estimate of the magnitude of the change of overall viscosity with time. In addition, the times at which the transition began,  $t_b$ , and ended,  $t_e$ , are given. It would appear that the viscosity reduction occurred independently of degasification rate which was estimated from the density data. An upper bound on the time rate of change of the density was available from Equation 3.6 as

$$\frac{d\rho}{dt} \leq -kb \quad (5.4)$$

where the values for  $k$  and  $b$  are available from Table 3.1. More important than the magnitude of the rate of change, however, was the continuous and slowly varying nature of the degasification reaction. It would be difficult to relate this reaction with the sudden viscosity reduction. Barnea and Mizrahi<sup>32</sup> discussed a similar reduction in the effective viscosity of a solid and liquid system when the volume fraction of solid passed a certain critical value of approximately fifty per cent. Equation 3.12 and Table 3.1 have shown, however, that the volume fraction of gas at the entrance at the onset of viscosity reduction varied from one per cent to seventy per cent. A critical volume fraction of solids, therefore, would not be expected as a cause for the sudden reduction of viscosity.

Table 5.3 An Estimate of the Time Rate of Change of Viscosity

Temperature	Pressure	run	$\frac{d\mu}{dt}$ *	$t_b$ **	$t_e$ **
(°C)	(nominal psi)		( $\frac{\text{poise}}{\text{second}}$ )	(second)	(second)
410	75	79	-36.1	95	115
410	100	77	-97.9	105	145
410	150	84	-35.5	95	110
450	50	85	-23.3	92	96
450	50	87	-32.1	94	102
450	100	90	-88.8	92	100
450	125	91	-23.4	92	100
450	125	92	-96.6	92	102

\* the rate of change of the apparent, overall viscosity with time

\*\* the beginning,  $t_b$ , and the end,  $t_e$ , of the time period in which this approximation was applied

## 5.5 Conclusion

Results of the measurements of the volumetric flow rate, temperature, pressure drop, density, and position of the piston head versus time were reported as an overall, apparent viscosity versus time at a constant temperature and pressure drop. Data were fitted to a second-order polynomial and the overall viscosity was shown to be accurately represented as constant for a specific time period. Within the accuracy of the experimental equipment the overall viscosity was Newtonian though a rheological classification based on a measurement of a multi-phase fluid is certainly inexact. The overall viscosity was a strong function of temperature. A lower-bound estimate for the time rate of change of viscosity was estimated and contrasted with the degasification rates. The change in solids content as a cause of the sudden reduction of viscosity was discounted. Finally, the measurements of the overall, apparent viscosity were compared with the fluidity data reported in the literature.

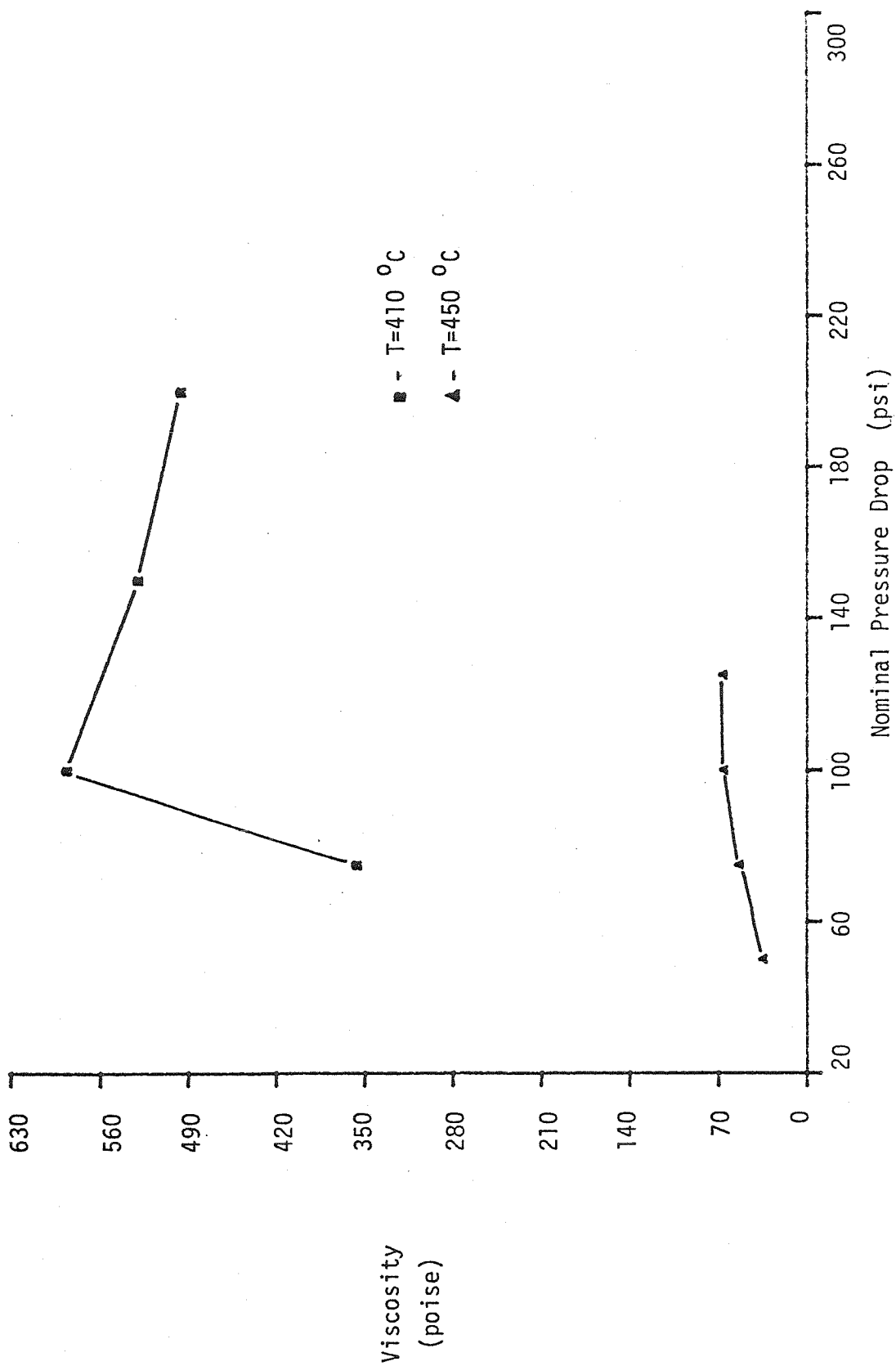


Figure 5.9. The overall viscosity of a Pitt 8 coal versus nominal pressure drop.

## **Chapter 6**

### **6.1 Introduction**

In this chapter, the complex nature of the coal melt is discussed, and a simplified model of the fluid is introduced. The major parameters of the flow are considered in light of the model and the assumptions within the model are detailed. Relevant correlations of pressure drop are reviewed, and a representational sample is detailed for use in the determination of the liquid viscosity. The Lockhart and Martinelli correlation was modified to match more closely the conditions of flow for the coal.

### **6.2 The Two-Component, Two-Phase Model**

The coal melt is a complex, heterogeneous, chemically-reacting fluid. Formation of gas produces a bubbly mixture in the reservoir that greatly complicates the rheological relationships. In addition, mineral solids are present, and perhaps some minerals are in solution. Thus the flow is at least three-phase; solid, liquid, and gas. Finally, because the amount of gas present is mainly due to chemical reactions, the density of the fluid is time dependent.

It is suggested that the correlations developed for two-component, two-phase flow would adequately provide the pressure-drop relationships necessary for an estimate of the viscosity of the liquid coal. In addition, the assumption of a frothy flow would be used in the selection of the appropriate correlations.

Before applying these correlations, some justification of the assumptions should be given. The treatment of the coal as a liquid and gas only may be checked by studying the model's representation of the data. If, in fact, the coal displays flow behavior related to the solids content, the apparent viscosity would be of a dilatant nature. If this behavior is not evident, however, then the assumption of gas-liquid flow would appear reasonable.

### 6.3 Flow Regime Determination

The coal melt in the reservoir was assumed to be a frothy or bubbly mixture of gas and liquid. This assumption was checked by examining the reservoir under the run conditions. The flow through the capillary tube must be examined, however, to determine the type of two-phase flow expected.

A recent paper by Husain et al.<sup>33</sup> reviewed the various methods of flow regime determination and presented an improved correlation for the prediction of frothy flow. Data for many different fluids including oils of relatively high viscosity were used to form and test this improved correlation. The inclusion of the high-viscosity oils indicated that the correlation would be applicable to the flow of coal melts. The correlation stated, quite simply, that the criterion for frothy flow was that the total mass velocity must exceed a certain value for frothy flow. That is, for frothy flow

$$G_T \geq 2 \times 10^6 \frac{\text{lb}}{(\text{hr ft}^2)} \quad (6.1)$$

where  $G_T$  is the total mass velocity. A analysis of the flow conditions of the coal melt showed a total mass velocity in the range of  $10^5$  to  $10^6$  lb/(hr ft<sup>2</sup>).

This range indicated that the flow was in a transition regime from frothy to slug flow. The initial frothiness of the coal in the reservoir indicated, however, that the entrance flow was frothy. The appearance of the coal at the exit suggested that the flow remained frothy throughout the capillary tube.

A reasonable interpretation of the transition flow would be to have it frothy upon entrance to the capillary tube with transition to slug flow at some point down the tube. This result can be understood physically by realizing that as the bubbles moved down the tube and experienced a reduction of pressure, the diameters of the bubbles expanded until they would attain the size of the capillary tube at which point the flow would be in the slug regime. Observation of the coal melt, however, at its exit from the capillary tube showed that it was frothy. In addition, the recordings of the piston-head movements indicated smooth motion with only the occasional spurts that might indicate slug flow.

These observations were interpreted as showing that the flow was frothy with occasional, and short-lived, transitions to slug flow. These occasional chugs were visible in the raw-data plots for the viscosity shown in Chapter 5, especially at the higher temperatures. Thus, in the following analyses and correlations, the flow was assumed to be principally frothy.

#### **6.4 Equations of Motion**

The equations of motion in Chapter 4 were specifically developed in a general manner in order to reduce the number of assumptions. The additional assumptions to be made in the two-phase, two-component model allowed a somewhat more detailed analysis.

Before considering the momentum equation, any phase-velocity differences should be addressed. A rough estimate of the relative velocity of a bubble in a liquid due to the pressure gradient was made by replacement of the hydrostatic pressure gradient in the relationship<sup>34</sup> for the buoyant velocity of a bubble at low Reynolds' number with the actual pressure gradient. The relative velocity of a bubble was a strongly increasing function of the radius of the bubble. With the radius of the bubble equal to half the radius of the capillary tube, the relative velocity of the bubble was less than 5 percent of the mean velocity of the liquid. Since the radius of a bubble in frothy flow would not be expected to be larger than half the radius of the capillary

tube, the assumption of no relative motion of the phases appeared correct.

A rigorous and systematic study of the conservation equations of two-phase flow has been undertaken within the last decade. Yadigaroglu and Lahey<sup>35</sup> have presented one form of these equations which agrees with the various developments found in the literature. It is important to link the developments of Chapter 4 with these general equations. Yadigaroglu and Lahey<sup>35</sup> gave the Lagrangian form of the momentum equation for the two-phase mixture as

$$-\frac{\partial P}{\partial z} - G - \tau_w \frac{C_f}{A_c} - E = I_L + I_G \quad (6.3)$$

where  $G$  is related to the forces arising from the gravitational field,  $C_f$  is the wetted circumference,  $E$  is the net volumetric force due to evaporation, "sometimes called the Meschersky force", and  $I_L$  and  $I_G$  are the inertia forces for the liquid and gas respectively. The inertia forces were shown to be insignificant in Chapter 4, and the buoyancy force was discussed above. Flow was considered to be two-component, thereby eliminating the evaporative term. Equation 6.3 therefore becomes

$$-\frac{\partial P}{\partial z} = \tau_w \frac{C_f}{A_c} \quad (6.4)$$

which is similar to Equation 4.50. The wetted circumference was also expressed as

$$\tau_w C_f = \tau_{wl} C_l + \tau_{wg} C_g \quad (6.5)$$

where  $\tau_{wl}$  and  $\tau_{wg}$  are the shear stresses at the wall exerted by the liquid and gas, respectively, and  $C_g$  and  $C_l$  are the circumferences touched by the gas and liquid, respectively. Equation 6.5 will be useful in a later development.

Two problems prevented the exact solution of Equation 6.4. The first problem was an exact development of the density as a function of pressure and temperature. A constitutive relationship for the density was developed in Section 7.3 that was consistent with the assumptions of the two-component, two-phase model. The second problem was involved with the definition of the volumetric-flow rate in Equations 4.38 and 4.39. The rate of strain must be known as a

function radius as well as axial position. Alternately, by using Equation 4.41, the shear stress was required as a function of radius. Equation 4.39 therefore requires a detailed knowledge of the radial distribution of the gas phase. This problem was sidestepped by taking various definitions for the mean apparent viscosity as a function of the volume fraction of gas. No further development of the equations of motion was necessary, however, in order to apply the various correlations available in the literature for two-phase pressure drop.

### **6.5 Liquid-Gas Correlations**

The two-phase flow of steam and water through pipes has been of engineering interest for many years. A search of the appropriate literature has shown that no exact solution has been obtained. Therefore, numerous correlations have been developed to help predict the pressure drop in flow of such a mixture. Idsinga et. al.<sup>36</sup>, provided a comprehensive evaluation of eighteen of these correlations. It was found that the various correlations were accurate in only very specific regions of the flow parameters such as volume fraction or Reynolds' Number. An accuracy of twenty to thirty per cent is about the best that can be expected.

Application of a steam-and-water correlation to the coal-rheology experiment presented many difficulties. The major differences between a steam-and-water flow and the flow of coal and gas were in turbulence, phase velocities, and buoyancy.

Most engineering interest has been focused on the turbulent flow of steam-and-water mixtures. The coal rheology experiment, however, was laminar in both phases, due to the relatively high viscosity of the coal. The analytical methods used for laminar flow are less complex than those used for turbulent flow and should provide a greater degree of accuracy. The historical lack of interest in the high viscosity, laminar flow of two-phase mixtures may explain why the accuracy for correlations applying to these conditions are no better than those for more difficult flow parameters.

The second principal difference in the two types of flow was the differing velocities of the phases. In steam-and-water mixtures buoyancy plays a key role in laminar flow whereas

buoyancy is not important in the flow of coal and gas. Brown and Kranich<sup>37</sup> have shown that in the laminar flow of steam and water, buoyancy is an important force for both horizontal and vertical orientations. Again, the somewhat simpler parameters of the flow of the coal mixture should, but did not, allow a more accurate correlation.

The Lockhart and Martinelli correlation<sup>38</sup> has been a standard for steam and water flows since its publication in 1949. It is felt that any study of two-component, two-phase pressure drop should be compared with this standard. The Lockhart and Martinelli correlation is based on the equation

$$\left(\frac{\Delta P}{L}\right)_{TP} = \varphi^2(\chi) \left(\frac{\Delta P}{L}\right)_l \quad (6.6)$$

where  $\left(\frac{\Delta P}{L}\right)_{TP}$  is the two-phase pressure drop,  $\varphi$  is the correlation function,  $\chi$  is the correlation variable defined below, and  $\left(\frac{\Delta P}{L}\right)_l$  is the pressure drop for the liquid flow rate alone in the same pipe. The correlation variable  $\chi$  is defined as

$$\chi \equiv \frac{\left(\frac{\Delta P}{L}\right)_l}{\left(\frac{\Delta P}{L}\right)_g} = \frac{\omega_l \rho_g \mu_l}{\omega_g \rho_l \mu_g} \quad (6.7)$$

where  $\left(\frac{\Delta P}{L}\right)_g$  is the pressure drop for the gas-flow rate alone,  $\omega$  is the mass-flow rate for the liquid or gas,  $\rho$  is the density for the liquid or gas, and  $\mu$  is the viscosity for the liquid or gas. The Lockhart and Martinelli correlation was used by selecting the appropriate  $\chi$  based on the flow conditions, determining the appropriate value of  $\varphi$  from the correlation, and then using Equation 6.6. Since  $\chi$  is directly proportional, however, to the density of the gas, this model is based on the assumption of an incompressible gas phase. The gas density is then determined by the 'average' pressure. Since the pressure distribution is unknown and probably non-linear, this 'average' pressure is somewhat nebulous.

The variable of correlation for the correlation of Lockhart and Martinelli<sup>38</sup> was given by Equation 6.7 as

$$\chi = \frac{\omega_l \rho_g \mu_l}{\omega_g \rho_l \mu_g} \quad (6.8)$$

Since

$$\frac{\omega}{\rho} = \frac{\rho Q}{\rho} = Q \quad (6.9)$$

and

$$Q_l = \alpha_l Q \quad Q_g = \alpha_g Q \quad , \quad (6.10)$$

the correlation variable of Equation 6.8 becomes

$$\chi = \frac{\alpha_l \mu_l}{\alpha_g \mu_g} \quad (6.11)$$

The correlation itself was given in Equation 6.6 as

$$\left( \frac{\Delta P}{L} \right)_{TP} = \varphi^2(\chi) \left( \frac{\Delta P}{L} \right)_l \quad (6.12)$$

The pressure gradient for the two-phase mixture was given by the length of the capillary tube and the pressure drop, and was expressed in Chapter 4 as Equation 4.51, the defining equation for the overall, apparent viscosity. The pressure gradient of the liquid alone is given as

$$\left( \frac{\Delta P}{L} \right)_l = \frac{8 \mu_l Q_l}{\pi r_o^4} \quad (6.13)$$

Substitution of Equations 6.13, 6.10, and 4.51 into Equation 6.12 gives

$$\mu_l = \frac{\mu}{\varphi^2(\chi) \alpha_l} \quad (6.14)$$

Equation 6.14 was solved in an iterative manner by first estimating  $\chi$ , computing  $\mu_l$  from Equation 6.14, and then estimating a new  $\chi$  from Equation 6.11. The viscosity of the gas was taken to be the viscosity of methane at the run temperature. The volume fractions were taken to be the values at the entrance to the capillary tube.

Table 6.1 displays the results of the application of the correlation of Lockhart and Martinelli to the overall-viscosity data of Chapter 5. Due to the large magnitude of the ratio of the

estimated viscosity of the liquid to the viscosity of the gas, the values of  $\chi$  were always greater than the range of the correlation. The value of  $\phi$  used, therefore, was based on the largest given value of  $\chi$ .

The inadequateness of applying conventional steam-water correlations to the flow of heated coal is exemplified by the Lockhart and Martinelli correlation. The magnitude of  $\chi$ , as given in Equation 6.11, was much larger than steam-water, or even most oil-water flows. The application of the correlation of Lockhart and Martinelli was, therefore, considered to be only an estimate of the viscosity of the liquid.

Table 6.1 An Estimate of the Viscosity of the Liquid				
Based on the Correlation by Lockhart and Martinelli <sup>38</sup>				
Temperature	Pressure	$\alpha_g  _{in}^*$	Overall Viscosity	Liquid Viscosity
(°C)	(psi nominal)		(poise)	(poise)
410	75	0.41	356	490
410	100	0.33	586	710
410	150	0.14	528	498
410	200	0.01	494	404
450	50	0.68	34	86
450	75	0.47	53	87
450	100	0.42	65	91
450	125	0.19	65	65

\* the volume fraction of gas at the time period defined in Table 5.2 and evaluated at the entrance to the capillary tube.

The assumption of an incompressible gas phase was appropriate to the types of flows that were used for the correlation. In the coal rheology experiment, however, pressure drops were observed which were much greater than those used by Lockhart and Martinelli. Therefore, it was proposed that the two-phase pressure drop given by Lockhart and Martinelli,  $(\frac{\Delta P}{L})_{TP}$ , be approximated as

$$(\frac{\Delta P}{L})_{TP} \approx \frac{dP}{dz} \quad (6.15)$$

and then Equation 6.6 becomes

$$\frac{dP}{dz} = \varphi^2(\chi) (\frac{\Delta P}{L})_l \quad (6.16)$$

From Equation 6.7

$$\chi = k_3 P \quad (6.17)$$

where the density of the gas was assumed to follow the ideal gas law,  $P$  is the pressure, and  $k_3$  is defined as

$$k_3 = \frac{\omega_l \mu_l}{\omega_g \mu_g R T} \quad (6.18)$$

where  $R$  is the specific gas constant, and  $T$  is the absolute temperature. Thus, from Equation 6.17

$$d\chi = k_3 dP \quad (6.19)$$

and substitution of Equations 6.15 and 6.19 into Equation 6.6 yields

$$\frac{dP}{\varphi^2(\chi)} = \frac{d\chi}{k_3 \varphi^2(\chi)} = (\frac{\Delta P}{L})_l dz \quad (6.20)$$

Rearranging and then integrating over the length of the pipe,  $L$ , gives

$$\int_{\chi(0)}^{\chi(L)} \frac{d\chi'}{\varphi^2(\chi')} = k_3 (\frac{\Delta P}{L})_l L \quad (6.21)$$

where  $\chi(0)$  is the initial condition. Equation 6.21 was solved in an iterative manner by

estimating  $\chi$  at the entrance and exit, solving for the viscosity in  $k_3$ , and then using the new value of the viscosity for a better estimate of the range of the integration. This modification was similar to the correlation of Martinelli and Nelson<sup>45</sup>, which was developed for the flow of boiling water. Once again, the magnitude of  $\chi$ , as given in Equation 6.11, was much larger than what it would be for steam-water, or even most oil-water flows. The application of this modified correlation of Lockhart and Martinelli was not, therefore, applied to the viscosity data.

Husain et. al.<sup>33</sup> recently compiled a review of the various theories and correlations for frothy pressure drop. In addition to presenting their own pressure-drop theory, they computed the average fractional deviation and the standard deviation of these various correlations by applying these correlations to the data bank of pipeline pressure drops compiled by Mandhane et. al.<sup>39</sup>. For volume fractions of gas less than 0.5, the correlation of Happel<sup>40</sup> developed for the viscosity of suspensions of solid spheres provides the best prediction of pressure drop. Happel's correlation is

$$\mu_{TP} = \mu_l e^{\frac{2.5\alpha_g}{1 - \frac{39\alpha_g}{64}}} \quad (6.22)$$

where  $\mu_{TP}$  is the viscosity of the two-phase mixture,  $\alpha_g$  is the volume fraction of gas, and  $\mu_l$  is the viscosity of the liquid. Equation 6.22 was used to provide one estimate of the viscosity of the liquid based on the overall viscosity found in Chapter 5 and the volume fraction of gas found in Chapter 3. It should be noted that the estimate based on Happel used the entrance conditions for the volume fraction of gas and therefore neglected the change of volume fraction of gas with axial position. Since Happel's correlation was developed for solid and liquid flow, it is surprising that this correlation gave the best results for liquid and gas.

The correlation developed by Happel, Equation 6.22,

$$\mu_{TP} = \mu_l e^{\frac{2.5\alpha_g}{1 - \frac{39\alpha_g}{64}}} \quad (6.23)$$

was applied to the viscosity data based on the volume fraction of gas at the inlet,  $\alpha_g|_{in}$ ; and

based on an estimate of the length-averaged volume fraction of gas,  $\bar{\alpha}_g$ . The length-averaged volume fraction of gas was estimated as

$$\bar{\alpha}_g = \frac{\alpha_g|_i + \alpha_g|_o}{2} \quad (6.24)$$

where  $\alpha_g|_o$  is the volume fraction of gas at the exit of the capillary tube. The volume fraction of gas at the exit was calculated from the estimate of the density at the exit of the capillary tube. Table 6.2 shows the application of the correlation developed by Happel to the viscosity data.

The estimates of the volume fraction of gas showed that the optimum range for Happel's correlation had been exceeded, especially for the runs at the higher temperature. It is important to note, however, that the effect of a solid phase on the flow behavior of the liquid is given by Happel's correlation. The volume fraction of gas might be increased by the volume of a solid phase with minimal effect on the estimates of the viscosity of the liquid since the volume fraction of gas was large.

Table 6.2 An Estimate of the Viscosity of the Liquid					
Based on the Correlation by Happel <sup>40</sup>					
Temperature	Pressure	$\alpha_g _{in}$ *	$\bar{\alpha}_g$ *	$\mu_l(\alpha_g _{in})$ *	$\mu_l(\bar{\alpha}_g)$ *
(°C)	(nominal psi)			(poise)	(poise)
410	75	0.41	0.56	91	41
410	100	0.33	0.52	212	86
410	150	0.14	0.43	365	124
410	200	0.01	0.37	476	151
450	50	0.68	0.74	1.87	1.17
450	75	0.47	0.64	12.5	4.72
450	100	0.42	0.61	15.9	5.74
450	125	0.19	0.50	38.0	10.8

\* nomenclature:

$\alpha_g|_{in}$  the volume fraction of gas at the time period defined in Table 5.2 and evaluated at the entrance to the capillary tube.

$\bar{\alpha}_g$  the length-averaged volume fraction of gas as given in Equation 6.24.

$\mu_l(\alpha_g|_{in})$  estimated viscosity of the liquid based on the volume fraction of gas at the entrance.

$\mu_l(\bar{\alpha}_g)$  estimated viscosity of the liquid based on the length-averaged volume fraction of gas.

For volume fractions of gas greater than 0.5, Husain<sup>33</sup> recommends a modification of Happel's correlation as follows

$$\mu_{TP} = \mu_g + (\mu_c - \mu_g) \left( \frac{1}{\alpha_g} - 1 \right)^3 \quad (6.25)$$

where

$$\mu_c \equiv \mu_l e^{\frac{2.5\alpha_g}{1 - \frac{39\alpha_g}{64}}} \Big|_{\alpha_g=0.5} = 6.036 \mu_l \quad (6.26)$$

Substitution of Equation 6.26 into Equation 6.25 gives

$$\mu_l = \left( \frac{\mu_{TP} - \mu_g}{\left( \frac{1}{\alpha_g} - 1 \right)^3} + \mu_g \right) / 6.036 \quad (6.27)$$

Table 6.3 shows the application of the modification by Husain of the correlation developed by Happel to the viscosity data.

Table 6.3 An Estimate of the Viscosity of the Liquid					
Based on the Correlation by Husain <sup>83</sup>					
Temperature	Pressure	$\alpha_g  _{in}^*$	$\bar{\alpha}_g^*$	$\mu_l(\alpha_g  _{in})^*$	$\mu_l(\bar{\alpha}_g)^*$
(°C)	(nominal psi)			(poise)	(poise)
410	75	0.41	0.56	19	121
410	100	0.33	0.52	11	123
410	150	0.14	0.43	0.38	37
410	200	0.01	0.37	-	16
450	50	0.68	0.74	54	130
450	75	0.47	0.64	6.1	49
450	100	0.42	0.61	4.1	41
450	125	0.19	0.50	-	11

\* nomenclature:

$\alpha_g |_{in}$  the volume fraction of gas at the time period defined in Table 5.2 and evaluated at the entrance to the capillary tube.

$\bar{\alpha}_g$  the length-averaged volume fraction of gas as given in Equation 6.24.

$\mu_l(\alpha_g |_{in})$  estimated viscosity of the liquid based on the volume fraction of gas at the entrance.

$\mu_l(\bar{\alpha}_g)$  estimated viscosity of the liquid based on the length-averaged volume fraction of gas.

## 6.6 Conclusion

The complex, multi-phase, multi-component flow of heated coal was considered to be a simple, two-component, liquid and gas flow. The flow regime was calculated to be in transition from frothy to slug flow but because of the unusual conditions of the flow of coal the flow regime was considered frothy. Various correlations were applied to the overall-viscosity data in order to estimate the viscosity of the liquid. The inadequacies of these correlations were related to the parameters of the flow and, as demonstrated by Table 6.4, the predictions of the viscosity of the liquid were somewhat erratic. The Lockhart and Martinelli correlation was modified to match more closely the conditions of flow for the coal.

Table 6.4 A Summary of the Estimates of the Viscosity of the Liquid					
Temperature	Pressure	Overall	Viscosity Estimate		
		Viscosity	L and M *	Happel <sup>40</sup>	Husain <sup>83</sup>
(°C)	(nominal psi)	(poise)	(poise)	(poise)	(poise)
410	75	356	490	41	121
410	100	586	710	86	123
410	150	528	498	124	37
410	200	494	404	151	16
450	50	34	86	1.2	130
450	75	53	81	4.7	49
450	100	65	91	5.7	41
450	125	65	65	11	11

\* Lockhart and Martinelli<sup>88</sup>

## Chapter 7

### 7.1 Introduction

In this chapter, a detailed model of the density was developed and then applied to the density measurements. The equations of motion were established with the use of the density model. A mean-apparent viscosity was defined, and the momentum equation was solved in closed form for the determination of the viscosity of the liquid.

### 7.2 The Two-Component, Two-Phase Model

It is suggested that a two-component, two-phase model composed of an ideal gas and an incompressible liquid would adequately provide the rheological relationships necessary for a quantitative measurement of the viscosity of the liquid coal. In addition, the assumptions of a frothy flow and a density as a function of only pressure and time at constant temperature, would be used in the analysis of this model fluid.

As was discussed in Chapter 4, the time dependence of the density was important in the continuity equation but not the momentum equation. Once the mass fraction of gas had been determined at the entrance of the capillary tube, the important changes in density down the tube were caused by the reduction in pressure, not by devolatilization. The residence time of approximately four tenths of a second rein-

forced this assumption. The assumption of frothy flow was discussed in Chapter 6.

### 7.3 Density Model

As was stated in Section 6.4, the equations of motion could not be developed further without a constitutive relationship for the density. For the conditions of time, temperature, and pressure in the coal-rheology experiment, the system was a chemically-reacting, and consisted of three phases, a solid, a liquid, and a gas. To simplify the heterogeneous nature of the system, the density model considered the fluid to be an incompressible liquid and an ideal gas. Though the gas, in particular, was a mixture of many different products, it was treated as a single gas with an average molecular weight. Additionally, a mean solubility was considered as a function of time and temperature. The phases were considered to be at the same pressure, thereby neglecting any forces due to surface tension. With these simplifications, the system was treated as a two-phase, two-component mixture with three degrees of freedom. Thus, at equilibrium, the density would be completely determined by three independent properties. By specifying an equation of state, however, for the simplified two-component system, the density could be determined by two properties, say temperature and pressure, at any given time. The non-equilibrium factors were initially neglected. The density of the model fluid was therefore given by

$$\rho = \frac{\rho_l \left(1 + \frac{\tau_g}{1 - \tau_g}\right)}{\frac{\tau_g}{1 - \tau_g} \frac{P^*}{P} + 1} \quad (7.1)$$

where  $\rho$  is the density,  $P$  is the pressure,  $\rho_l$  is the density of the liquid,  $\tau_g$  is the mass fraction of gas not in solution, and  $P^*$  is defined as

$$P^* \equiv \rho_l R^* T \quad (7.2)$$

here  $T$  is the temperature, and  $R^*$  is the specific gas constant for the average behavior of the gas products. Equation 7.1 is similar to a development by Ryason and Lewis<sup>41</sup>.

The model given by Equation 7.1 estimated the mass fraction of gas not in solution with the assumption that the change in the overall density was due to a gas phase which occupied a volume predicted by the ideal-gas law at equilibrium and with no surface tension. The mass fraction of gas not in solution at a certain time and temperature was found to vary with pressure. A total mass fraction of gas,  $r_t$ , was therefore assumed to be both a function of temperature and time only, and expressible as a function of a solubility constant which also was a function of time and temperature only. That is, the mass fraction of gas not in solution was given by

$$r_g(T, P, t) = r_t(T, t) - s(T, t) \times P \quad (7.3)$$

where  $r_t$ , the total mass fraction of gas, and  $s$ , the solubility constant, were functions of temperature and time. This model considered the gas in solution to occupy an insignificant volume. The density of the liquid was available from the measurements given in Chapter 3. It should be noted that this model in its present form was only applicable when there was gas present in excess of the solubility limit. For this reason, the model was only applied to densities significantly less than the density of the liquid. In addition, if the reservoir contained gas in solution only, the difficulties presented by the change in solubility with pressure as the coal moved down the tube would lead to a critical point, where some gas would suddenly come out of solution. The difficulties of such a flow situation was discussed in detail by C. D. Han et. al.<sup>42</sup>, and such a flow situation was studiously avoided in this investigation.

The mass fraction of gas was expected to be small so that Equation 7.1 was simplified to

$$\rho = \frac{\rho_l(1+r_g)}{\frac{r_g P^*}{P} + 1} \quad (7.4)$$

Tables 7.1 and 7.2 present the applications of Equation 7.4 to the density data at 410°C and 450°C respectively.

Table 7.1 Estimate of the Mass Fraction of Gas in the Reservoir at 410 °C			
Time	Total Mass	Solubility Constant	Mean Molecular
(seconds)	Fraction of Gas	$(\frac{cm^2}{dyne} \times 10^{10})$	Weight
90	0.00079	0.050	1
100	0.0016	0.103	2
110	0.0024	0.148	3
120	0.0031	0.191	4
130	0.0039	0.229	5
140	0.0039	0.222	5
150	0.0081	0.443	10
160	0.0082	0.432	10
170	0.0121	0.608	15
180	0.0177	0.872	20
190	0.0227	1.085	25
200	0.0280	1.297	30
250	0.0490	1.866	55
300	0.0775	2.444	80

Table 7.2 Estimate of the Mass Fraction of Gas in the Reservoir at 450 °C			
Time	Total Mass	Solubility Constant	Mean Molecular
(seconds)	Fraction of Gas	( $\frac{cm^2}{dyne} \times 10^{10}$ )	Weight
90	0.010	0.898	6
100	0.020	1.65	11
110	0.030	2.41	16
120	0.031	2.38	16
130	0.031	2.35	16
140	0.032	2.15	17
150	0.032	2.25	16
160	0.034	2.27	16
170	0.035	2.25	16
180	0.036	2.21	16
190	0.036	2.15	16
200	0.036	2.05	16
250	0.044	1.71	20
300	0.050	0.68	25

In the reservoir, the mass fraction of gas changed slowly at constant pressure and temperature and therefore allowed equilibrium modeling of the solubility. For the modeling of the mass fraction of gas in the capillary tube, the residence time of less than a half of a second precluded an equilibrium calculation of the solubility. Thus, for the density model applied within the capillary tube, the mass fraction of gas was considered constant for two reasons. First, as previously discussed, the production of gas due to devolatilization was considered insignificant within the capillary tube due to the short residence time and small volume. Second, again due to the short residence time, the change in the mass fraction of gas not in solution due to the pressure change was not considered significant. Thus, the mass fraction of gas not in solution throughout the capillary tube was taken to be the value found at the entrance to the tube at a given temperature, pressure, and time.

#### 7.4 Viscosity Model

The two-component, two-phase model of the coal melt combined with the density model and a definition of mean-apparent viscosity allowed an approximate solution of the equations of motion.

The result of the force balance in Chapter 4 produced Equation 4.35

$$-(P_o - P_i)A_c = C \int_0^L \tau_w dz \quad (7.5)$$

or, in differential form

$$-\frac{dP}{dz} \frac{A_c}{C} = \tau_w(z) \quad (7.6)$$

Additionally, Equation 4.39 for the volumetric flow rate gave

$$Q = -2\pi \int_0^{r_o} \frac{\partial u}{\partial r} \frac{r^2}{2} dr \quad (7.7)$$

By assuming a mean-apparent viscosity,  $\bar{\mu}$ , such that

$$\bar{\mu} = \frac{\tau}{-\frac{\partial u}{\partial r}} \quad (7.8)$$

where  $\bar{\mu}$  is a function of axial and radial position, Equation 7.7 may be written as

$$Q = 2\pi \int_0^{r_0} \frac{\tau}{\bar{\mu}} \frac{r^2}{2} dr \quad (7.9)$$

As in Chapter 4, any non-Newtonian behavior of the fluid should be evident from various runs at different pressures.

By use of Equation 4.44, Equation 7.9 may be written as

$$Q = 2\pi \int_0^{r_0} \frac{\tau_w}{\bar{\mu}} \frac{r^3}{2r_0} dr \quad (7.10)$$

The shear stress at the wall,  $\tau_w$ , was taken outside of the integral. In addition, the mean-apparent viscosity was assumed to be a function of gas and liquid viscosities and volume fractions of gas and liquid. Since frothy flow was assumed, the volume fractions were not considered to be functions of radial position. These assumptions neglect any bubble migrations. Thus, Equation 7.10 simplifies to

$$Q = \frac{\pi \tau_w}{\bar{\mu} r_0} \int_0^{r_0} r^3 dr \quad (7.11)$$

or

$$Q = \frac{\pi \tau_w r_0^3}{4\bar{\mu}} \quad (7.12)$$

where  $Q$ ,  $\tau_w$ , and  $\bar{\mu}$  are functions of axial position only. Rearranging Equation 7.12 for  $\tau_w$  yields

$$\tau_w = \frac{4\bar{\mu}Q}{\pi r_0^3} \quad (7.13)$$

and substituting Equation 7.9 into Equation 7.6 produces

$$-\frac{dP}{dz} \frac{A_c}{C} = \frac{4\bar{\mu}Q}{\pi r_o^3} \quad (7.14)$$

Since

$$A_c = \pi r_o^2 \quad (7.15)$$

and

$$C = 2\pi r_o \quad (7.16)$$

Equation 7.14 simplifies to

$$-\frac{dP}{dz} = \frac{8\bar{\mu}Q}{\pi r_o^4} \quad (7.17)$$

Equations 4.16 and 4.17 allow the volumetric flow rate to be written as

$$Q(z) = \frac{\dot{m}}{\rho(z)} \quad (7.18)$$

Substitution of Equation 7.4, the density model, gives

$$Q(z) = \frac{\dot{m} \left( \frac{r_g P^*}{P} + 1 \right)}{\rho_l (1 + r_g)} \quad (7.19)$$

where the mass fraction of gas not in solution,  $r_g$ , was considered constant. A combination of Equations 7.19 and 7.17 produces

$$-\frac{dP}{dz} = \frac{8\bar{\mu}}{\pi r_o^4} \frac{\dot{m} \left( \frac{r_g P^*}{P} + 1 \right)}{\rho_l (1 + r_g)} \quad (7.20)$$

Finally, the mean-apparent viscosity was taken to be

$$\bar{\mu} \equiv \alpha_g \mu_g + \alpha_l \mu_l \quad (7.21)$$

Additional possible forms of the mean-apparent viscosity, such as a form used successfully by McAdams<sup>43</sup>, were also considered. Though these alternate forms for the mean viscosity also lead to closed-form solutions of the momentum equation, applica-

tion of these solutions to the data was difficult and these forms of the solution were not considered as accurate nor as appropriate as the solution generated by Equation 7.21.

The substitution of Equation 7.21 in Equation 7.20 gave

$$-\frac{dP}{dz} = \frac{8\dot{m}_L}{\pi r_o^4} \frac{\left(\frac{\tau_g P^*}{P} + 1\right)}{\rho_l(1+\tau_g)} (\alpha_g \mu_g + \alpha_l \mu_l) \quad (7.22)$$

Use of Equation 7.4 to form the volume fractions leads to

$$\alpha_l = \frac{1}{1 + \frac{\tau_g P^*}{P}} \quad (7.23)$$

and

$$\alpha_g = \frac{\frac{\tau_g P^*}{P}}{1 + \frac{\tau_g P^*}{P}} \quad (7.24)$$

Substitution of these results into Equation 7.22 produces

$$-\frac{dP}{dz} = \frac{8\dot{m}_L \mu_l}{\pi r_o^4 \rho_l (1+\tau_g)} \left( \frac{\tau_g P^*}{P} \frac{\mu_g}{\mu_l} + 1 \right) \quad (7.25)$$

Defining

$$-k_1 \equiv \frac{8\dot{m}_L \mu_l}{\pi r_o^4 \rho_l (1+\tau_g)} \quad (7.26)$$

and

$$k_2 \equiv \frac{\tau_g P^* \mu_g}{\mu_l} \quad (7.27)$$

where  $k_1$  and  $k_2$  are not functions of axial or radial position, and using these definitions, Equation 7.25 becomes

$$\frac{dP}{dz} = k_1 \left( 1 + \frac{k_2}{P} \right) \quad (7.28)$$

Rearrangement and integration by parts yields

$$\int \left( 1 - \frac{k_2}{P+k_2} \right) dP = \int k_1 dz + C_1 \quad (7.29)$$

or

$$P - k_2 \ln(P+k_2) = k_1 z + C_1 \quad (7.30)$$

where  $C_1$  is a constant of integration. Applying the boundary condition

$$P = P_i \quad \text{at} \quad z = 0 \quad (7.31)$$

gives

$$C_1 = P_i - k_2 \ln(P_i + k_2) \quad (7.32)$$

Additionally, since

$$P = P_o \quad \text{at} \quad z = L \quad (7.33)$$

Equation 7.30 becomes

$$P_o - k_2 \ln(P_o + k_2) = k_1 L + C_1 \quad (7.34)$$

Substitution of Equation 7.32 for  $C_1$  gives

$$P_o - k_2 \ln(P_o + k_2) = k_1 L + P_i - k_2 \ln(P_i + k_2) \quad (7.35)$$

or

$$P_o - P_i - k_2 \ln \left( \frac{P_o + k_2}{P_i + k_2} \right) = k_1 L \quad (7.36)$$

Examination of the definitions of  $k_1$  and  $k_2$  in Equations 7.26 and 7.27 shows that the only unknowns in Equation 7.36 are the viscosities of the liquid and the gas. The viscosity of the gas was taken to be the viscosity of methane at that temperature, as was done in Chapter 6.

In order to most easily apply Equation 7.36, a rearrangement of Equation 7.26 was made by substitution of the definition of the overall, apparent viscosity . That is, since

$$\dot{m} = \frac{\rho_r \pi r_o^4}{8\mu} \left( \frac{\Delta P}{L} \right) \quad (7.37)$$

from Equation 5.2, Equation 7.26 becomes

$$k_1 = \frac{\rho}{\rho_l(1+r_g)} \frac{\mu_l}{\mu} \left( \frac{\Delta P}{L} \right) \quad (7.38)$$

Substitution of the density model, Equation 7.4, and Equation 7.23, Equation 7.38 produces

$$k_1 = \frac{\alpha_l \dot{m}}{1+r_g} \frac{\mu_l}{\mu} \left( \frac{\Delta P}{L} \right) \quad (7.39)$$

Since the mass fraction of gas in Equation 7.27 and the volume fraction of liquid in Equation 7.39 were functions of time, an estimate of these values was made based on the mid-point of the times reported in Table 5.2. In addition, the mass fraction of gas in Equation 7.27 was based on the mass fraction of gas not in solution. These values were taken from the density model of the previous section, based on the model that included the effects of solubility. As was discussed in Section 7.3, the mass fraction of gas not in solution was considered constant in the capillary tube.

The values needed for the application of Equation 7.36 are given in Table 7.3. The actual solution of Equation 7.36 was done in an iterative manner, and the results of that application are shown in Table 7.4.

The main advantage of the solution of Equation 7.30 was considered to be the establishment of the pressure distribution as a function of axial position. With this solution and the density model of Equation 7.4, the volumetric flow rate and the shear stress at the wall were determined as a function of axial position, and these values were used to provide an estimate of the viscosity of the liquid that was not dependent

upon the conditions under which the experiment was conducted. Thus, the viscosity of the liquid was more accurately estimated, though the definition of a mean-apparent viscosity was somewhat arbitrary.

Table 7.3 The Mass Fraction of Gas Not in Solution				
Temperature	Pressure	$\tau_g$	$\alpha_g _{t=0}$	Time
(°C)	(nominal psi)			(second)
410	75	0.0082	0.41	170
410	100	0.0072	0.33	170
410	150	0.0050	0.14	170
410	200	0.0029	0.01	170
450	50	0.019	0.68	110
450	75	0.015	0.47	110
450	100	0.010	0.42	110
450	125	0.0062	0.19	110

\* nomenclature:

$\tau_g$  the mass fraction of gas not in solution at the entrance to the capillary tube

$\alpha_g|_{t=0}$  the volume fraction of gas at the entrance to the capillary tube

Table 7.4. An Estimate of the Viscosity of the Liquid

Temperature	Pressure	Mean Viscosity	Liquid Viscosity
(°C)	(nominal psi)	(poise)	(poise)
410	75	356	603
410	100	586	875
410	150	528	614
410	200	494	499
450	50	34	106
450	75	53	100
450	100	65	112
450	125	65	80.2

## **7.5 Conclusion**

An estimate of the mass fraction of gas not in solution was made through use of a model of the density. Since the mass fraction of gas not in solution was found to be a function of pressure in addition to temperature and time, a relationship for the total mass fraction of gas was developed based on a solubility parameter. The total mass fraction of gas provided a good indication of the rate of degasification. The momentum equation was developed with the use of the model of the density and, based on a mean viscosity, the resultant equation was solved for the viscosity of the liquid. Various forms of the mean viscosity were applied and the definition considered the most accurate and appropriate was applied to the data. This estimate of the viscosity of the liquid was tailored to the specific flow parameters and provided an estimate of the viscosity of the liquid that was considered more accurate than the estimates of Chapter 6.

## Chapter 8

### 8.1 Summary and Results

An experimental investigation of the fluidity of a rapidly heated, bituminous, highly volatile coal was conducted with a high-temperature capillary rheometer similar to the devices used in the polymer industry. The principal goal of this investigation was to provide a quantitative measurement of the fluidity of coal in its plastic state. The only instrument currently used for fluidity measurements of coal, the Gieseler plastometer, provides only qualitative measurements of viscosity. In addition, measurements with the capillary rheometer have shown that the transition from no flow to plastic flow occurs over ten to thirty seconds, which is quite different from the twenty minutes required in a Gieseler plastometer<sup>7,8</sup>.

The radius of the capillary tube in the rheometer was 0.026 centimeter and the length-to-diameter ratio was 51. The rheometer was operated at two temperatures, 410 °C and 450 °C, and pressures in the reservoir reached a maximum of 141 bars. A high-temperature seal insured retention of all products of decomposition in the reservoir. The capillary tube was removable and disposable. In addition, a solid tube replaced the capillary tube for density measurements. The rheometer was constructed with molybdenum because of its high thermal conductivity, and the rheometer had a

large thermal mass compared to the coal sample in order to insure rapid heating. Figures 2.1 through 2.3 presented schematic representations of the experimental equipment. Thermal analysis of the sample of coal in the reservoir was given in Section 3.3. This section also discussed the possible errors caused by the assumptions of the analysis, and concluded that isothermal conditions existed in the reservoir within ninety seconds of insertion of the coal. The rheometer was calibrated by measurement of the viscosity of a standard-calibration fluid. These measurements were made between 20 °C and 40 °C and viscosities between seventy poise and ten poise. This range of viscosities was the same as the lowest range of viscosities encountered in the coal-flow measurements. Section 2.10 described these calibration runs, and Figure 2.4 showed the results. Section 2.11 described the measurements of the density of water in order to insure that the measurements of density were accurate.

Measurements of the position of the piston head versus time at 410 °C and 450 °C and pressure drops of 35.3, 53.0, 70.6, 88.3, 106, and 141 bars were reported with both the capillary tube inserted for viscosity measurements (Chapter 5) and the solid rod inserted for density measurements (Chapter 3). The measurements of the density in the reservoir were fitted to the empirical function:

$$\rho_r = a + b \times e^{-k(t-t_0)} \quad (8.1)$$

where  $\rho_r$  is the density in the reservoir,  $t$  is time, and  $a, b, k,$  and  $t_0$  are the constants to be established for each temperature and pressure. The values of these constants were given in Table 3.1. Equation 8.1 modeled the density as a function of time with a maximum standard deviation of 0.0090 gm/cm<sup>3</sup>, or five percent of the minimum value for the density. Equation 8.1 shows that the greatest rate of change of density with time occurred before the warm-up period of ninety seconds. Section 4.2 and Table 4.1 showed that the time-rate of change of the density was important for calculation of the volumetric flow rate.

In Sections 4.2 and 4.3, the macroscopic continuity and momentum equations were applied to volumes containing the reservoir and the capillary tube. Equation 4.32 gave an expression of the momentum equation applied to the volume of the capillary tube in terms of experimentally measured variables. Based on Equation 4.32 and the laboratory data given in Table 4.2, the significant forces acting on the volume of the capillary tube were the shear stress at the wall and the pressure drop along the tube, as described by the following equation:

$$-(P_o - P_i)A_c = C \int_0^L \tau_w dz \quad (8.2)$$

where  $P_o$  and  $P_i$  are the pressures at the entrance and the exit to the capillary tube, respectively,  $A_c$  is the cross-sectional area;  $L$  is the length;  $C$  is the circumference of the capillary tube;  $z$  is the axial coordinate; and  $\tau_w$  is the shear stress at the wall.

In Section 4.4, the difficulties associated with the multi-component, multi-phase flow of coal became evident upon introduction of the definition of viscosity through the rate of strain described by the following equation:

$$Q = -2\pi \int_0^{r_o} \frac{\partial u}{\partial r} \frac{r^2}{2} dr \quad (8.3)$$

where  $Q$  is the volumetric flow rate;  $r_o$  is the radius of the capillary tube;  $u$  is the axial velocity; and  $r$  is the radial coordinate. Without detailed knowledge of the distribution of the gaseous phase, both the velocity distribution and the radial gradient of the velocity distribution were unknown. It was necessary, therefore, to put the results of the measurements of the position of the piston head versus time in terms of an overall viscosity. Sometimes called the "effective" viscosity, the overall viscosity was computed using the value of volumetric rate of flow at the entrance to the capillary tube. Because the volumetric flow rate was a function of axial position due to the gaseous phase, the overall viscosity was not a constant of the material but rather a result of the

conditions under which the experiment was conducted. In addition, this overall viscosity was based on an initial assumption of a Newtonian fluid, and was, therefore, more accurately termed an apparent, overall viscosity.

In Chapter 5, the measurements of the overall, apparent viscosity were fitted to the empirical function:

$$\mu(t) = a + b(t - t_0) + c(t - t_0)^2 \quad (8.4)$$

where  $\mu$  is the overall, apparent viscosity, and  $a, b, c,$  and  $t_0$  are the constants to be established for each temperature and pressure drop. The values of these constants are given in Table 5.1. Equation 8.4 modeled the overall, apparent viscosity as a function of time with a maximum standard deviation of 53 poise, or ten percent of the minimum value for  $\mu$ , at 410 °C, and a maximum standard deviation of 14 poise, or thirty percent of the minimum value for  $\mu$ , at 450 °C. The behavior with time of the apparent, overall viscosity was consistent over all the temperatures and pressure drops. An initial and quite sudden transition from no flow to the maximum flow rate was followed by a constant-flow rate until the distance between the piston head and the bottom of the reservoir was of the same order of magnitude as the radius of the capillary tube at which time the flow rate decreased. Measurements based on this constant-flow rate gave a constant value for the overall, apparent viscosity during the specified time period with a maximum standard deviation of 57 poise, or 13 percent of the minimum  $\mu$ , at 410 °C, and a maximum standard deviation of 8 poise, or 12 percent of the minimum  $\mu$ , at 450 °C. Table 8.1 gave the actual values of the overall viscosity for each temperature and pressure drop, and Table 5.2 provided further detail. Within the accuracy of the experiment, the apparent, overall viscosity was not a function of pressure drop. This result was important because, if the solid phase were affecting the measurements of viscosity, then the apparent, overall viscosity would increase with pressure drop. Any rheological classification based on the overall viscosity of a multi-

phase system, however, must be considered approximate. Contrary to the measurements made with the Gieseler plastometer<sup>9,7,12</sup>, the transition from no flow to flow was swift, sudden, and independent of the volume of gas produced. Measurements with the Gieseler plastometer<sup>5,6,8,13</sup> had also linked the maximum rate of production of gas with the minimum viscosity while the present experiments consistently showed that transition from no flow to flow occurred after the maximum rate of production of gas. Because conditions for heat transfer were much better in the capillary rheometer than in the Gieseler plastometer, it is suggested that the assumption of isothermal conditions in the plastometer was incorrect and that non-isothermal conditions caused these discrepancies.

A nother goal of this present investigation was to determine the viscosity of the continuous phase in order to allow scaling of process equipment. It is important to recognize that any measurement of viscosity as a property of the coal, and therefore independent of the conditions under which the measurement was conducted, must be expressed as a viscosity of the continuous phase. In Chapter 6, the flow regime was determined to be frothy, and the flow was considered to be a two-phase, two-component system. The density of the liquid phase was taken to be the maximum density measured during the warm-up period. This maximum density was 1.32 gm/cm<sup>3</sup> with a standard deviation of 0.057 gm/cm<sup>3</sup> at 410 °C, and 1.14 gm/cm<sup>3</sup> with a standard deviation of 0.02 gm/cm<sup>3</sup> at 450 °C. Use of the measurements of the density of the liquid and of the overall-density measurements allowed the calculation of the volume fraction of gas in the reservoir for the period of time for which the flow rate was constant. These values of the volume fraction of gas are given in Table 8.1, and were found to be relatively insensitive to variations in the density of the liquid phase. Estimates of the viscosity of the liquid, based on two-phase correlations found in the literature<sup>32,33,36,38,40</sup> and the volume fraction of gas at the entrance to the tube, were considered inadequate because the flow parameters of the coal were significantly

different from the conditions for which the correlations were developed. In addition, because the high overall viscosity of the coal caused large pressure drops, the volume fraction of gas was a strong function of axial position. None of the correlations reviewed by Idsinga<sup>36</sup> or Husain<sup>33</sup> were able to deal with such large variations in the volume fraction of gas. The most reasonable values for the viscosity of the liquid based on these correlations were those values given by the application of the Lockhart and Martinelli<sup>38</sup> correlation. Table 8.1 gave the viscosity of the liquid based on the application of this correlation to the overall viscosity.

An estimate of the viscosity of the liquid based on the flow parameters encountered in the flow of coal was developed in Chapter 7. A model of the density of the coal was developed in Section 7.3 by considering the liquid to be incompressible and the volume occupied by the gas to be given by the ideal-gas law, that is,

$$\rho = \frac{\rho_l(1+\tau_g)}{\frac{\tau_g P^*}{P} + 1} \quad (8.5)$$

where  $\tau_g$  is the mass fraction of gas not in solution;  $P$  is the pressure;  $\rho$  is the overall density;  $\rho_l$  is the density of the liquid phase; and  $P^*$  is a constant related to the ideal-gas law and defined by Equation 7.2. Since decomposition could be considered to be a function of temperature alone, the density model included solubility as a function of pressure as follows:

$$\tau_g(T, P, t) = \tau_t(T, t) - s(T, t) \times P \quad (8.6)$$

where  $T$  is the temperature,  $\tau_t$  is the total-mass fraction of gas, and  $s$ , a function of temperature and time, represents a linear relationship between the pressure and the mass fraction of gas in solution. The total-mass fraction of gas was a function of temperature and time, and the mass fraction of gas not in solution gave reasonable predictions of the overall density. The mass fraction of gas was constrained to increase with time, and more measurements of the density at different pressures would increase the

accuracy of this model. Figures 8.1 and 8.2 show the mass fraction of gas in the reservoir versus time, and the standard deviation of the prediction of the density in the reservoir based on Equations 8.5 and 8.6. By developing this model of the overall density, one degree of freedom for the simplified, two-phase, two-component system was removed.

In Section 7.4, the momentum equation was re-examined with the model for the density included. By taking a definition for the mean viscosity of the fluid as a function of the viscosities of the liquid and the gas and as a function of the volume fractions of the liquid and the gas, several closed-form solutions of the momentum equation were generated. These solutions showed pressure distributions that were not linear, as expected, though the deviations from linearity were quite small. One particular function for the mean viscosity ( $\bar{\mu}$ ),

$$\bar{\mu} = \alpha_g \mu_g + \alpha_l \mu_l \quad , \quad (8.7)$$

where  $\mu_l$  and  $\mu_g$  are the viscosities of the liquid and gas, respectively, and  $\alpha_l$  and  $\alpha_g$  are the volume fractions of the liquid and gas, respectively, was applied to the viscosity data, and the results are given in Table 8.1. Under the flow conditions of the coal-rheology experiment, the non-linear term in the solution of the pressure distribution was insignificant, and, therefore, the solution was written as

$$-(P_o - P_i) = \frac{8\dot{m}\mu_l L}{\pi r_o^4 \rho_l (1 + r_g)} \quad (8.8)$$

where  $\dot{m}$  is the mass-flow rate,  $r_o$  is the radius of the capillary tube, and  $\rho_l$  is the density of the liquid phase. Equation 8.8 allowed measurement of the viscosity of the liquid from experiments on gas-liquid capillary flow. Though the application of this solution of the momentum equation appeared quite reasonable, the results were affected by an arbitrary selection of the form of a mean viscosity.

## 8.2 Conclusions

The major conclusions related to the initial goals of this investigation are listed below.

1. The capillary rheometer provided quantitative measurements of the overall viscosity of coal in its plastic state with the following relationship:

$$\mu = \frac{\pi r_o^3}{4Q_i} \left[ \frac{-(P_o - P_i)A_c}{CL} \right] \quad (8.9)$$

where  $\mu$  is the overall viscosity, and  $Q_i$  is the volumetric flow rate at the entrance to the capillary tube. The empirical representation of the overall viscosity had a standard deviation of less than twenty percent. The accuracy of these measurements was quite good for multi-phase flow, and it was transition from frothy flow to slug flow that prevented even greater accuracy. Though measurements of the overall viscosity were dependent upon the conditions under which the experiments were conducted, these results indicated a significant improvement over the qualitative measurements of fluidity made by the Gieseler plastometer. Comparison of these results with measurements made with a plastometer was not possible because the relationship between a plastometer measurement and viscosity is complex and unknown.

2. The differences between the measurements made with the capillary rheometer and the measurements made with a Gieseler plastometer were most noticeable in their descriptions of the transition from no flow to flow at the maximum flow rate. The plastometer indicated that this transition occurred over a time period of twenty minutes, while the capillary rheometer showed a time period of transition of about twenty seconds. In addition, the plastometer showed decreasing viscosity until the effects of coking began to increase the viscosity. The capillary rheometer, in contrast, measured a constant viscosity once transition had occurred.

These measurements by the capillary rheometer were quite short, however, lasting about forty seconds at 410 °C and ten seconds at 450 °C. This different description of transition was attributable to the superior heat-transfer characteristics of the capillary rheometer, and suggests that a large number of theories on coal in its plastic state<sup>4,5,6,8,9,13</sup> must be revised.

3. A review of the theory of two-phase flow did not uncover an accurate method of determining the viscosity of the liquid. The correlations reviewed by Idsigna<sup>36</sup> and Husain<sup>33</sup> were developed for flow conditions so different from the flow of coal that use of these correlations was questionable. In general, the gas produced by decomposition made the overall viscosity less than the viscosity of the continuous phase.
4. Development of a model for the density of the coal in Section 7.3, and selection of a form for the mean viscosity in Section 7.4, resulted in a solution of the momentum equation that was specifically tailored for the flow of coal in a capillary tube. Use of the density model,

$$\rho = \frac{\rho_l(1+r_g)}{\frac{r_g P^*}{P} + 1} \quad (8.5)$$

resulted in the solution for the pressure drop:

$$-(P_o - P_i) = \frac{8\dot{m}\mu_l L}{\pi r_o^4 \rho_l (1+r_g)} \quad (8.8)$$

The viscosity of the liquid was calculated from this solution and the experimental data, and this result was independent of the conditions under which the experiment was performed. Though the experimental data may not be used to confirm or deny the validity of this solution, comparison of this solution with the correlations discussed in Chapter 6 showed that this solution was reasonable, well-behaved, and appropriate.

The plasticity of coal has piqued the curiosity of researchers for almost a hundred years. The development of an instrument that allows a quantitative description of this plasticity is important in many ways. The descriptions of plasticity and the transition to plasticity provided by this instrument will be of great interest to the chemists and chemical engineers who are concerned with the basic structure of coal. The overall viscosity data and the estimates of the viscosity of the liquid phase will enable the design of equipment to take advantage of the temporary fluidity of bituminous coals. Finally, the application with perhaps the greatest potential would be the treatment of coal in its plastic state to reduce its pollutants and improve its usefulness as an alternate fossil fuel. The predictions of pressure drops and transition to plasticity are essential in the development of these applications.

Table 8.1 Summary of the Viscosity Measurements

Temperature	Pressure	Gas Volume	Overall	Liquid Viscosity	
	Drop	Fraction *	Viscosity	L and M **	Density Model
(°Celsius)	( bars )		(poise)	(poise)	(poise)
410	53.0	0.41	356	490	603
410	70.6	0.33	586	710	875
410	106	0.14	528	498	614
410	141	0.01	494	404	499
450	35.3	0.68	34	86	106
450	53.0	0.47	53	87	100
450	70.6	0.42	65	91	112
450	88.3	0.19	65	65	80

\* at the entrance to the capillary tube and during constant flow

\*\* correlation of Lockhart and Martinelli<sup>38</sup>

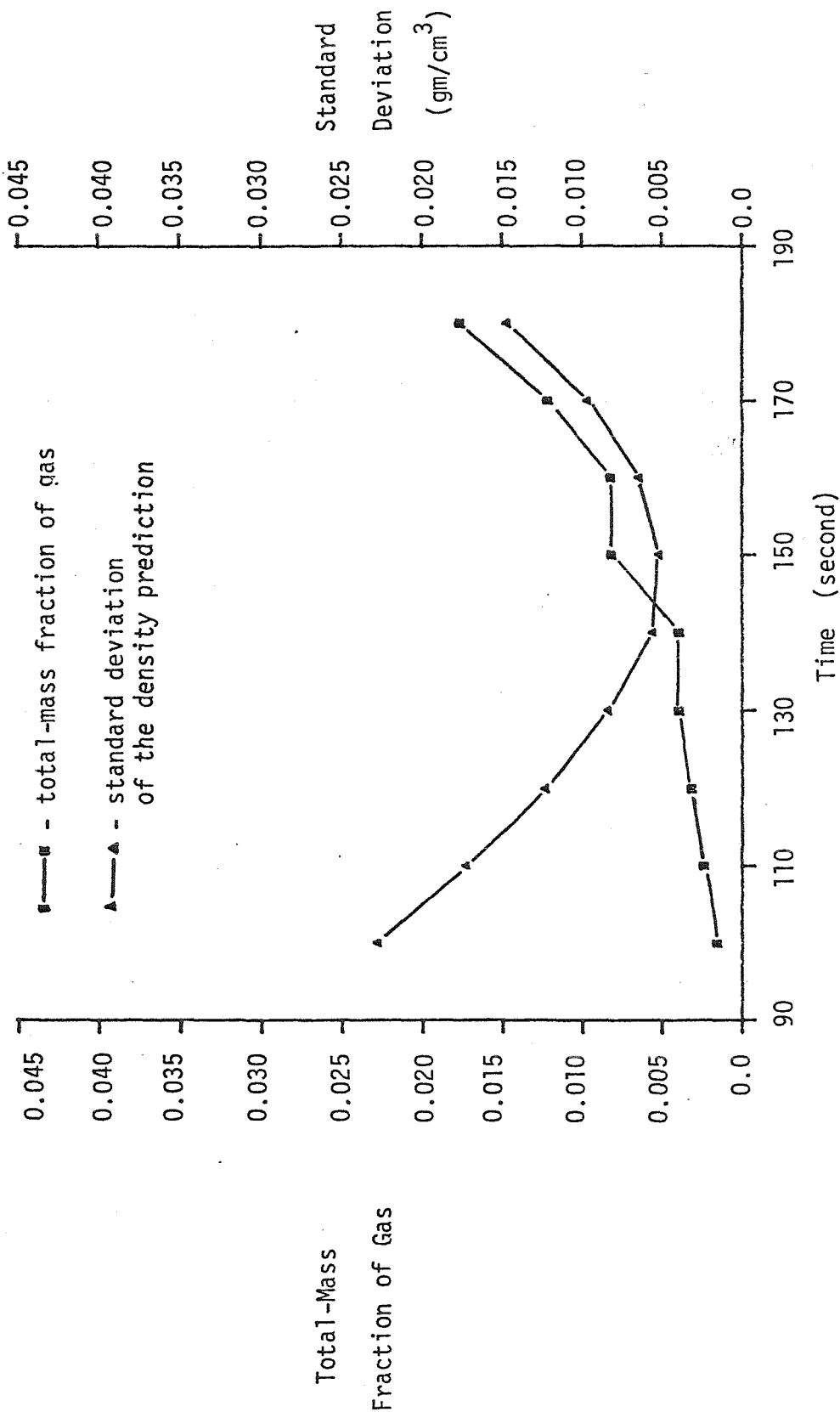


Figure 8.1. The total-mass fraction of gas versus time and the standard deviation of the prediction of the overall density based on total-mass fraction of gas in the reservoir at 410 °C.

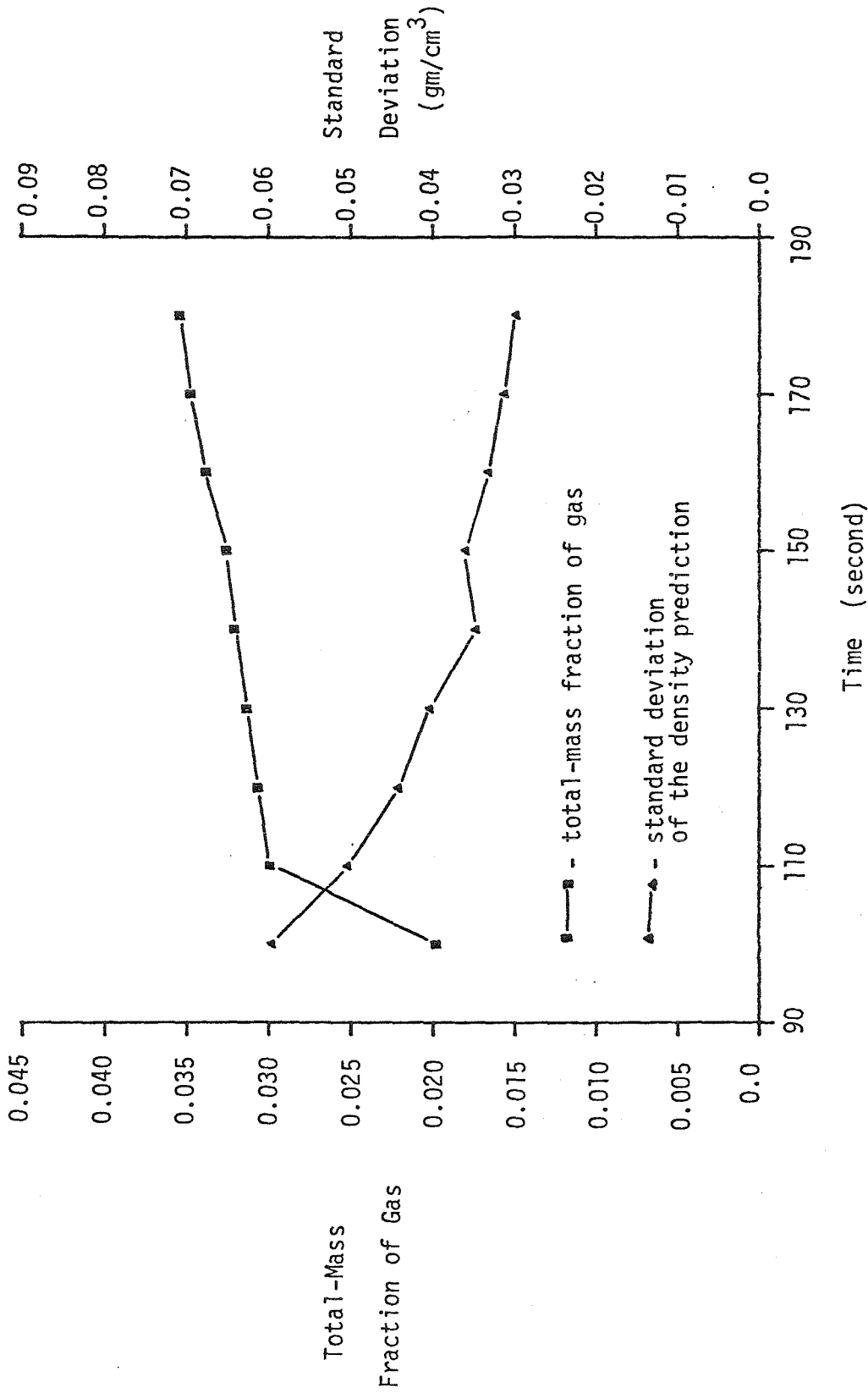


Figure 8.2. The total-mass fraction of gas in the reservoir versus time and the standard deviation of the prediction of the overall density based on the total-mass fraction of gas at 450°C.

List of References

1. M. L. Gorbaty, F. J. Wright, R. K. Lyon, R. B. Long, R. H. Schlosberg, Zeinab Baset, Ronald Liotta, B. G. Silbernagel, and D. R. Neskora, 'Coal Science: Basic Research Opportunities', *Science*, **206**, 4422 (1979), pp 1029-1034.
2. K. Gieseler, *Gluckauf*, **70**, 178 (1934).
3. ASTM Method D 2639-74, American Society for Testing and Materials, Philadelphia, Pa. (1974).
4. W. G. Lloyd, 'Experimental Laboratory Measurements of Selected Coal Types', JPL Report No. 9950-344, Institute of Mining and Minerals Research, University of Kentucky (1979).
5. D. Fitzgerald, 'Kinetic Study of Coal Carbonization in the Plastic Zone', *Fuel*, **35**, 178 (1956).
6. D. W. van Krevelen and J. Schuyer, **Coal Science Aspects of Coal Composition**, Elsevier Publishing Company, Amsterdam (1957).
7. W. G. Lloyd, 'Developments of Methods of Characterizing Coal in Its Plastic State', Office of Research and Engineering Services, Institute of Mining and Minerals Research, University of Kentucky (1978).
8. W. G. Lloyd, H. E. Francis, M. R. Tewell Jr., R. O. Kushida and V. D. Sankur, 'A Model for the Isothermal Plastometric Behavior of Coals', pp 99-104 of reference (4), (1979).
9. D. W. van Krevelen, F. J. Huntjens, H. N. M. Dormans, 'Chemical Structure and Properties of Coal XVI Plastic Behavior on Heating', *Fuel*, **35**, 462 (1956).
10. J. D. Davis, 'Dependence of Yields of Products on Temperature and Rate of Heating', **Chemistry of Coal Utilization**, H. H. Lowry editor, John Wiley and

Sons, New York (1945), pp 834-847.

11. E. Audibert, *Fuel*, **5**, 229 (1926).
12. P. L. Waters, 'Rheological Properties of Coal during the Early Stage of Thermal Softening', *Fuel*, **41**, 3 (1962).
13. D. W. van Krevelen and H. A. G. Cherrin, 'Chemical Structure and Properties of Coal XVII A Mathematical Model of Coal Pyrolysis', *Fuel*, **36**, 85 (1957).
14. C. E. England and P. R. Ryason, 'New method of feeding coal: continuous extrusion of fully plastic coal', *Fuel*, **57** (1978), pp 241-244.
15. S. P. Feinstein, 'Rheology', Coal Pump Development Phase I Feasibility Report, JPL Report No. 5030-235 (1978), pp 632-642.
16. S. P. Feinstein, personal communication (1980).
17. W. G. Lloyd, 'Experimental Laboratory Measurements of Selected Coal Types', JPL Report No. 9950-344, Institute of Mining and Minerals Research, University of Kentucky (1979), pg. 22.
18. C. D. Hodgman editor, **Handbook of Chemistry and Physics**, Chemical Rubber Publishing Company, Ohio (1949), pg. 1774.
19. C. D. Hodgman editor, **Handbook of Chemistry and Physics**, Chemical Rubber Publishing Company, Ohio (1949), pg. 1716.
20. E. T. Severs, **Rheology of Polymers**, Reinhold Publishing Corporation, New York (1962), pg. 86.
21. H. S. Carslaw and J. C. Jaeger, **Conduction of Heat in Solids**, Clarendon Press, Oxford (1959).
22. D. W. van Krevelen and J. Schuyer, **Coal Science Aspects of Coal Composition**, Elsevier Publishing Company, Amsterdam (1957), pp 282-284.

23. R. Bird, W. Stewart and E. Lightfoot, **Transport Phenomena**, John Wiley and Sons, New York (1960), pg. 85.
24. J. R. van Wazer, J. W. Lyons, K. Y. Kim and R. E. Colwell, **Viscosity and Flow Measurement**, Interscience, New York (1963), pp. 15-22.
25. R. Bird, W. Stewart and E. Lightfoot, **Transport Phenomena**, John Wiley and Sons, New York (1960), pg. 89.
26. J. R. van Wazer, J. W. Lyons, K. Y. Kim and R. E. Colwell, **Viscosity and Flow Measurement**, Interscience, New York (1963), pp. 199-214.
27. D. C. Bogue, 'Entrance Effects and Prediction of Turbulence in Non-Newtonian Flow', *Industrial and Engineering Chemistry*, **51**, 875 (1959).
28. E. H. Merz and R. E. Colwell, 'A High Shear Rate Capillary Rheometer for Polymer Melts', *ASTM Bulletin*, **232**, 63 (1958).
29. D. W. Dodge and A. M. Metzner, 'Turbulent Flow of Non-Newtonian Systems', *Journal of the American Institute of Chemical Engineers*, **5**, 2 (1959) pg. 189.
30. J. R. van Wazer, J. W. Lyons, K. Y. Kim and R. E. Colwell, **Viscosity and Flow Measurement**, Interscience, New York (1963), pp. 199-214.
31. H. L. Toor, 'Heat Generation and Conduction in the Flow of a Viscous Compressible Liquid', *Transactions of the Society of Rheology*, **1**, 177 (1959).
32. E. Barnea and J. Mizrahi, 'A General Approach to the Fluid Dynamics of Particulate Systems Part I. General Correlations for Fluidization and Sedimentation in Solid Multiparticle Systems', *Chemical Engineering Journal*, **5** (1973), pp. 171-189.
33. A. Husain, W. G. Choe and J. Wersman, 'Applicability of the Homogeneous Flow Model to Two-Phase Pressure Drop in Straight Pipe and Across Area Changes', *American Institute of Chemical Engineers Symposium Series*, **74**, 174 (1978), pp.

205-214.

34. G. K. Batchelor, **An Introduction to Fluid Dynamics**, University Press, Cambridge (1967).
35. G. Yardigargolu and R. T. Lahey Jr., 'On the Various Forms of the Conservation Equations in Two-Phase Flow', *International Journal of Multiphase Flow*, **2** (1975), pp. 477-494.
36. W. Idsinga, N. Todreas and R. Bowling, 'An Assessment of Two-Phase Pressure Drop Correlations for Steam-Water Systems', *International Journal of Two-Phase Flow*, **3** (1977), pp. 401-413.
37. F. C. Brown and W. L. Kranich, 'Model for the Prediction of Velocity and Void Fraction Profiles in Two-Phase Flow', *Journal of the American Institute of Chemical Engineers*, **14**, 750 (1968).
38. R. W. Lockhart and R. C. Martinelli, 'Proposed Correlation of Data for Isothermal Two-Phase, Two-Component Flow in Pipes', *Chemical Engineering Progress*, **45**, 1 (1949), pp. 39-48.
39. J. M. Mandhane, G. A. Gregory and K. Aziz, 'A Flow Pattern Map for Gas-Liquid Flow in Horizontal Pipes', *International Journal of Multiphase Flow*, **1**, 537 (1974).
40. J. Happel, 'Viscous Flow in Multiparticle Systems: Slow Motion of Fluids Relative to Beds of Spherical Particles', *Journal of the American Institute of Chemical Engineers*, **4**, 197 (1958).
41. D. H. Lewis Jr. and P. R. Ryason, 'The Apparent Viscosity of a Fluid-Gas Mixture', to be published (1981).
42. C. D. Han, Y. W. Kim and K. D. Malhotra, 'A Study of Foam Extrusion Using a Chemical Blowing Agent', *Journal of Applied Polymer Science*, **20** (1976), pp.

1583-1595.

43. W. H. McAdams, W. K. Woods and L. C. Heroman Jr., 'Vaporization Inside Horizontal Tubes - Benzene-Oil Mixtures', Transactions of the ASME, **64**, 193 (1942).
44. Viscosity Standard S2000-78103, Cannon Instrument Company, P. O. Box 16, State College, Pennsylvania 16801.
45. R. C. Martinelli and D. B. Nelson, 'Prediction of Pressure Drop During Forced-Circulation Boiling of Water', Transactions of the ASME, **70**, 695 (1948).

Appendix A

Density Data

The overall density was computed from the mass of the sample and the volume of the reservoir. The volume of the reservoir was a function of time, and was computed as a cylinder with a radius of 1.0 centimeter and a height given by the position of the piston head. Each sample was a Pitt 8 coal, and the data were taken at the indicated temperatures, pressures, and sampling rates. "Time starts at" indicates the period of time that occurred between insertion of the sample and initiation of the collection of data. Nominal pressure is converted to absolute pressure with the following two relationships:

$$F_p = \pi 3.2^2 \times (P_g + 14.7) \times C_{E-CGS} \text{ dynes} \quad (2.1)$$

where  $F_p$  is the force,  $P_g$  is the nominal pressure, and  $C_{E-CGS}$  converted psi to dynes per centimeter squared, and

$$P_r = \frac{F_p}{\pi R_o^2} \frac{\text{dynes}}{\text{cm}^2} \quad (2.2)$$

where  $P_r$  is the pressure in the reservoir, and  $R_o$  is the radius of the reservoir.

density run

run number 11

sampling interval (seconds) 30.00

nominal pressure (psig) 100.00

temperature 408.0

time starts at ninety secs

mass (grams) 1.9779

position of piston head (centimeters)

0.675 0.683 0.700 0.700 0.718 0.742 0.758 0.783 0.800 0.812

0.825 0.852 0.858 0.868 0.882 0.887 0.900 0.917 0.925 0.932

0.938 0.947

density run not used

run number 12

sampling interval (seconds) 30.00

nominal pressure (psig) 100.00

temperature 408.0

time starts at ninety secs

mass (grams) 1.9704

position of piston head (centimeters)

0.720 0.720 0.742 0.767 0.775 0.775 0.775 0.785 0.803 0.827

0.842 0.863 0.872 0.882 0.890 0.913 0.918 0.928 0.937 0.948

density run not used

run number 13

sampling interval (seconds) 30.00

nominal pressure (psig) 100.00

temperature 408.0

time starts at ninety secs

mass (grams) 1.3740

position of piston head (centimeters)

0.382 0.393 0.397 0.405 0.410 0.417 0.420 0.425 0.430 0.433

0.437 0.443 0.447 0.450 0.458 0.467

density run

run number 14

sampling interval (seconds) 30.00

nominal pressure (psig) 100.00

temperature 408.0

time starts at ninety secs

mass (grams) 1.3730

position of piston head (centimeters)

0.442 0.462 0.482 0.498 0.517 0.530 0.562 0.575 0.587 0.598  
0.608 0.620 0.633

density run

run number 15

sampling interval (seconds) 30.00

nominal pressure (psig) 100.00

temperature 408.0

time starts at ninety secs

mass (grams) 1.3734

position of piston head (centimeters)

0.410 0.422 0.432 0.442 0.450 0.462 0.470 0.480 0.488 0.502  
0.513 0.525 0.533 0.545

density run not used

run number 17

sampling interval (seconds) 30.00

nominal pressure (psig) 100.00

temperature 410.0

time starts at ninety secs

mass (grams) 1.2780

position of piston head (centimeters)

0.363 0.377 0.383 0.392 0.398 0.405 0.415 0.427 0.437 0.445  
0.455

density run

run number 18

sampling interval (seconds) 30.00

nominal pressure (psig) 100.00

temperature 408.0

time starts at ninety secs

mass (grams) 1.2830

position of piston head (centimeters)

0.417 0.428 0.433 0.435 0.438 0.450 0.457 0.472 0.483 0.497

0.505 0.515 0.520

density run not used

run number 20

sampling interval (seconds) 30.00

nominal pressure (psig) 100.00

temperature 410.0

time starts at ninety secs

mass (grams) 1.3090

position of piston head (centimeters)

0.457 0.477 0.478 0.478 0.478 0.488 0.503 0.518 0.530 0.542

0.557 0.565 0.577 0.587 0.600 0.610 0.618

density run

run number 23

sampling interval (seconds) 30.00

nominal pressure (psig) 150.00

temperature 410.0

time starts at ninety secs

mass (grams) 1.3034

position of piston head (centimeters)

0.353 0.353 0.355 0.362 0.372 0.378 0.392 0.400 0.408 0.415  
0.425 0.430 0.438 0.443 0.452

density run

run number 24

sampling interval (seconds) 30.00

nominal pressure (psig) 150.00

temperature 410.0

time starts at ninety secs

mass (grams) 1.1488

position of piston head (centimeters)

0.323 0.333 0.342 0.350 0.358 0.367 0.375 0.383 0.390 0.397  
0.405 0.412 0.420 0.425 0.430

density run not used

run number 22

sampling interval (seconds) 30.00

nominal pressure (psig) 150.00

temperature 410.0

time starts at ninety secs

mass (grams) 1.3240

position of piston head (centimeters)

0.273 0.275 0.280 0.292 0.300 0.307 0.317 0.325 0.332 0.340  
0.347 0.353 0.360 0.367 0.373 0.380

density run

run number 25

sampling interval (seconds) 30.00

nominal pressure (psig) 150.00

temperature 410.0

time starts at ninety secs

mass (grams) 1.2769

position of piston head (centimeters)

0.342 0.342 0.352 0.353 0.363 0.377 0.383 0.395 0.403 0.408

0.415 0.423 0.432 0.438 0.445 0.448 0.455

density run not used

run number 26

sampling interval (seconds) 30.00

nominal pressure (psig) 200.00

temperature 410.0

time starts at ninety secs

mass (grams) 1.2766

position of piston head (centimeters)

0.347 0.353 0.362 0.363 0.373 0.378 0.388 0.395 0.400 0.407

0.413 0.418 0.422 0.427

density run

run number 27

sampling interval (seconds) 30.00

nominal pressure (psig) 200.00

temperature 410.0

time starts at ninety secs

mass (grams) 1.2698

position of piston head (centimeters)

0.298 0.310 0.328 0.337 0.338 0.358 0.363 0.373 0.378 0.378

0.383 0.392

density run

run number 29

sampling interval (seconds) 30.00

nominal pressure (psig) 200.00

temperature 410.0

time starts at ninety secs

mass (grams) 1.3197

position of piston head (centimeters)

0.318 0.328 0.343 0.367 0.373 0.373 0.393 0.400 0.408 0.415

0.422 0.427 0.433 0.440 0.443 0.450

density run not used

run number 30

sampling interval (seconds) 30.00

nominal pressure (psig) 200.00

temperature 410.0

time starts at ninety secs

mass (grams) 1.3624

position of piston head (centimeters)

0.305 0.293 0.288 0.305 0.338 0.342 0.348 0.353 0.372 0.378

0.363 0.390 0.395 0.403 0.408 0.413

density run

run number 31

sampling interval (seconds) 30.00

nominal pressure (psig) 75.00

temperature 410.0

time starts at ninety secs

mass (grams) 1.1117

position of piston head (centimeters)

0.357 0.378 0.402 0.422 0.440 0.458 0.477 0.495 0.510 0.523  
0.537 0.550 0.563 0.577 0.587 0.600

density run not used

run number 32

sampling interval (seconds) 30.00

nominal pressure (psig) 75.00

temperature 410.0

time starts at ninety secs

mass (grams) 1.1024

position of piston head (centimeters)

0.315 0.330 0.345 0.358 0.368 0.383 0.403 0.422 0.438 0.455  
0.465 0.478 0.495 0.510 0.522 0.532 0.542

density run

run number 35

sampling interval (seconds) 5.00

nominal pressure (psig) 50.00

temperature 450.0

time starts at forty seconds

mass (grams) 1.1029

position of piston head (centimeters)

0.342 0.373 0.397 0.435 0.463 0.487 0.512 0.538 0.558 0.577  
0.590 0.602 0.613 0.628 0.637 0.650

density run

run number 36

sampling interval (seconds) 10.00

nominal pressure (psig) 50.00

temperature 450.0

time starts at forty secs

mass (grams) 0.8040

position of piston head (centimeters)

0.278 0.283 0.365 0.438 0.485 0.525 0.563 0.588 0.617 0.640

0.667 0.688

density run

run number 38

sampling interval (seconds) 5.00

nominal pressure (psig) 50.00

temperature 450.0

time starts at forty secs

mass (grams) 1.1457

position of piston head (centimeters)

0.388 0.427 0.468 0.507 0.542 0.577 0.645 0.673 0.705 0.728

density run

run number 33

sampling interval (seconds) 30.00

nominal pressure (psig) 75.00

temperature 410.0

time starts at ninety secs

mass (grams) 1.2112

position of piston head (centimeters)

0.445 0.475 0.498 0.525 0.545 0.563 0.580 0.597 0.612 0.628

0.643 0.657 0.670 0.683 0.693 0.705

density run not used

run number 34

sampling interval (seconds) 30.00

nominal pressure (psig) 75.00

temperature 410.0

time starts at ninety secs

mass (grams) 1.1834

position of piston head (centimeters)

0.357 0.405 0.427 0.448 0.467 0.480 0.492 0.505 0.525 0.540

0.553 0.565 0.577 0.590 0.603 0.612 0.622 0.632 0.640 0.645

density run

run number 39

sampling interval (seconds) 10.00

nominal pressure (psig) 100.00

temperature 450.0

time starts at ninety secs

mass (grams) 1.1048

position of piston head (centimeters)

0.497 0.498 0.500 0.522 0.542 0.562 0.583 0.597 0.622 0.658

0.677 0.688 0.700 0.712

density run

run number 40

sampling interval (seconds) 10.00

nominal pressure (psig) 100.00

temperature 450.0

time starts at ninety secs

mass (grams) 1.0128

position of piston head (centimeters)

0.528 0.527 0.527 0.542 0.553 0.575 0.590 0.603 0.617 0.635  
0.650 0.663 0.675 0.687 0.695 0.707 0.715

density run

run number 41

sampling interval (seconds) 10.00

nominal pressure (psig) 75.00

temperature 450.0

time starts at ninety secs

mass (grams) 1.0358

position of piston head (centimeters)

0.583 0.583 0.585 0.607 0.633 0.658 0.678 0.703 0.725 0.745  
0.770 0.785 0.805

density run

run number 42

sampling interval (seconds) 10.00

nominal pressure (psig) 125.00

temperature 450.0

time starts at ninety secs

mass (grams) 1.1123

position of piston head (centimeters)

0.375 0.375 0.378 0.397 0.402 0.417 0.433 0.442 0.460 0.470  
0.483 0.493 0.500 0.510 0.518 0.525

density run

run number 43

sampling interval (seconds) 10.00

nominal pressure (psig) 125.00

temperature 450.0

time starts at ninety secs

mass (grams) 0.9131

position of piston head (centimeters)

0.300 0.305 0.307 0.338 0.357 0.372 0.387 0.398 0.410 0.423

0.433 0.443 0.457 0.467 0.477 0.487 0.495 0.505 0.512

density run

run number 44

sampling interval (seconds) 10.00

nominal pressure (psig) 75.00

temperature 450.0

time starts at ninety secs

mass (grams) 1.0231

position of piston head (centimeters)

0.518 0.518 0.518 0.520 0.547 0.572 0.593 0.612 0.628 0.643

0.657 0.675 0.690 0.697 0.708 0.723 0.730 0.740 0.750 0.760

0.775

density run

run number 45

sampling interval (seconds) 10.00

nominal pressure (psig) 100.00

temperature 450.0

time starts at ninety secs

mass (grams) 0.9856

position of piston head (centimeters)

0.417 0.417 0.422 0.443 0.462 0.480 0.497 0.510 0.525 0.540

0.552 0.565 0.573 0.585 0.593 0.605 0.612 0.622

## Appendix B

### Viscosity Data

The volumetric flow rate was computed from the time rate of change of the volume of the reservoir, separate measurements of the density, and the radius of the capillary tube, 0.026 centimeter. The volume of the reservoir was a function of time, and was computed as a cylinder with a radius of 1.0 centimeter and a height given by the position of the piston head. Each sample was a Pitt 8 coal, and the data were taken at the indicated temperatures, pressures, and sampling rates. 'Time starts at' indicates the period of time that occurred between insertion of the sample and initiation of the collection of data. Nominal pressure is converted to pressure drop with the following two relationships:

$$F_p = \pi 3.2^2 \times P_g \times C_{E-CGS} \text{ dynes} \quad (2.1)$$

where  $F_p$  is the force,  $P_g$  is the nominal pressure, and  $C_{E-CGS}$  converted psi to dynes per centimeter squared, and

$$P_r = \frac{F_p}{\pi R_o^2} \frac{\text{dynes}}{\text{cm}^2} \quad (2.2)$$

where  $P_r$  is the pressure drop, and  $R_o$  is the radius of the reservoir. The relationships between volumetric flow rate, pressure drop, and viscosity were given in Chapter 4.

viscosity run not used

run number 75

sampling interval (seconds) 5.00

nominal pressure (psig) 100.00

temperature 410.0

time starts at ninety secs

mass (grams) 0.0000

position of piston head (centimeters)

0.437 0.437 0.437 0.437 0.437 0.437 0.435 0.432 0.428 0.418  
0.412 0.403 0.395 0.380 0.368 0.343 0.322 0.317 0.300 0.280  
0.255 0.238 0.208 0.190 0.162 0.135 0.095 0.080 0.050 0.013

viscosity run not used

run number 76

sampling interval (seconds) 5.00

nominal pressure (psig) 100.00

temperature 410.0

time starts at ninety secs

mass (grams) 0.0000

position of piston head (centimeters)

0.503 0.507 0.508 0.508 0.508 0.508 0.508 0.505 0.498 0.490  
0.480 0.463 0.443 0.418 0.398 0.347 0.362 0.340 0.320 0.297  
0.278 0.263 0.243 0.223 0.208 0.187 0.168 0.145 0.128 0.112  
0.097

viscosity run

run number 77

sampling interval (seconds) 5.00

nominal pressure (psig) 100.00

temperature 410.0

time starts at ninety secs

mass (grams) 0.0000

position of piston head (centimeters)

0.403 0.403 0.403 0.403 0.403 0.402 0.400 0.398 0.395 0.392  
0.387 0.378 0.370 0.362 0.353 0.343 0.335 0.325 0.313 0.305  
0.290 0.278 0.268 0.255 0.242 0.227 0.210 0.193 0.178 0.162  
0.147 0.130 0.112 0.095 0.082 0.068 0.055 0.043 0.033 0.028

0.023 0.017

viscosity run

run number 78

sampling interval (seconds) 5.00

nominal pressure (psig) 100.00

temperature 410.0

time starts at ninety secs

mass (grams) 0.0000

position of piston head (centimeters)

0.413 0.413 0.413 0.413 0.413 0.412 0.412 0.412 0.410 0.407

0.403 0.395 0.383 0.378 0.348 0.337 0.338 0.345 0.335 0.323

0.312 0.295 0.280 0.272 0.257 0.237 0.223 0.205 0.188 0.173

0.158 0.140 0.125 0.110 0.095 0.080 0.070 0.057 0.047 0.040

0.033 0.028 0.027 0.025

viscosity run

run number 79

sampling interval (seconds) 5.00

nominal pressure (psig) 75.00

temperature 410.0

time starts at ninety secs

mass (grams) 0.0000

position of piston head (centimeters)

0.487 0.485 0.483 0.478 0.472 0.463 0.453 0.443 0.425 0.415

0.405 0.370 0.372 0.357 0.340 0.323 0.302 0.252 0.270 0.255

0.235 0.207 0.195 0.178 0.155 0.140 0.120 0.103 0.092 0.078

0.072 0.062 0.057 0.047

viscosity run

run number 80

sampling interval (seconds) 5.00

nominal pressure (psig) 75.00

temperature 410.0

time starts at ninety secs

mass (grams) 0.0000

position of piston head (centimeters)

0.418 0.417 0.417 0.410 0.407 0.397 0.393 0.407 0.403 0.393  
0.358 0.350 0.352 0.358 0.348 0.328 0.312 0.305 0.275 0.262  
0.263 0.252 0.247 0.212 0.195 0.180 0.122 0.143 0.128 0.110  
0.103 0.097 0.090 0.082 0.078 0.075 0.072 0.068 0.065 0.063  
0.062 0.060 0.058

viscosity run

run number 81

sampling interval (seconds) 2.00

nominal pressure (psig) 200.00

temperature 410.0

time starts at ninety secs

mass (grams) 0.0000

position of piston head (centimeters)

0.238 0.217 0.207 0.190 0.167 0.153 0.138 0.123 0.107 0.100  
0.088 0.077 0.060 0.047 0.047 0.038 0.032

viscosity run

run number 82

sampling interval (seconds) 5.00

nominal pressure (psig) 150.00

temperature 410.0

time starts at ninety secs

mass (grams) 0.0000

position of piston head (centimeters)

0.347 0.327 0.307 0.282 0.257 0.220 0.200 0.172 0.137 0.107

0.082 0.063 0.052 0.043 0.040

viscosity run

run number 83

sampling interval (seconds) 5.00

nominal pressure (psig) 150.00

temperature 410.0

time starts at ninety secs

mass (grams) 0.0000

position of piston head (centimeters)

0.345 0.303 0.275 0.275 0.248 0.220 0.202 0.153 0.122 0.098

0.065 0.055 0.040 0.033 0.028

viscosity run

run number 84

sampling interval (seconds) 5.00

nominal pressure (psig) 150.00

temperature 410.0

time starts at ninety secs

mass (grams) 0.0000

position of piston head (centimeters)

0.383 0.375 0.362 0.348 0.333 0.298 0.292 0.272 0.248 0.222

0.212 0.162 0.133 0.107 0.077 0.042 0.048 0.037

viscosity run

run number 85

sampling interval (seconds) 2.00

nominal pressure (psig) 50.00

temperature 450.0

time starts at ninety secs

mass (grams) 1.6320

position of piston head (centimeters)

0.697 0.693 0.685 0.658 0.628 0.595 0.562 0.528 0.498 0.463

0.397 0.322 0.168 0.128 0.112 0.102 0.088

viscosity run

run number 87

sampling interval (seconds) 2.00

nominal pressure (psig) 50.00

temperature 450.0

time starts at ninety secs

mass (grams) 1.6516

position of piston head (centimeters)

0.673 0.678 0.678 0.678 0.678 0.675 0.658 0.612 0.568 0.520

0.442 0.358 0.275 0.107 0.083 0.050

viscosity run

run number 89

sampling interval (seconds) 1.00

nominal pressure (psig) 100.00

temperature 450.0

time starts at ninety secs

mass (grams) 1.0831

position of piston head (centimeters)

0.333 0.310 0.292 0.275 0.260 0.243 0.232 0.215 0.200 0.187  
0.173 0.153 0.140 0.128 0.113

viscosity run

run number 90

sampling interval (seconds) 2.00

nominal pressure (psig) 100.00

temperature 450.0

time starts at ninety secs

mass (grams) 1.6195

position of piston head (centimeters)

0.600 0.600 0.600 0.600 0.597 0.583 0.567 0.548 0.525 0.492  
0.457 0.400 0.350 0.323 0.273 0.237 0.183 0.127

viscosity run

run number 91

sampling interval (seconds) 2.00

nominal pressure (psig) 125.00

temperature 450.0

time starts at ninety secs

mass (grams) 1.5854

position of piston head (centimeters)

0.537 0.525 0.513 0.490 0.460 0.422 0.367 0.307 0.240 0.168  
0.108

viscosity run

run number 92

sampling interval (seconds) 2.00

nominal pressure (psig) 125.00

temperature 450.0

time starts at ninety secs

mass (grams) 1.6714

position of piston head (centimeters)

0.562 0.562 0.562 0.545 0.530 0.508 0.473 0.420 0.363 0.267

0.208 0.138 0.072

viscosity run

run number 94

sampling interval (seconds) 1.00

nominal pressure (psig) 75.00

temperature 450.0

time starts at ninety secs

mass (grams) 1.4348

position of piston head (centimeters)

0.568 0.553 0.535 0.518 0.498 0.477 0.462 0.442 0.423 0.400

0.378 0.362 0.340 0.325 0.308 0.272 0.245 0.222

viscosity run

run number 95

sampling interval (seconds) 1.00

nominal pressure (psig) 75.00

temperature 450.0

time starts at ninety secs

mass (grams) 1.3717

position of piston head (centimeters)

0.512 0.487 0.468 0.450 0.428 0.410 0.388 0.360 0.328 0.293

0.262 0.220 0.203 0.188

APPENDIX C

A sample of Gieseler plastometer data for the Pitt 8 coal by Lloyd.<sup>4</sup>

